Probability of Derailment under Earthquake Conditions

by

Lucile M. Guillaud

Diplôme d'Ingénieur

Ecole Spéciale des Travaux Publics, Paris, France (2005)

SUBMITTED TO THE DEPARTMENT OF CIVIL AND ENVIRONMENTAL ENGINEERING IN PARTIAL

FULFILLMENT OF THE REQUIREMENTS FOR THE DEGREE OF

MASTER OF SCIENCE IN TRANSPORTATION

AT THE

MASSACHUSETTS INSTITUTE OF TECHNOLOGY

September 2006

Signature of Author: _____

Department of Civil and Environmental Engineering

August 9, 2006

Certified by: _____

Daniele Veneziano

Professor of Civil and Environmental Engineering

Thesis Supervisor

Certified by: _____

Joseph Sussman

Professor of Civil and Environmental Engineering and Engineering Systems

JR East Professor

Thesis Reader

Accepted by: _____

Andrew J. Whittle

Chairman, Departmental Committee for Graduate Students

Probability of Derailment under Earthquake Conditions

by

Lucile M. Guillaud

Submitted to the Department of Civil and Environmental Engineering on August 9, 2006
in Partial Fulfillment of the Requirements for the
Degree of Master of Science in Transportation

ABSTRACT

A quantitative assessment of the probability of derailment under earthquake conditions is presented. Two derailment modes are considered: by vibratory motion – during the ground motion – and by permanent track deformation – after the motion ended. Criteria for derailment that apply to both modes are derived in terms of peak transversal acceleration and peak transversal displacement. This allows a direct comparison between the two causes of derailment. We find that the first mode of derailment (by vibratory motion) dominates over the second mode (by track damage).

The model considers the effect of spatial non-homogeneities in soil and structural characteristic and the incoherence of the ground motion into the assessment of derailment risk. The lateral motion experienced by the train under non-synchronous vibration of the track is obtained as the superposition of two contributions: one is the track motion at a fixed location and the other is the motion as the train travels on deformed tracks. Under linear elastic conditions, a method to obtain the power spectral density function for ground acceleration is presented and used to obtain acceleration and displacement response spectra. The second component of motion depends on speed. It is found that the train motion due to track deformation has small effects at ordinary speeds but that it becomes noticeable as the speed increases and the support spacing decreases. In general, it is shown that changes in soil and structural properties present a higher risk for derailment by vibratory motion. In some cases, the second component of train motion may increase the acceleration due to track motion at a single location by a factor of two.

The analysis is first done assuming linear behavior of the soil and structure and then nonlinearities and permanent deformations are included. The elastic analysis is found to be adequate, except for structures with natural periods exceeding 1 second where the elastic analysis yields conservative estimates in comparison with the inelastic case.

Thesis Supervisor: Daniele Veneziano
Title: Professor of Civil and Environmental Engineering

ACKNOWLEDGMENTS

I gratefully acknowledge the financial support provided by the *East Japan Railway Company.*

I would like to express my sincerest gratitude to Professor Veneziano. It has been a privilege and a pleasure to work under his supervision. I sincerely thank him for sharing his knowledge with an extraordinary patience.

I am thankful to Professor Sussman for his support throughout these years at MIT. His constant encouragement and friendliness made these years more bearable. I sincerely thank him for giving me the opportunity to take part in a variety of research groups.

I would like to thank Tyler for his friendship over the years. It has been a pleasure to work with him. Most importantly, he made these years very enjoyable.

Finally, I am most grateful to my parents for their love and support.

TABLE OF CONTENTS

LIST OF FIGURES

LIST OF TABLES

1 Introduction

From an engineering point of view, train derailment under earthquakes may occur under two distinct conditions. During the strong ground motion phase, the accelerations and displacements of the track may exceed limits that cause the train to derail. This first mode of derailment is referred to as derailment by vibratory motion. If the train survives the strong motion phase, it may subsequently encounter damaged tracks and derail (derailment by permanent track deformation). In the past (e.g., Papadimitriou, 1995), it has been assumed that the risk of derailment by vibratory motion is small relative to the risk of derailment by permanent track deformation. More recent work by JR East shows that this is not necessarily the case. For example, in the Niigata earthquake of 2004 sudden variation in site conditions may have induced differential structural responses sufficient to trigger derailment of a Shinkansen train by vibratory motion. In general, changes in soil and structural properties present a higher risk for derailment by vibratory motion. In addition, recent work on spatial variation of ground motion has shown that during the ground motion, spatially extended structures such as viaducts and embankments experience excitations that vary along the structure and possibly develop very large local deformations. It is not quite clear whether derailment by track damage dominates over derailment during the ground motion.

Our objective is to make a detailed quantitative assessment of the two derailment modes, in particular to improve the current earthquake risk analysis of the JR East Shinkansen system.

The first step of this study is to develop criteria for derailment under earthquake conditions that apply to both modes of derailment. Criteria for derailment in terms of peak transversal acceleration and peak transversal displacement are presented. This allows a direct comparison between the two causes of derailment.

The second step is to present a model that considers the effect of spatial non-homogeneities in soil and structural characteristic and the incoherence of the ground motion into the assessment of derailment risk. The lateral motion experienced by the train under non-synchronous vibration of the track can be obtained as the superposition of two contributions: One is the track motion at a fixed location and the other is the motion as the train travels on deformed tracks. First we characterize the vibratory motion of the track using the dynamic properties of the soil and the structure at a single location. This gives the first component of train motion. Then we consider the effect of spatial non-homogeneities in soil and structural characteristics and the incoherence of the ground motion to obtain a second component of lateral train acceleration. This second component of motion is sensitive to train speed. Speed has actually two effects. It may facilitate derailment under synchronous track motion and contributes to lateral acceleration and displacement under non-synchronous track motion. The later effect is considered, whereas the former effect is being ignored.

The analysis is first done assuming linear behavior of the soil and structure and then nonlinearities in the structural response and permanent deformations are included. Excessive residual deformation appears as a pertinent criterion when considering the derailment of a train running on permanently damaged tracks. Clearly, any permanent deformation at the end of the ground motion would be equaled or exceeded during the motion itself. However, spatial dependence of damage and train speed must also be accounted for.

We find that the first mode of derailment dominates over the second mode. The elastic analysis is found to be adequate, except for structures with natural periods exceeding 1 second. In this case, the elastic analysis yields quite conservative estimates in comparison with the inelastic case. However, natural periods over 1 second are not common. It is also found that the train motion due to track deformation has small effects at ordinary speeds but that it becomes noticeable as the speed increases and the support spacing decreases. In some cases, this second component of train motion may increase the base acceleration due to track motion at a fixed location by a factor of two.

The thesis is organized as follows:

Chapter 2 analyzes derailment under earthquake conditions assuming linear behavior of the soil and the structure that supports the tracks.
In Section 2.1, criteria for derailment under earthquake conditions are derived and the first mode of derailment (by vibratory motion) is investigated for the case of a stationary train. For this purpose, it is sufficient to consider the dynamic properties of the soil and the structure at a single location. Under linear elastic conditions, a method to obtain the power spectral density function for ground acceleration is presented and used to obtain acceleration and displacement response spectra. Section 2.2 considers the effect of train speed and asynchronous motion at different locations along the track. For this purpose, we consider the effect of spatial non-homogeneities in soil and structural characteristics and the incoherence of the ground motion to obtain a second component of lateral train motion. This component depends on train speed.

Chapter 3 considers the effects of nonlinearities in the structural response and the development of permanent deformations of the track, which may trigger derailment events of the second type.
First, we re-evaluate derailment due to vibratory motion by considering inelastic behaviour of the structure. This is done in Section 3.1. The soil response remains linear elastic, and the structure is assumed to behave as an elasto-plastic single degree of freedom system. In Section 3.2, permanent deformations are included, and the second mode of derailment (by track damage) is considered.

Chapter 4 summarizes our main findings and conclusions and makes recommendation for future work.

2 Elastic Analysis

Derailment is most likely to occur when a large lateral force occurs simultaneously with a reduced vertical load on wheel. A commonly used limit is expressed in terms of the ratio between the lateral and vertical forces.

During the strong ground motion phase, the lateral acceleration and displacement of the track may exceed limits that cause the train to derail. This cause of derailment is referred to as derailment by vibratory motion. In this section, we consider this mode of derailment under the assumption that the support and the rail system behave linearly.

The lateral motion experienced by the train under non-synchronous vibration of the track can be obtained as the superposition of two contributions: 1) The shaking of the track at the location of the train, and 2) The pseudo-static motion of the train due to the waviness of the track induced by differences in support displacements. This second component of motion depends on train speed.

First we characterize the vibratory motion of the track using the dynamic properties of the soil and the structure at a single location. This first component of train motion, with peak acceleration *Sa* and peak displacement *Sd* is considered in Section 2.1. Then we consider the effect of spatial non-homogeneities and discontinuities in soil and structural characteristics and the incoherence of the ground motion to obtain the second component of lateral train acceleration, Sa_d. This component characterizes the differential displacements of the track during the ground motion. This is discussed in Section 2.2.

In all cases, we assume linear dynamic behavior of the soil and the structure.

2.1 Derailment of a Stationary Train due to Vibratory Motion

In this section, we consider the first component of vibratory motion, namely the shaking of the track at a single location with peak acceleration *Sa* and peak absolute

displacement *Sd*. Section 2.1.1 presents general derailment criteria for trains under dynamic but not necessarily seismic conditions. During the strong ground motion phase, the acceleration and the displacement of the track may exceed threshold values, causing the train to derail. An important objective is to determine those critical conditions. This is done in Section 2.1.2. Criteria for derailment in terms of peak transversal acceleration and peak transversal displacement are presented, and applied to selected scenarios. Section 2.1.3 relates the levels of shaking *Sa* and *Sd* to earthquake magnitude, epicentral distance, local site conditions and structural period. This is done in a way that allows discussion of non-homogeneous site conditions when dealing with derailment of a moving train (see Section 2.2). Acceleration and displacement response spectra are derived, and a discussion concerning the contribution of the ground motion to the critical level of shaking is proposed. Finally, in Section 2.1.4, we derive probabilities of derailment by vibratory motion for selected earthquake scenarios. One aspect that has been disregarded is the effect of speed under homogeneous site conditions. This section considers vibratory motion of a stationary train, independently of train speed. Speed may facilitate derailment under synchronous track motion. The problem of including train speed is discussed at the end of this section, with a case study of the Niigata earthquake.

2.1.1 General Derailment Criteria

This section presents a review of what is known concerning train derailment under dynamic but not necessarily seismic conditions.

Derailment is most likely to occur when a large lateral force occurs simultaneously with a reduced vertical load on wheel. During train motion, vertical, transversal and longitudinal forces are applied to the train, even in the absence of ground motion. An excessive transversal force H is the main cause of train derailment. Transversal forces have both a static and a dynamic component. Static forces are due to centrifugal acceleration whereas transverse dynamic forces are caused by track and rolling stock defects. It is commonly assumed in railway engineering that the wheels and the rail are free of defects (Railway Engineering, 2000) and static analysis that omits the dynamic

loads caused by defects is often considered adequate (Profillidis, 2000). Also in this study we ignore rail and track defects.

Under certain conditions and when exceeding certain limits, lateral forces may cause a train to derail. Derailments occur for various reasons: wheel climbing, vehicle overturning, track lateral shift, overall unstable equilibrium, etc... A commonly used limit is expressed in terms of the ratio Y/Q of the lateral to vertical wheel forces (Dynamics of Railway Vehicle Systems, 1984). The Y/Q ratio is especially important in predicting wheel climb (Simulation in Railway Dynamics, 1988). Derailment generally occurs when the ratio Y/Q exceeds a limit that depends on the angle and coefficient of friction between wheel and rail (Dynamics of Railway Vehicle Systems, 1984); see Figure 2-1.

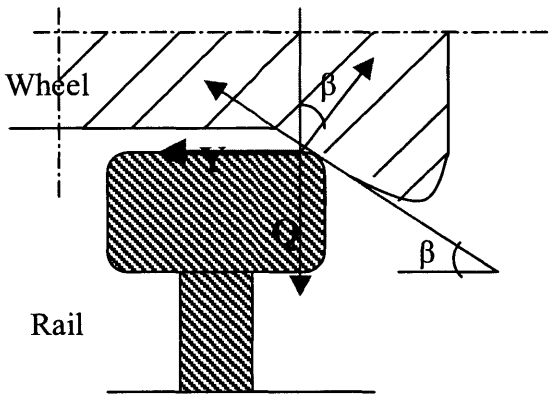

Figure 2-1 Lateral and vertical forces between wheel and rail

A conservative estimate of the region of safe operation is given by Nadal's formula:

$$\frac{Y}{Q} \leq \frac{\tan\beta - f}{1 + f\tan\beta} \tag{1}$$

where f is the wheel-rail friction coefficient and β the angle between wheel and rail; see Figure 2-1. A typical value for the coefficient of friction f is 0.3 (Fundamentals of rail vehicle dynamics: guidance and stability, 2003). The wheel-to-rail angle β takes

values between 60° and 80°. A coefficient of friction f =0.27 and a wheel-to-rail angle β=60° have been used in the past to determine that the Y/Q ratio should not exceed 1. Studies of various cases of derailment have shown that $\frac{Y}{Q} \leq 1.2 \text{ or } 1.3$ provides an adequate safety factor (Alias, 1982). However, it has been shown (Japanese National Railway -Yokose, Matsudaria) that the critical value of Y/Q may actually range from values of about 0.8 to over 2 due to changes in the angle of flange to rail attack and the duration of the occurrence. The Y/Q ratio can therefore reach values up to 2 without leaving the region of safe operation (Interaction between Train and Track, 1966). The criticality of a given ratio Y/Q depends also on the dynamic conditions and a ratio that may be a problem at high speeds may not be at lower speeds. There is nevertheless consensus that a ratio of 0.8 is a minimum for wheel climb to occur (Computer-aided Simulation in Railway Dynamics, 1988). Values in excess of twice to three times have been observed, but because of their short duration, wheel climbing did not occur. An accepted duration for the onset of wheel climbing is approximately 0.3second (Computer-aided Simulation in Railway Dynamics, 1988).

The requirements for acceptable riding quality demand that the vertical acceleration should not exceed 0.2g (Interaction between Train and Track, 1966) and that the ratio of the lateral-to-vertical accelerations does not exceed 0.75. For example, a vertical acceleration of 0.064g and a lateral acceleration of 0.048g are judged acceptable; whereas a lateral acceleration close to 0.3g is unacceptable. Table 2-1 shows the correspondence between ride quality and lateral and vertical acceleration (Interaction between Train and Track, 1966). The British Railways Ride Quality Index (Bahatti, 1984) ranks from 1 (very good ride quality) to 5 (dangerous); as reported in Dynamic of Railway Vehicle Systems (1984).

Ride Index	Ride Quality	Lateral acceleration	Vertical acceleration	Ratio Y/Q
3	satisfactory	0.048g	0.064g	0.75
4	Tolerable	0.120g	0.164g	0.73
5	Dangerous	0.265g	0.35g	0.76

Table 2-1 Safety values of lateral and vertical acceleration, British Railways Ride Quality index.

It is apparent that derailment is most likely to occur when a large lateral force occurs simultaneously with a reduced vertical load on wheel. Also in the case of a Y/Q ratio that does not exceed 0.8, a lateral acceleration of 0.3g is considered dangerous.

It is mentioned in Fundamentals of Rail Vehicle Dynamics (2003) and Railway Engineering (2000) that another mode of derailment is the track shifting laterally, when the lateral forces imposed by the vehicle are sufficient to shift the track laterally under high transverse loads. This form of derailment occurs mainly at high-speeds when the total transverse force H exceeds the transverse resistance L. Finally, the train may overturn due to loss of overall equilibrium (Railway Engineering, 2000). It was found (Amans, Sauvage, 1969) that in the worst case – with the center of mass 2.25m above the track and for standard-gauge track, a train overturns when the transverse acceleration reaches g/3: $A_{transverse} \geq g/3$.

Since the most frequent mode of derailment is by wheel climbing (see, for example, Interaction Between Vehicle and Track, 1966; Dynamics of Railway Vehicle Systems, 1984; Fundamentals of Rail Vehicle Dynamics, 2003), this is the mode of failure considered in our model of derailment.

Influence of Curves

One last factor to be mentioned is the effect of track curvature. From elementary physics, a vehicle running at speed V on a curve of radius R develops a centrifugal acceleration $\gamma = V^2/R$ and a centrifugal force $F = mV^2/R$. In order to reduce this unfavorable effect, transverse cants are used to offset the centrifugal forces. Transverse

cant almost compensates transversal accelerations generated by centrifugal forces. The maximum non-compensated transverse acceleration for a vehicle at 300km/h (worst case scenario, French TGV) is of $0.67 m/s^2$ (or 0.067g). The UIC (International Union of Railways) sets limiting values of cant and acceleration, and in general, tracks are laid for a maximum value of non-compensated centrifugal acceleration ranging between 0.5 and $1 m/s^2$. Therefore in a first approximation one may neglect the curvature of the track when estimating the probability of derailment.

From this brief review of train dynamic, we conclude that no comprehensive theoretical formula exists to assess train derailment probability under different levels of shaking. Most of the existing relations are semi-empirical and are the result of tests conducted by different railroads. Nevertheless, the following observations are made:

1. Derailment may have several causes; mainly track shifting, train overturning or wheel climbing. The limit most often used to predict train derailment is in terms of the ratio Y/Q of the lateral to vertical wheel forces.
2. An excessive transversal force is the main cause of train derailment. The vertical component of the acceleration is not considered and is usually disregarded in earthquake-induced derailment risk analysis.
3. The critical transversal acceleration for overturning may be as low as 0.3g in a worst case scenario. The British Railway Index indicates that a lateral acceleration above 0.3g is unacceptable.
4. Transverse cants effectively compensate the transversal accelerations generated by curvature. Hence as a first approximation, curvature and cant will be omitted from derailment analysis.
5. A static analysis that omits the dynamic loads caused by defects is considered adequate (Profillidis, 2000). Also in this study we ignore rail and track defects.

2.1.2 Derailment under Earthquake Conditions

This section derives the critical levels of shaking in terms of transversal track displacement and transversal track acceleration beyond which the train is expected to derail. Previous simulations of train derailment under vibratory motion are considered. Two variables appear as critical when dealing with train derailment: the peak transversal acceleration and the peak transversal displacement. Criteria for derailment in terms of these two quantities are presented, and applied to selected scenarios.

Simulations and tests have been conducted by the Safety Research Laboratory of the East Japanese Railroad Company (JR East) to determine the conditions under which earthquakes may induce derailment. The analysis includes two derailment modes. The first mode is derailment by vibratory motion whereas the second mode refers to derailment due to permanent deformation of the track at the end of the ground motion. Each evaluation starts with a given earthquake scenario, defined by magnitude M and distance to the source R, in addition to the natural period of the structure T_{st} (see Figure 2-2). Empirical attenuation relations are used to assess ground motion intensity at the site using Spectral Intensity. Spectral Intensity (SI) is obtained from the velocity spectra S_v:

$SI_{cm/s}(T_{st}) = \frac{1}{(b-a)} \int_a^b S_v(T, T_{st}) dT$ thus yielding SI in kine value (cm/sec). JR East also uses spectral intensity in units of displacement (mm). SI values expressed in mm rather than in cm/s are defined as: $SI_{mm}(T_{st}) = (b-a) * SI_{cm/s}(T_{st}) = \int_a^b S_v(T, T_{st}) dT$.

Semi-empirical fragility curves derived from dynamic simulations are used to assess the probability of derailment given the spectral intensity $SI_{cm/s}$ (T_{st}) at the site.

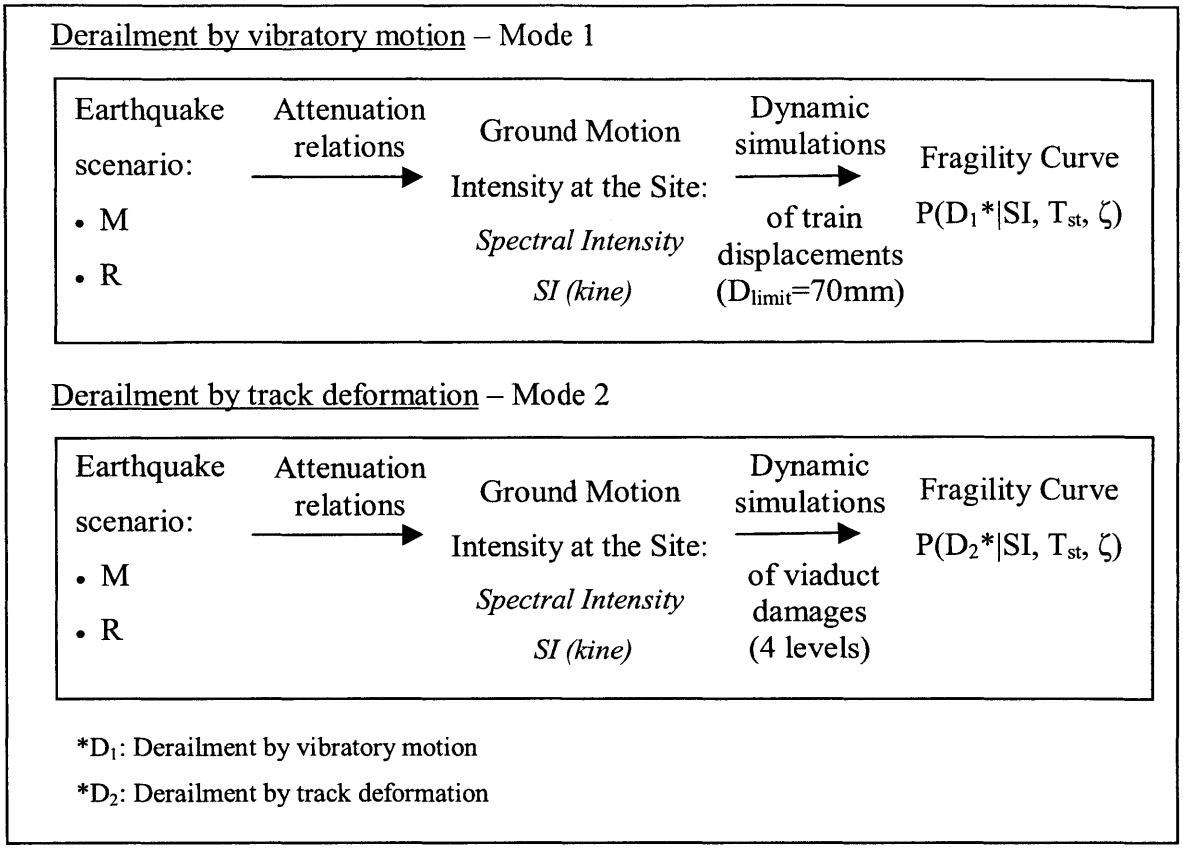

Figure 2-2 Derailments by vibration and derailments by track deformation – As evaluated by JR East Safety Research Laboratory

As observed in the previous literature review, the assessment of train safety is largely based on test results. However, in the case of seismic loads, testing is difficult. Therefore, JR East has developed methods to assess safety by computer simulation; see the dynamic train model in Figure 2-3. In addition, JR East has conducted experiments using a bogie test device where conditions can be easily changed. Results for the first mode of derailment (by vibration during the ground motion) are presented in this section. Results for the second mode (derailment by damaged tracks) will be presented in Section 3.2 where we consider inelastic behavior and track damage.

To assess the probability of derailment by vibratory motion, JR East conducted a series of numerical analyses. Using the dynamic model in Figure 2-3, they determined the limiting levels of shaking that the track can experience before triggering displacements between wheel and rail exceeding the derailment limit of 70mm.

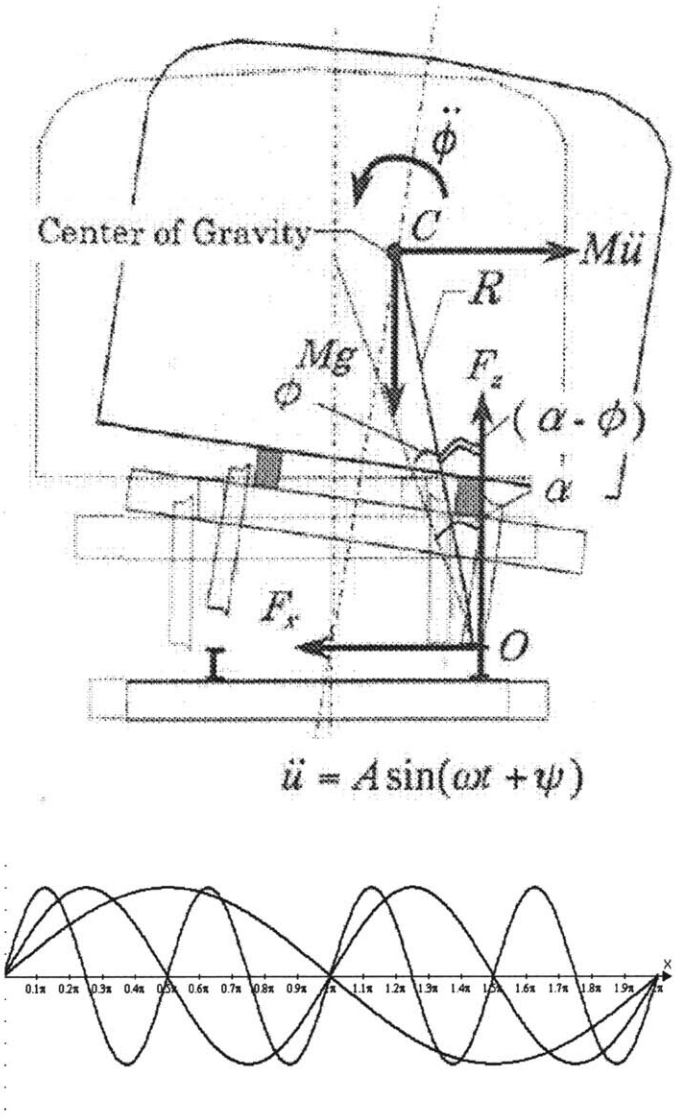

Figure 2-3 Train dynamic model - From JR East Manual

The conditions of the simulations are as follows (Shimamura and Yamamura, 2005):

1) The Shinkansen cars are subjected to earthquake-induced vibrations when they are running at constant speed over straight undistorted track;
2) The tracks are slab tracks with high rail supporting rigidity;
3) The input excitation is transversal to the track direction and is transmitted to the rail by a structure with given natural period. The range of natural periods considered is from 0.3 to 1.5s, with a damping of 5% for all structures.

4) Stability of the train depends on the relative horizontal displacement between wheels and rails, with a limiting value of 70mm.

The evaluation of the critical level of shaking and the variability of these quantities is done in two stages: First, the critical level of shaking that induces displacements between wheel and rail in excess of 70mm was evaluated by using the train dynamic model shown in Figure 2-3 with sinusoidal inputs modeling in approximation the vibratory motion generated by the earthquake. These first series of simulations yield deterministic values for the critical levels of shaking D_{limit} and A_{limit}. Second, the variability of these quantities was estimated by using actual recordings of earthquake ground motion as inputs to the train dynamic model.

From the sinusoidal inputs simulations, the amplitude D_{limit} of the sinusoidal motion yielding displacements between wheel and rail in excess of 70mm is evaluated as a function of the period of the vibration T_{st}. Figure 2-4 shows how D_{limit} depends on T_{st} for both Shinkansen and regular trains.

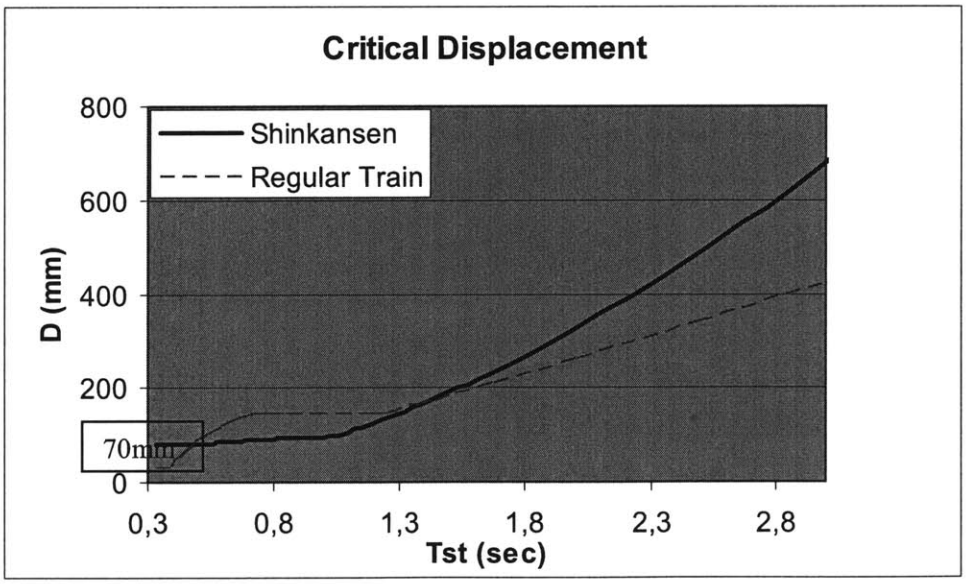

Figure 2-4 Relationship between critical amplitude D_{limit} and period of vibration T_{st} (JREast Dynamic Model)

In the case of Shinkansen trains, at periods smaller than about 1 second, D_{limit} is close to 70mm. For longer periods, D_{limit} increases in an approximately quadratic way with T_{st}.

Figure 2-5 shows the same results in terms of acceleration limit A_{limit}. Note that D_{limit} and A_{limit} are related as $A_{\text{limit}} = \omega_{st}^2 D_{\text{limit}}$ where $\omega_{st} = \frac{2\pi}{T_{st}}$ is the frequency of vibration. Interestingly, for Shinkansen trains, the critical acceleration for $T_{st} \geq 1\,\text{sec}$ is approximately constant and equal to 0.3g.

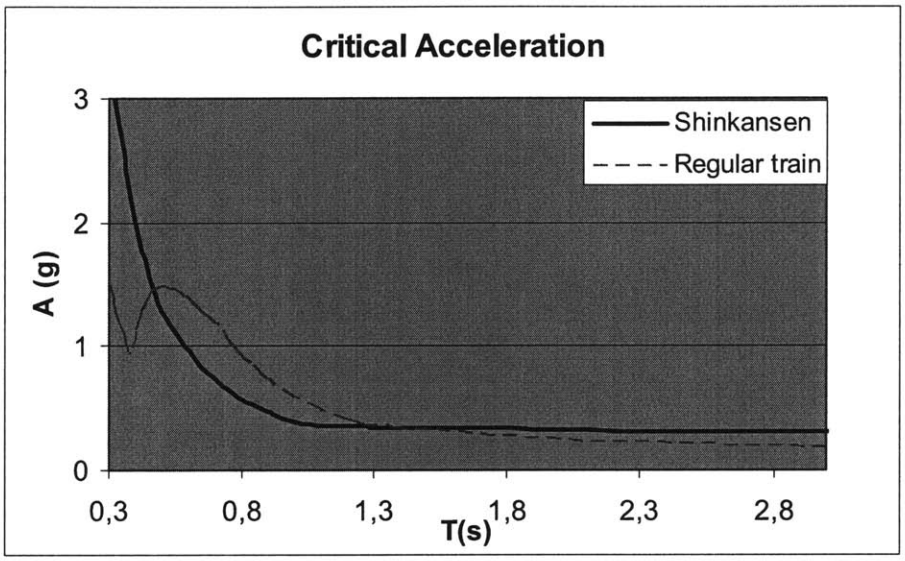

Figure 2-5 Relationship between critical acceleration A_{limit} and period of vibration T_{st} - derived from Figure 2-4 with $A_{\text{limit}} = \omega_{st}^2 D_{\text{limit}}$

The JR East simulations provide estimates of the critical amplitude D_{limit} and critical acceleration A_{limit} of the sinusoidal input yielding wheel-rail displacements in excess of 70mm, as a function of the period of vibration T_{st}.

As a rough analogy for the wheel sliding on the rail of a stationary train, one may consider the sliding block model of Newmark (1965). The results of this analysis are presented in Appendix I. The trends of A_{limit} derived by JR East are in general in good

agreement with those from the sliding block model. The sliding block model is nevertheless very conservative for periods of excitation lower than 1 second. Indeed, a train is more stable than a block sliding only in one direction; hence the higher levels of critical acceleration found by JR East.

To predict whether derailment occurs or not, we approximate the motion of the viaduct as sinusoidal with period T_{st}. The peak acceleration A equals the spectral acceleration $Sa(T_{st})$, and the peak displacement D equals the spectral absolute displacement $Sd(T_{st})$. At periods below 1 second, the displacement limits obtained by JR East are close to 70mm (Figure 2-4); whereas at periods above 1 second, the acceleration limits are close to 0.3g (Figure 2-5). These limits of 0.3g at T_{st}>1s and 70mm at T_{st}<1s are used in Figure 2-6 where the acceleration limits obtained by simulations are compared with the acceleration limits derived using the two aforementioned criteria. These criteria reproduce JR East's results very accurately for Shinkansen trains. For commuter trains, the agreement is not as good. One reason may be the functional forms used to approximate the displacement limits obtained by simulation of regular trains.

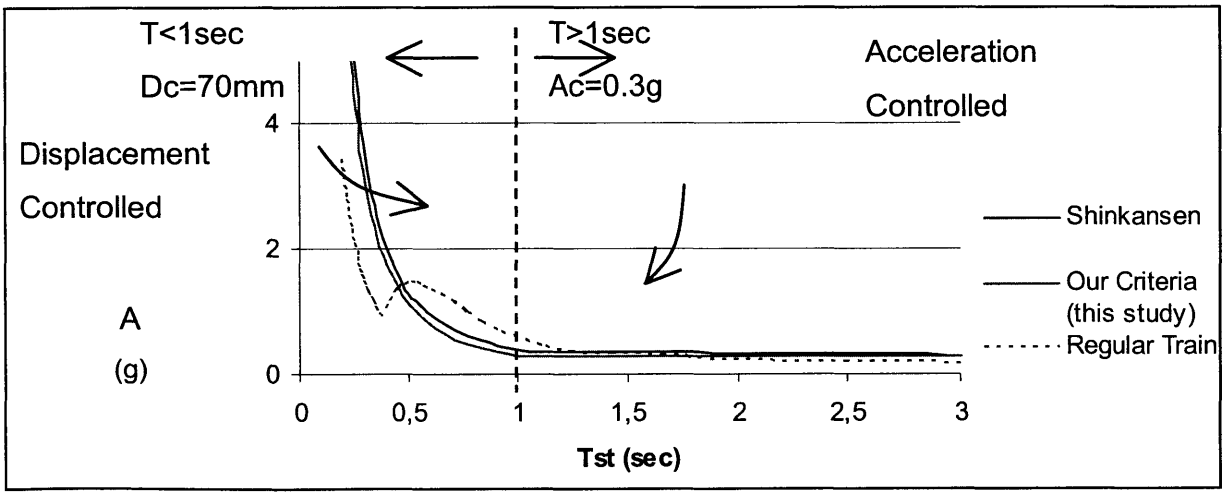

Figure 2-6 Composite model for the criteria for derailment'

Then, we assume that the train derails if:

$$\begin{cases} A_{abs} \geq 0.3g \\ \quad and \\ D_{abs} \geq 70mm \end{cases} \tag{2}$$

Note that the criterion for displacement is in terms of the absolute displacement D_{abs}, thus taking into account the contribution of the ground motion (PGD) and the displacement of the structure relatively to the ground (D_{rel}). Statistically, D_{abs} may be related to D_{rel} and PGD as follow:

$$D_{abs} = \sqrt{PGD^2 + D_{rel}^2} = \sqrt{PGD^2 + \frac{A_{abs}^2}{\omega_{st}^4}}.$$

Derailment occurs when both criteria in Equation (2) are met; see Figure 2-7. Derailment occurs in the shaded area.

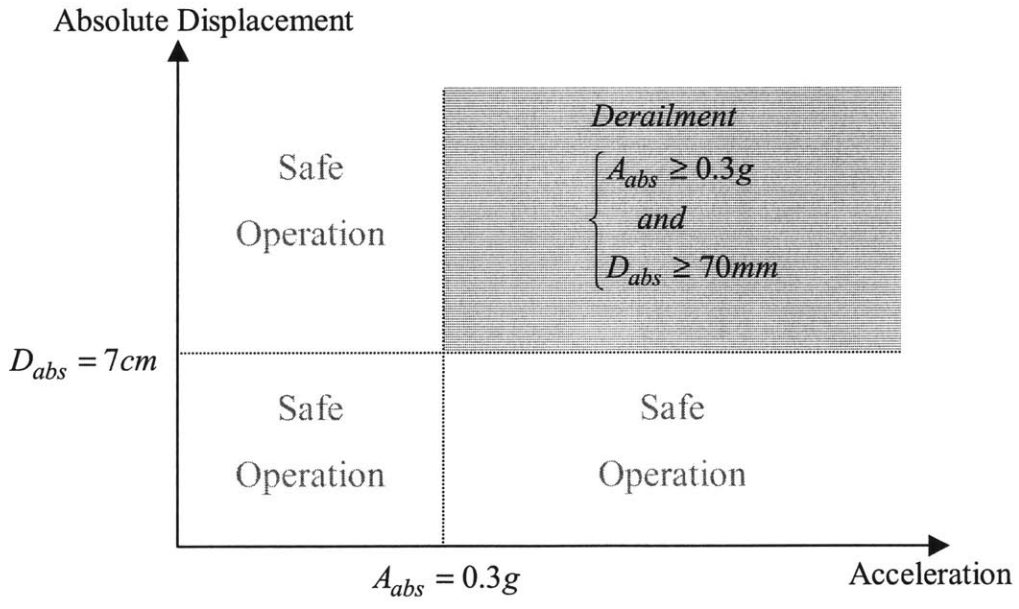

Figure 2-7 Criteria for derailment by vibratory motion

The derailment criteria should be expressed in probabilistic terms. Here, we consider sharp boundaries between the safe and unsafe regions. In reality, it is stochastic: There is a probability that the train derails in the safe region, and there is a probability that the train does not derail in the unsafe region. Nevertheless, if this type of uncertainty is small relative to the uncertainty on $\{(D,A)|M,R\}$, then assuming deterministic boundaries yields satisfactory results. The variability of D_{limit} and A_{limit} was estimated by JR East Research Laboratory, using actual recordings of earthquake ground motion as inputs to the train dynamic model. It was estimated that $0.2 \le \sigma_{\ln A_{limit}} \le 0.4$. The variability of the peak motion about the median value, based on the scatter of peak acceleration of individual recordings about the median empirical attenuation relationship, is typically larger: $\sigma_{\ln Sa_{|M,R}} \ge 0.60$ (Youngs et al., 1997). Thus, an analysis that considers only the uncertainty on $\{(D,A)|M,R\}$ is considered adequate.

To assess the probability of derailment, the natural logarithm of Sa and Sd are assumed to follow a normal distribution. Assuming that Sa and Sd are independent, the probability to exceed the criteria for derailment (Equation 2) is expressed as:

$$P[(Sa \ge 0.3g) \cap (Sd \ge 7cm)] = \Phi\left[-\frac{\ln 0.3g - m_{\ln Sa}}{\sigma_{\ln Sa}}\right] * \Phi\left[-\frac{\ln 7cm - m_{\ln Sd}}{\sigma_{\ln Sd}}\right] \qquad (3)$$

where Φ is the standard normal cumulative distribution function. The spectral acceleration $Sa(T_{st})$ equals the peak acceleration A and the spectral displacement $Sd(T_{st})$ equals the peak absolute displacement D. $\sigma_{\ln Sd}$ and $\sigma_{\ln Sa}$ are the standard deviations of $\ln(Sd)$ and $\ln(Sa)$ respectively.

The variability of the peak motion about the median value is based on the scatter of peak acceleration of individual recordings about the median empirical attenuation relationship.

Accelerations at a site resulting from earthquakes of a given magnitude and distance are commonly assumed to be lognormal distributed with standard deviation σ. For example, McGuire (1978), Joyner and Boore (1981), and Campbell (1981) confirmed evidence for a lognormal distribution of peak ground acceleration with corresponding value of σ between 0.37 and 0.62. Bender (1984) in a review of ground motion variability, concludes that the lognormal standard deviation σ appears to be somewhere in the range $0.35 < \sigma < 0.65$. More recently, Youngs (1997) presented a review of the state of the art in terms of ground motion variability. Youngs et al. (1988) had found that the scatter of peak acceleration data about the median attenuation relationship decreased with increasing magnitudes. Figure 2-8 presents the results of ground motion variability from Youngs et al. (1997). Abrahamson and Silva (1997) empirical response spectra relations present a similar model for the standard error. The results are presented in Figure 2-9.

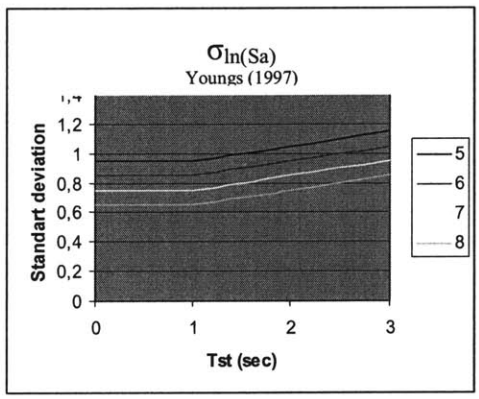

Figure 2-8 Standard deviation of ln(Sa), Youngs (1997)

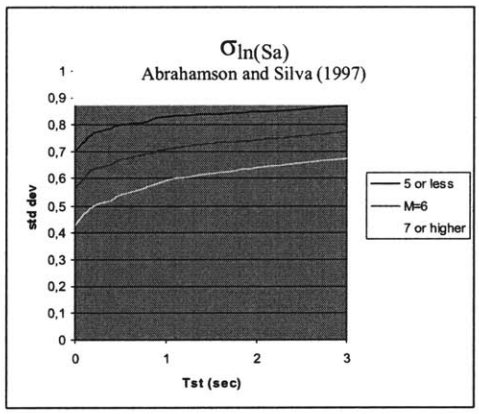

Figure 2-9 Standard deviation of ln(Sa), Abrahamson and Silva (1997)

Youngs (1997) and Abrahamson & Silva (1997) found standard deviations larger than previously reported. The standard deviation of the normal distribution, $\sigma_{\ln(Sa)}$, appears to be somewhere in the range $0.54 < \sigma < 1.05$. A lognormal standard deviation of 0.65 for Sa is used in our study as it reflects the larger standard deviations found more recently. The lognormal standard deviation of Sd is typically higher, and a value of 0.75 is used in this study.

Figure 2-10 shows probability of derailment given different expected peak accelerations *Sa* and expected peak absolute displacements *Sd*. The probabilities are evaluated according to equation (3), where *Sa* and *Sd* are assumed independent and follow lognormal distributions with corresponding standard deviations $\sigma_{\ln Sa} = 0.65$ and $\sigma_{\ln Sd} = 0.75$.

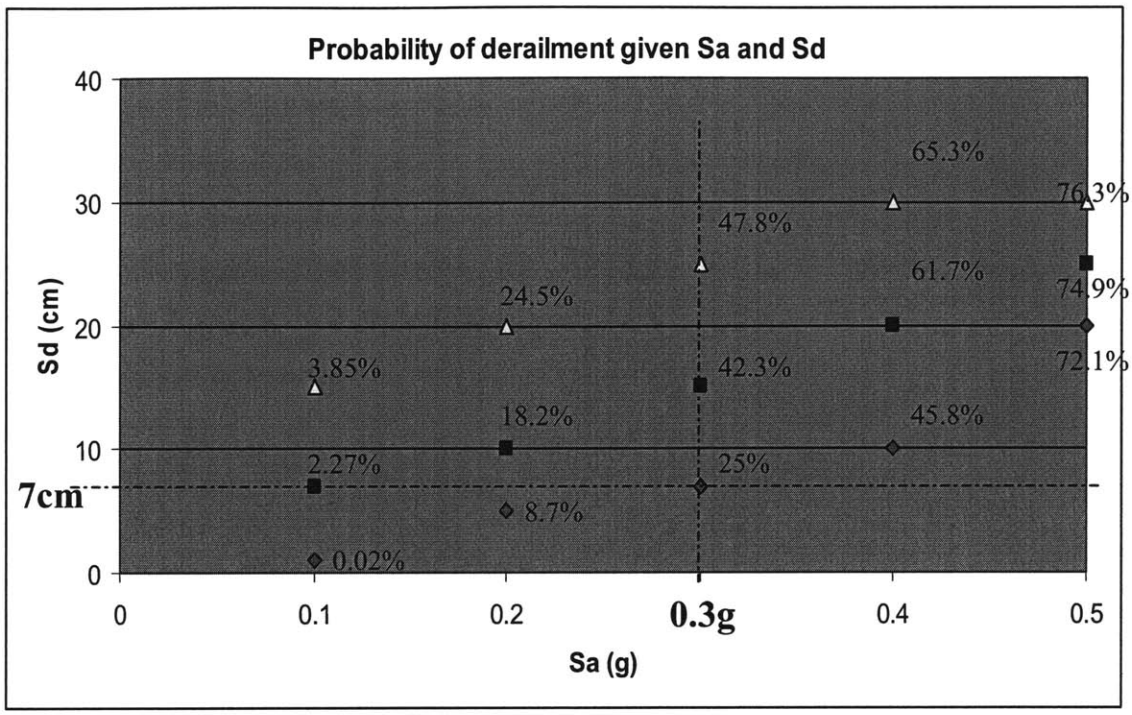

Figure 2-10 Probability of derailment given peak absolute acceleration Sa (g) and peak absolute displacement Sd (cm)

Table 2-2 shows typical values of peak ground acceleration (PGA) and corresponding peak ground displacement (PGD) for different Modified Mercalli Intensities in the Western United States (Trifunac and Brady, 1975). The last column shows the probability that the PGA exceeds 0.3g and the PGD exceeds 7cm. According to Table 2-2, scenarios where $Sa \leq 0.3g$ and $Sd \geq 7cm$ or $Sa \geq 0.3g$ and $Sd \leq 7cm$ have a low probability of occurrence.

M.M.Intensity	M	PGA (g)	PGD (cm)	P(PGA>0.3g and PGD>7cm)
III		0.013	1.25	0.000001%
IV	M<4.3	0.017	1.83	0.000016%
V	4.4<M<4.8	0.037	1.92	0.003%
VI	4.9<M<5.4	0.082	3.69	0.46%
VII	5.6<M<6.1	0.131	8.41	6.08%
VIII	6.2<M<6.5	0.167	8.58	11.11%
X	7<M<7.3	0.688	19.50	82.17%
		1.088	24.00	92.72%

Table 2-2 probability of derailment given PGA(g) and PGD(cm)

We have derived criteria for derailment in terms of peak acceleration Sa and peak absolute displacement Sd. In the next section, we relate the peak spectral acceleration Sa and the peak spectral displacement Sd to earthquake magnitude, epicentral distance, local site conditions, and structural period T_{st}.

2.1.3 Model for Displacement and Acceleration Response Spectra

This section presents methods to relate the level of shaking of the track to earthquake magnitude, epicentral distance, and local site conditions. The characterisation is in terms of spectral acceleration $Sa(\omega_{st})$ and spectral displacement $Sd(\omega_{st})$ where ω_{st} is the natural frequency of a single degree of freedom oscillator with 5% damping. In Section 2.1.2, criteria for derailment by vibratory motion have been expressed in terms of $Sa(\omega_{st})$ and $Sd(\omega_{st})$. There are several ways to obtain acceleration and displacement response spectra at given points along the track. One is to use recorded data and derive empirical attenuation relations by regression analysis (see, for example, the attenuation relationships derived by Abrahamson and Silva, 1997 or Youngs, Chiou, Silva and Humphrey, 1997). Although empirical spectral attenuation relations are commonly used to assess the response of a structure at a single point, to evaluate the differential motion at two points along the track in the case of horizontally heterogeneous soils and structures, one should follow a more engineering approach in which the dynamic properties of the soil and the structures are considered through appropriate transfer functions $H(\omega)$ (see, for example, the work of Monti & Pinto,1998; Shinozuka et al., 2000; or Sextos et al., 2003). For consistency, the same approach can be used for the motion at a single point. In what follows, the response spectra are derived from the acceleration power spectral density function, which accounts for the effects of source, path and local site conditions. Specifically, the acceleration power spectral density function of the track is expressed as:

$$S_A(\omega) = S_0 \left|H(\omega|M,R)\right|^2_{rock} \left|H(\omega|soil)\right|^2_{soil} \left|H(\omega|\omega_{st},\xi_{st})\right|^2_{structure} \qquad (4)$$

Where $\left|H(\omega|M,R)\right|^2_{rock}$ models the propagation of the seismic waves from the source to the site bedrock, $\left|H(\omega|soil)\right|^2_{soil}$ models the effect of local soil conditions, and $\left|H(\omega|\omega_{st})\right|^2_{structure}$ is the contribution from the response of the structure that supports the tracks. S_0 is a scale factor. Integration of $S_A(\omega)$ gives the variance of the track

acceleration from which the acceleration response spectra $Sa(\omega_{st})$ can be estimated. In essence, we are using the spectrum for ground motion acceleration compiled by Boore (2003) and others. Because we needed to model the soil effect continuously and with parameters related to the soil physical properties, we slightly modified the model to obtain a continuous representation of the local soil conditions. The soil response is therefore treated analytically by propagating the bedrock motion through a specified soil column, using an equivalent linear soil-response methodology. Response spectra for displacement are derived directly from the acceleration power spectral density function using the relation $S_D(\omega) = \frac{1}{\omega^4} S_A(\omega)$. Integration of $S_D(\omega)$ gives the variance of the track displacement from which the displacement response spectra $Sd(\omega_{st})$ can be estimated. Next, we discuss in greater detail the various terms in Equation (4).

1) The Spectrum of Ground Motion on Very Hard Rock $S_{rock} = S_0 |H|^2_{rock}$

Aki (1967) was one of the first seismologists to derive a theoretical source spectrum, referred to as the ω-squared model:

$$A(\omega|M) = \frac{1}{1 + \left(\omega / \omega_a(M)\right)^2} \tag{5}$$

The corner frequency $\omega_a = 2\pi f_a$ depends on magnitude M. Aki's work has been extensively used and refined by including path effects (attenuations with distance R and spreading) and site condition effects (amplifications). Boore (2003) presents a review of a general spectrum for ground motion that he and others have developed in the last few decades. It is a compilation of previous work on the subject, by Brune (1970), Hanks and McGuire (1981), Boore (1983), Atkinson (1984), Atkinson and Silva (1997, 2000) and others. This spectrum is presented below.

The Fourier spectrum of ground motion at a very hard rock site $H_{rock}(\omega|M,R)$ in Equation (4) and represented as:

$$H(\omega|M,R)_{rock} = CM_0\ A(\omega|M)\ D(\omega)\ P(\omega|R)\ \ I(\omega) \qquad (6)$$

is broken into contributions from earthquake source $CM_0\ A(\omega|M)\ D(\omega)$, path $P(\omega|R)$, and type of motion $I(\omega)$. The scale factor S_0 is included in the formulation of H_{rock}. H_{rock} is the Fourier spectrum of ground motion displacement if $I(\omega)=1$ and of ground motion acceleration for $I(\omega)=-\omega^2$.

C is a constant given by $C=\dfrac{R_e\ V_e\ F}{4\pi\ R_0\ \rho\ \beta^3}$, where R_e is the radiation pattern, usually averaged over a range of azimuths and take-off angles (Boore and Boatwright, 1984) and is estimated to be 0.55 on average for shear waves. V_e represents the partition of total shear wave energy into horizontal components $V_e = 1/\sqrt{2}$, F is the effect of free-surface amplification, taken as 2 in almost all applications, R_0 is a reference distance, usually set equal to 1 km; and ρ and β are the density and shear wave velocity respectively. M is the moment magnitude, related to the seismic moment M_0 through: $M=\frac{2}{3}\log(M_0)-10.7$. Atkinson and Silva (2000) use the following parameter values:

$$\begin{cases} R_e : radiation\ patern = .55 \\ V_e = 1/\sqrt{2} \\ F = 2 \\ \rho = 2.8 gm/cc = 2.8.10^6\ gm/m^3 \\ \beta = 3.2 km/s \end{cases}$$

The shape and amplitude of the source spectrum $A(\omega|M)$ depends on the magnitude of the earthquake. Although the most popular form of the source spectrum is the ω-squared model (see Equation 5), also referred to as the single-corner Brune model (Brune, 1970), other models have been developed. Among others is the 2-corner frequency model:

$$A(\omega|M) = \frac{1-\varepsilon}{1+\left(\omega/\omega_a\right)^2} + \frac{\varepsilon}{1+\left(\omega/\omega_b\right)^2} \tag{7}$$

used, for example by Atkinson and Silva (2000). The corner frequencies $f_a = \omega_a/2\pi$ and $f_b = \omega_b/2\pi$ depend on magnitude M. The lower corner frequency f_a is determined by the source duration $T_0 = 1/2f_a$ (Boatwright and Choy, 1992). From empirical data, Atkinson (1993) founds $\log(f_a) = 2.181 - 0.496M$. The higher corner frequency f_b is the frequency at which the spectrum attains half of the high frequency amplitude level. It has been found that $\log(f_b) = 2.41 - 0.408M$ (e.g., Atkinson and Silva, 2000). The constant ε in Equation (7) is a weighting parameter taking values between 0 and 1. For $\varepsilon = 1$, the 2-corner model is equivalent to the ω^2 model (Equation 5). Atkinson and Silva (2000) are using $\log(\varepsilon) = 0.605 - 0.255M$. $A(\omega|M)$, as presented above in Equation 5 or 7, is the Fourier spectrum of source displacement. It has to be multiplied by ω^2 to obtain the acceleration source spectrum shown below. The 2-corner frequency model source spectrum for acceleration is presented in Figure 2-11 for 3 magnitudes. It is the spectrum used in our model.

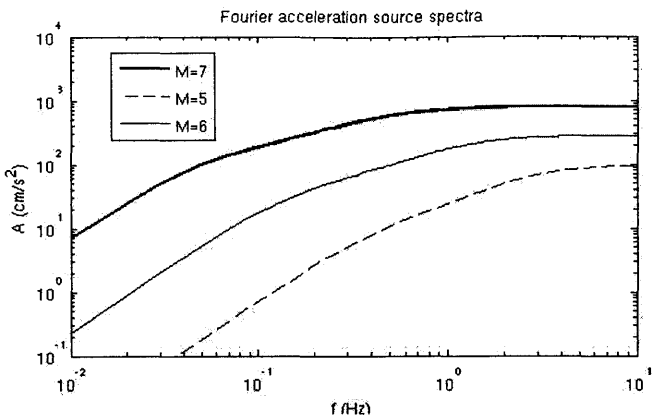

Figure 2-11 Source spectrum for acceleration, 2-corner frequency model

The decrease of the motion at high-frequency is modelled through the kappa operator $D(\omega) = \exp\left[-\frac{\omega k}{2}\right]$ where k is the diminution parameter. The attenuation operator $D(\omega)$ accounts for loss of high-frequency in the ground motion independent of the path. This loss is considered as a source effect by Papageorgiou and Aki (1983), a site effect by Hanks (1982) and Boore (2003) suggests a combination of these effects as plausible. From comparison with data, Boore and Joyner (1997) suggest that a value of k near 0.04 is appropriate for California. The diminution parameter in the Atkinson and Silva study (2000) is of 0.03, and Boore (2003) suggests that values between 0.02 and 0.04 are appropriate. In our model, we use $k = 0.035$ as in Boore & Joyner (1997). This value is close to the average reported by Anderson & Hough (1984), Boore *et al.* (1992), Atkinson & Silva (1997) and Boore & Joyner (1997). The diminution factor is plotted in Figure 2-12 for $k = 0.02$, 0.03 and 0.04.

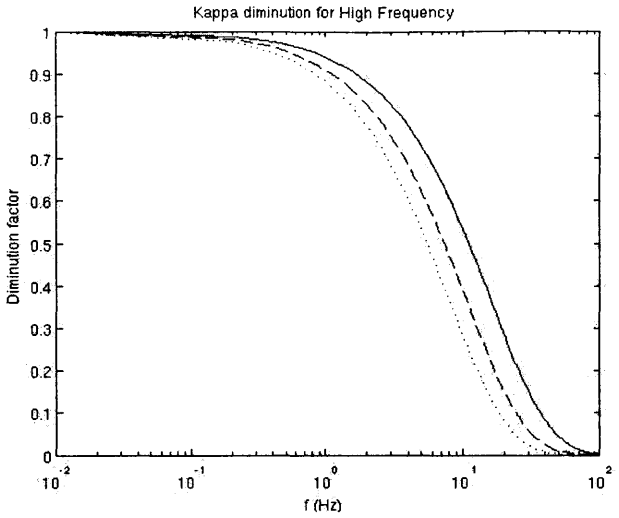

Figure 2-12 Kappa diminution factors at high frequency for k=0.02, 0.03 and0.04.

Figure 2-13 presents the 2-corner frequency source spectrum for acceleration for M = 5 and 7. The roll-off at high frequency is a result of the kappa factor with $k = 0.035$.

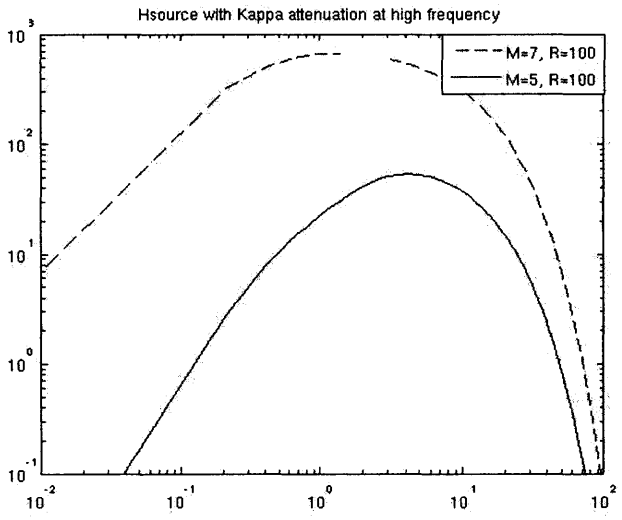

Figure 2-13 Source spectrum for acceleration, 2-corner frequency model with kappa $k = 0.035$

The second component of the ground motion spectrum in Equation (6) is the propagation and attenuation from the source to the site, denoted $P(\omega|R)$. This term is generally expressed as the product of two factors, $P(\omega|R) = G(R) * Q(\omega|R)$ (Boore, 2003). The geometric spreading, modeling the attenuation with distance relative to the

source $G(R)$, and the anelastic attenuation $Q(\omega|R)$, may be taken as (Raoof *et al.*, 1999):

$$G(R)=\begin{cases}\dfrac{1}{R} & R<40km\\ \dfrac{1}{40}\sqrt{\dfrac{40}{R}} & R>40km\end{cases} \tag{8}$$

and

$$Q(\omega|R)=\exp\left[\frac{-\omega R}{2*180\left(\omega/2\pi\right)^{0.45}\beta}\right] \tag{9}$$

where R is the distance to the source $R=\sqrt{d^2+h^2}$ with d the closest distance to the fault plane, and h the source depth; β is the shear wave velocity ($\beta=3.2km/s$).The functional forms and parameters in Equations (8) and (9) were obtained by fitting empirical data (Raoof *et al.*, 1999; Atkinson and Silva, 2000).

Figure 2-14 shows the attenuation with distance relative to the source (Equation 8).

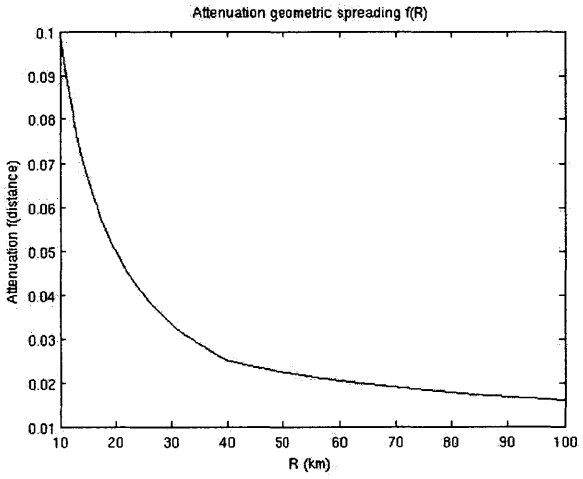

Figure 2-14 Geometric spreading as a function of distance to source

Figure 2-15 shows the anelastic attenuation in frequency content, Equation (9), for two distances R=50 and 100km.

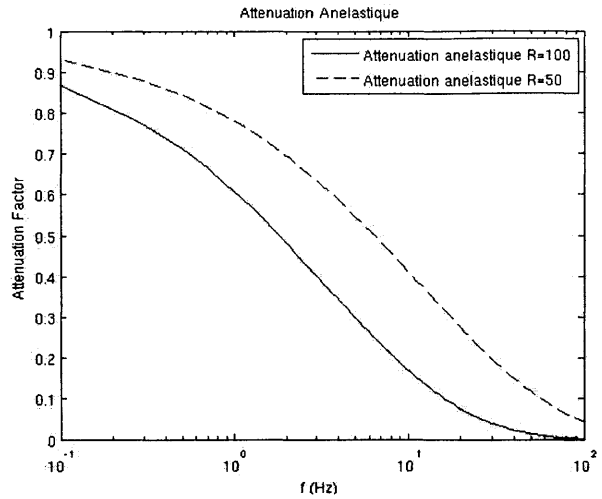

Figure 2-15 Anelastic attenuation in frequency content

For very hard bedrock sites ($\beta = 3.2km/s$) the spectrum is completely described by the source spectrum modified by the earlier two processes (kappa and attenuation). For softer soil conditions, we must also consider site amplifications through the soil column.

2) Soil transfer functions $|H(\omega|soil)|^2_{soil}$

As it propagates from the source region where the shear wave velocity is 3.2km/s, toward the surface where the shear wave velocity decreases, the bedrock spectrum is amplified. In Boore (2003), this phenomenon is modelled through frequency-dependent crustal amplification factors that depends on the shear wave velocity at the site, such as those of Boore and Joyner (1997) plotted in Figure 2-16-a. The reference soil – amplification of 1 – is very hard rock (shear wave velocity above 3km/s). Figure 2-16-b shows the amplifications factors combined with the loss of high-frequency (kappa operator with k=0.035).

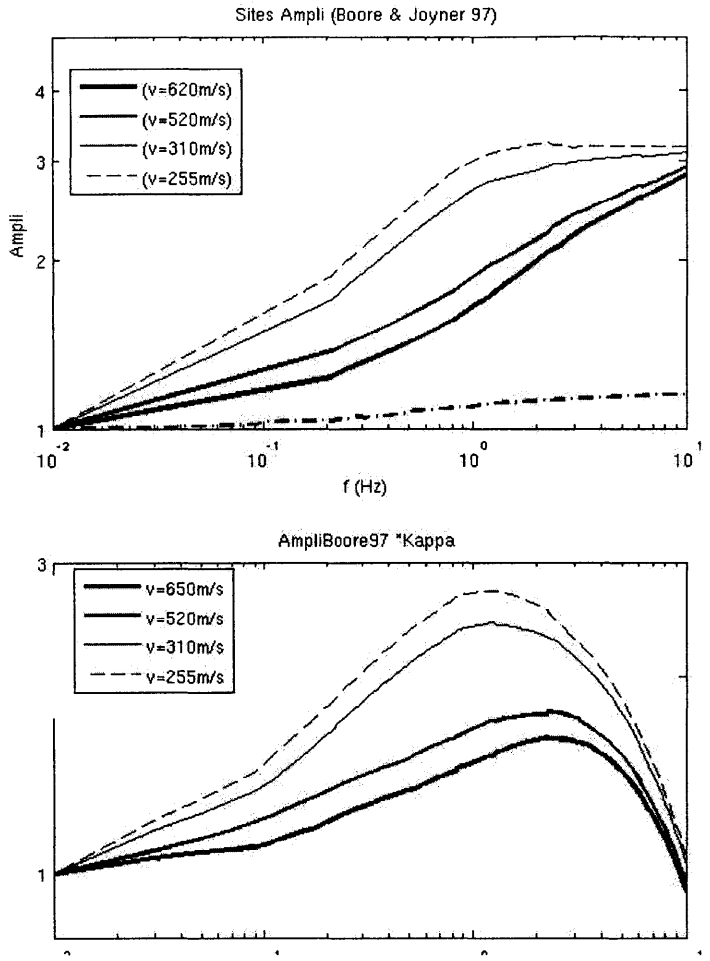

Figure 2-16 Crustal amplifications factors, from Boore and Joyner, 1997

The amplification factors in Figure 2-16 have been obtained by simulations (see Boore & Joyner, 1997). No analytical forms are available.

The total Fourier spectrum for acceleration is plotted below, for an earthquake of magnitude 7 and distance to the epicentre of 100km. The different plots correspond to different site conditions $v_{s_{30}} = 620, 520, 310 \; and \; 255 \; m/s$, as defined by the Boore and Joyner amplification factors.

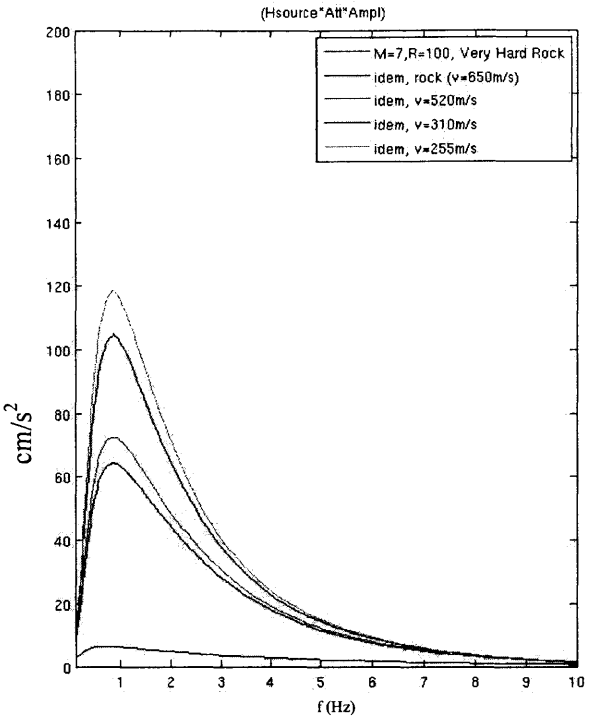

Figure 2-17 Total Fourier spectrum (source, attenuations and amplifications) for different soil conditions (v=650m/s to 255m/s)

The dynamic response of a single-degree-of-freedom system is characterized by the transfer function:

$$\left|H(\omega|\omega_{st},\xi_{st})\right|^2_{structure} = \frac{1+4\xi_{st}^2(\omega/\omega_{st})^2}{\left(1-(\omega/\omega_{st})^2\right)^2+4\xi_{st}^2(\omega/\omega_{st})^2}$$

Where $H(\omega|\omega_{st},\xi_{st})_{structure}$ is the complex function $\frac{1+2i\xi_{st}(\omega/\omega_{st})}{1-(\omega/\omega_{st})^2+2i\xi_{st}(\omega/\omega_{st})}$, ω_{st} is the natural frequency of the SDOF system considered, and ξ_{st} the fraction of damping (ξ_{st}=5%).

The mean power spectral density of structural acceleration is obtained as:

$$S_A(\omega|M,R,soil,\omega_{st},\xi_{st}) = \left|H(\omega|M,R)\right|^2_{rock}\left|H(\omega|soil)\right|^2_{soil}\left|H(\omega|\omega_{st},\xi_{st})\right|^2_{structure}$$

with $I(\omega)=-\omega^2$. The soil conditions are accounted for through the Boore and Joyner (1997) amplification factors. Although they do not offer a continuous modelling of soil conditions, they propose 4 different conditions.

Acceleration response spectra Sa can be derived using random vibration theory, assuming a stationary process of finite duration. We use the following relation between the peak motion Sa and the standard deviation of the process $\sigma_{A_{track}}$:

$$Sa(\omega_{st}) = c(\omega_{st}) * \sqrt{\sigma^2_{A_{track}}}$$

where

$$\sigma^2_{A_{track}}(\omega_{st}) = \int_{-\infty}^{+\infty} S_A(\omega) d\omega = \int_{-\infty}^{+\infty} \left|H(\omega|M,R)\right|^2_{rock} \left|H(\omega|soil)\right|^2_{soil} \left|H(\omega|\omega_{st},\xi_{st})\right|^2_{structure} d\omega$$

and $c(\omega_{st})$ is the peak-to-standard deviation ratio. This ratio has been variously estimated, usually starting from the classic result of Rice (1954) for the mean upcrossing rate of a stationary random process. For example, Vanmarcke (1977) has suggested:

$$c(\Omega) = \sqrt{2\ln(2.8 * \frac{\Omega}{2\pi} * t_p)} \qquad (10)$$

with Ω^2 the ratio of the variance of the derivative of the process to the variance of the process and t_p the duration of the process. Vanmarcke's equation (Equation 10) is used, for example, by Monti, Nuti & Pinto (1996) to derive peak ground motion for soils with different natural periods. As a first approximation, Ω can be set equal to the natural frequency of the system. This gives $c(\omega_{st}) = \sqrt{2\ln(2.8 * \frac{\omega_{st}}{2\pi} * T_{gm})}$ where ω_{st} is the natural frequency of the structure and T_{gm} the duration of the ground motion.

Acceleration response spectra for selected (M, R) are presented below. Three earthquake scenarios, one of magnitude M = 7 and epicentral distance R=100km, and two of magnitude M= 6, with R = 50 or 100km. For each scenario, 7 response spectra

are plotted. Five response spectra are obtained from the Boore formulation, and are plotted with simple lines. The lower one is for bedrock (source spectrum with kappa and propagation attenuation, but without site amplification: i.e., $v_{s_{30}} = 3.5\ km/s$ and $H(\omega|soil)_{soil} = 1$). The 4 remaining plots assume different soil conditions with $v_{s_{30}} = 620, 520, 310\ and\ 255\ m/s$ and $H(\omega|soil)_{soil}$ the corresponding amplification factor of Boore and Joyner (1997). For comparison, two empirical attenuation relations are plotted as dotted lines (Youngs, 1997, empirical attenuation relations). These are denoted by 'Rock' and 'Soil'. By comparing the amplification from 'Rock' to 'Soil' in the empirical relation and their own site factors, Boore and Joyner (1997) recommend to compare 'Rock' with with $v_{s_{30}}$ equals 620m/s and 'Soil' with $v_{s_{30}}$ equals to 310m/s .

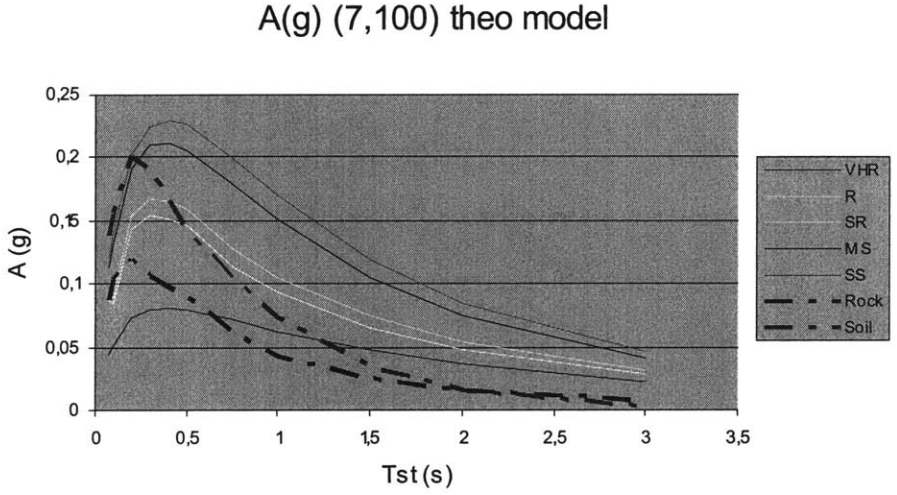

Figure 2-18 Acceleration response spectra, Boore model for M=7, R=100

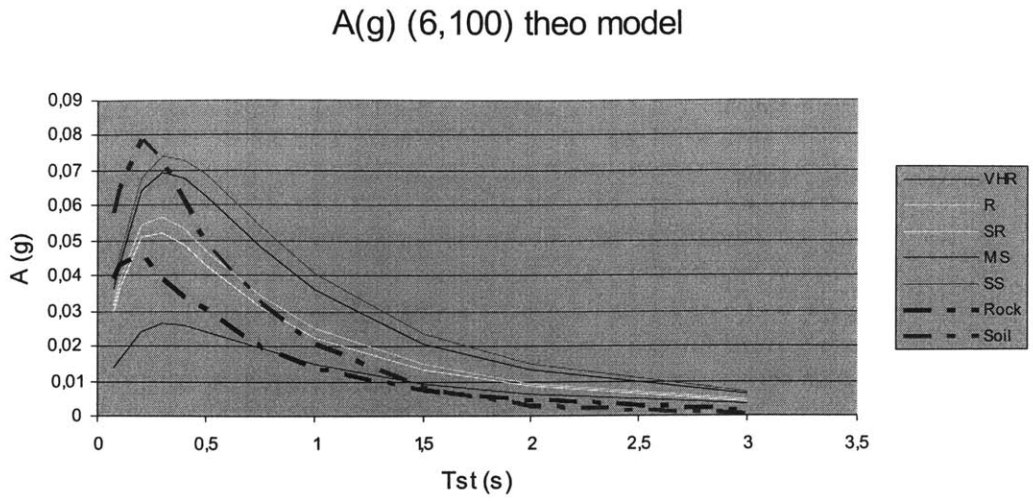

Figure 2-19 Acceleration response spectra, Boore model for M=6, R=100

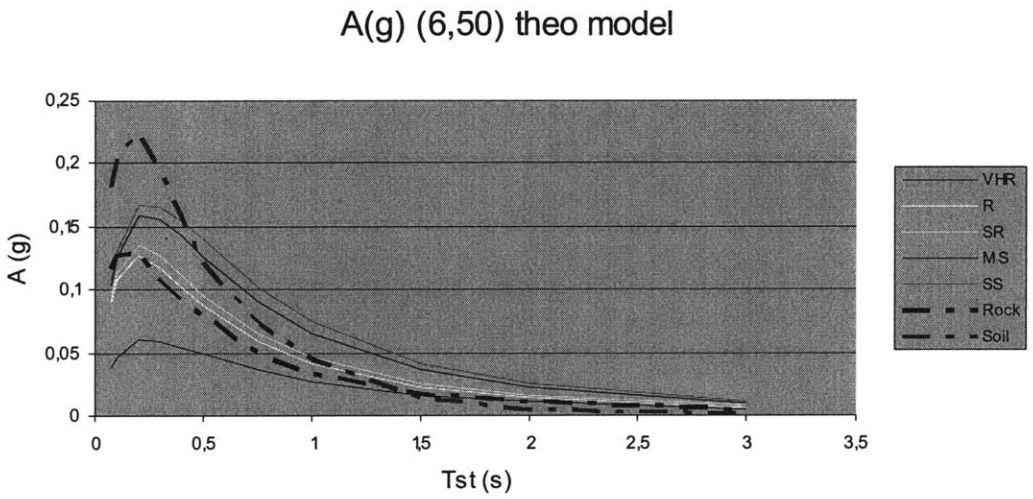

Figure 2-20 Acceleration response spectra, Boore model for M=6, R=50

In the short periods range, the shape of the theoretical spectra is close to the empirical ones, whereas in the long period range, the theoretical spectra overpredict the motion. This phenomenon is also reported in Atkinson & Silva (2000). Boore (2003) suggests a method to overcome this problem. We shall implement his method later when computing response spectra that include the continuous soil transfer function.

One of the main shortcomings of the Boore model is that the local soil conditions are treated empirically with amplification factors that are derived for a limited numbers of soil conditions (soils with average shear-wave velocity in the upper 30m of 620m/s,

520m/s, 310m/s and 255m/s). The section below proposes a model with a continuous representation of the local soil conditions.

Continuous model of the local soil conditions

The soil response can be treated analytically by propagating the rock motion through a specified soil column. Considerations of the filtering effect of a soil column through linear one-dimensional soil transfer functions $|H(\omega|soil)|^2_{soil}$ provide a tool to obtain a continuous model of the local soil conditions. Two models have been considered, the modified Kanai-Tajimi spectrum, presented in Appendix II and which considers only the first mode of vibration of the soil layer; and a linear one-dimensional soil transfer function which includes also the higher modes. The latter, combined with the spectrum for ground motion derived earlier, provides an attractive framework to include soil conditions. This second method is presented below and integrated into the spectrum of ground motion afterward.

The transfer functions are denoted H and verify

$$Sa_{soil} = |H(\omega)|^2 Sa_{rock}$$

where Sa_{rock} is the spectrum of ground motion at bedrock, e.g. as derived by Boore (2003).

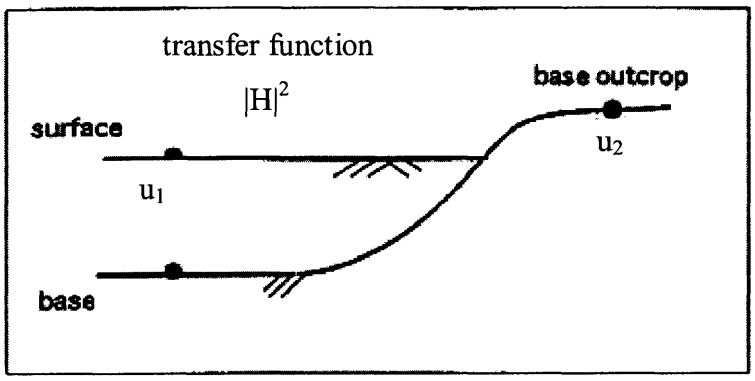

Figure 2-21 Transfer function for soil, adapted from Yamazaki

The most widely used technique for the study of one-dimensional amplification of vertically propagating seismic waves involves solution in the frequency domain of the

dynamic equations for linearly visco-elastic material. The soil is idealized as a horizontal layer overlaying rock with parameters as shown in Figure 2-22. The incident waves are assumed to be plane waves propagating in a known direction through the rock. The analytical solution to this soil amplification problem was given by Thomson (1950).

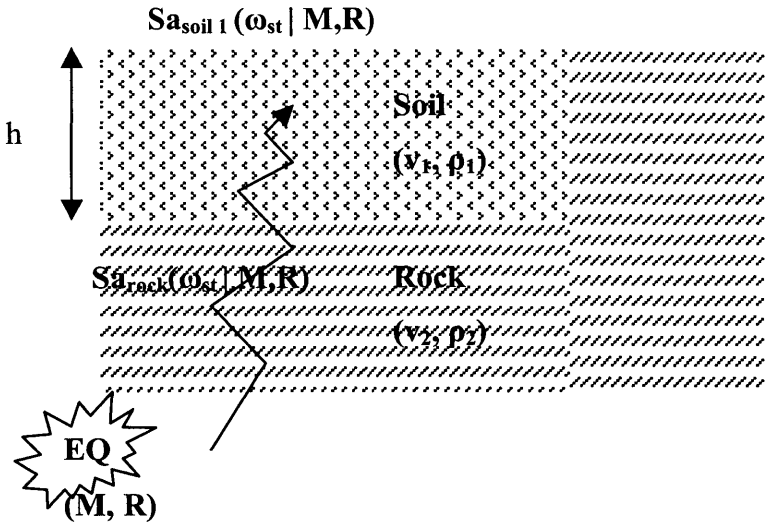

Figure 2-22 Parameters of the transfer function for soil

The transfer function of a soil layer of depth h , mass density ρ_1 and and shear-wave velocity v_1 is (Kausel, personal communication):

$$\left|H(\omega|h,k)\right|^2_{soil} = \frac{k^2}{\left|ik\cos(\theta(1-i\xi))-\sin(\theta(1-i\xi))\right|^2} \qquad (11)$$

where $\theta = \frac{\omega h}{v_1}$ and $k = \frac{\rho_2 v_2}{\rho_1 v_1}$ is the impedance contrast between rock (subscript 2) and soil (subscript 1). As k increases, the soil becomes softer (see Table 2-3). In Equation (11), ξ is the fraction of damping, we assume a linear hysteretic damping, independent of frequency. Material damping is normally a function of amplitude.

Plots of the transfer function for soil (Equation 11) are shown in Figure 2-23. It can be seen that the amplitude decreases for increasing values of f. Also, the amplification

increases with increasing k: soft soils amplify the ground motions. Conversely, for smaller values of k the amplification decreases.

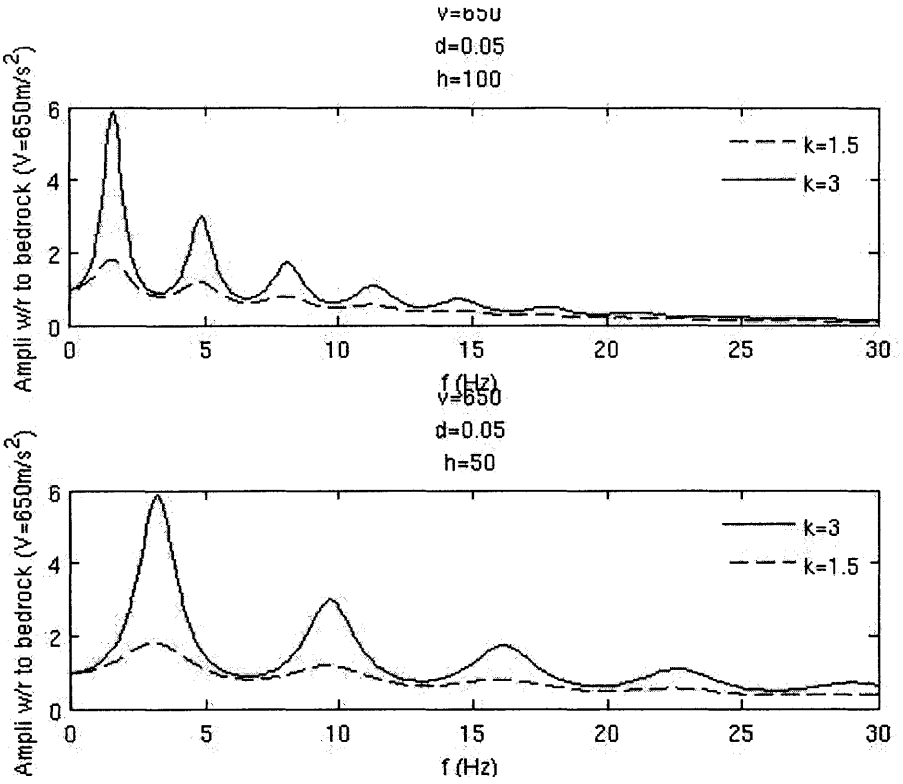

Figure 2-23 Amplification functions for soil: amplitude of motion at free surface, for different values of depth h, and different impedance contrast k.

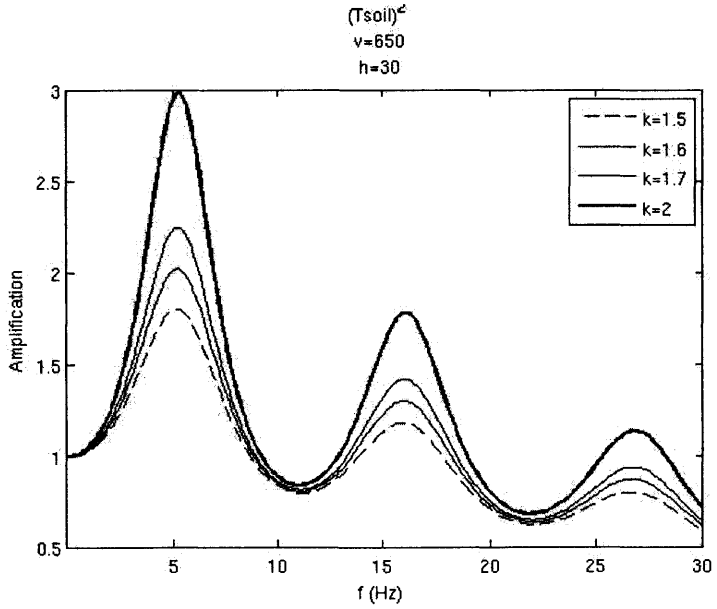

Figure 2-24 Amplification Functions: amplitude of motion at free surface

Table 2-3 provides ranges for k. Typically, k would range between 1 and 5 with respect to bedrock.

Soil	Wave Velocity (m/s)	Unit Weight (kg/m^3)	k (w/r to rock)
Very soft	220	1,600	4
	280	1,920	2.7
medium	370	2,000	1.9
	400	2,000	1.8
	450	2,160	1.5
Bedrock	650	2,200	1
Hard Rock	2440	2,400	

Table 2-3 Soil properties and typical values commonly used, adapted from Kausel and Roesset, 1984.

Derivation of our Engineering Model

Here we combine the Boore approach with an analytical transfer function for soil. The mean power spectral density of structural acceleration is therefore obtained as:

$$S_A(\omega) = \left|H(\omega|M,R,rock)\right|^2_{rock\ with\ v_{s30}=620m/s} \left|H(\omega|h,k)\right|^2_{soil} \left|H(\omega|\omega_{st},\xi_{st})\right|^2_{structure} \quad (12)$$

where the three terms in the right hand side (rhs) are as follows.

The first term is the mean power spectral density of ground acceleration at a rock site characterized by a shear wave velocity in the upper 30m of 620m/s:

$$\left|H(\omega|M,R,rock)\right|^2_{rock\ with\ v_{s30}=620m/s} = \left|CM_0\ A(\omega|M)\ D(\omega)\ P(\omega|R)\ V(\omega|rock)\ I(\omega)\right|^2 \quad (13)$$

The various terms on the rhs of Equation (13) were discussed in the previous section, and the amplification factors $V(\omega|rock)$ are for 'rock' (Boore and Joyner Amplification factor, 1997), with an average shear-wave velocity in the upper 30m of 620m/s. This is the value used by Atkinson and Silva (2000) to derive peak motion at rock sites. Thus, for rock sites with v=620m/s, the spectrum coincides with the Boore model.

The second term in Equation (12), $|H(\omega|h,k)|^2_{soil} = \frac{k^2}{|ik\cos(\theta(1-i\xi))-\sin(\theta(1-i\xi))|^2}$, is the transfer function for soil. Note that ρ_2, v_2 being the mass density and the shear wave velocity of the underlying bedrock, v_2 is therefore set equal to 620m/s to be consistent with the parameters used in the power spectral density of ground acceleration at a rock site (Equation 13). The soil layer above the rock takes different values depending on the soil condition to be modelled. The different soil conditions are parameterized by the couple (h,k) where h is depth of the soil layer, and k the coefficient of softness (e.g., k=1 rock; k=3 softer soil). Note that as it is currently set up, the shear wave velocity of the soil column above the bedrock must be less or equal to 620m/s.

The third term in Equation (12) is the response of the structure:

$$|H(\omega|\omega_{st},\xi_{st})|^2_{structure} = \frac{1+4\xi^2_{structure}(\omega/\omega_{structure})^2}{\left(1-(\omega/\omega_{structure})^2\right)^2+4\xi^2_{structure}(\omega/\omega_{structure})^2}$$

Using the mean power spectral density function of structural acceleration $S_A(\omega)$ (Equation 12), the acceleration response spectrum Sa is derived using random vibration theory, as mentioned earlier. However, Boore (2003) includes improvements in the random vibration results for earthquake ground motion, improvements that were not implemented in earlier versions of the theoretical attenuation approach. Those improvements are presented next, followed by the resulting acceleration response spectra.

The relation between the peak acceleration Sa and the standard deviation of the process $\sigma_{A_{track}}$, $Sa(\omega_{st}) = c(\omega_{st}) * \sqrt{\sigma^2_{A_{track}}}$ requires the variance of the process $\sigma^2_{A_{track}}$ and the peak-to-standard deviation ratio $c(\omega_{st})$. Random-vibration results provides an estimate of the ratio $c(\omega_{st})$ as mentioned earlier; and Parseval's theorem gives the variance as the integral of $S_A(\omega)$.

Boore (2003) notes that the random vibration results may not be appropriate for application to earthquake motion because seismic waves from earthquakes are inherently non-stationary. Also, one must consider that the response of resonant systems – local soils and mechanical oscillators – has significant correlation between adjacent peaks. Both characteristics violate basic assumptions of standard random vibration formulas. Boore suggests simple refinements when the oscillator period is longer than the duration of ground motion and for lightly damped oscillators, for which the response continues well past the ground motion excitation. This last phenomenon is thought to be responsible for the low-frequency discrepancy in Figure 2-18 and Figure 2-19 between empirical response spectra and theoretical results.

The durations to use in determining the two quantities of interest (peak-to-standard deviation ratio, and variance of the process) are modified. Boore and Joyner (1984) found that good results could be obtained if two durations were used:

- One duration, corresponding to the duration of the process i.e., the duration of ground motion, $T_{gm} = T_0(M) + T_{path}(R)$, for the evaluation of the ratio $c(\omega_{st}) = \sqrt{2\ln(2.8 * \frac{\omega_{st}}{2\pi} * T_{gm})}$
- And another one, longer, T_{rms} for the computation of the variance $\sigma^2_{A_{track}} = \frac{2}{T_{rms}} \int_0^\infty |H(\omega)|^2 d\omega$

The total duration of ground motion, T_{gm}, is the sum of 2 components: a source duration, T_0 and a path duration T_{path}. The source duration increases with magnitude and the path duration increases with distance, due to scattering and dispersion (Raoof *et al.*). A simple model that includes these dependencies is:

$$T_{gm} = T_0(M) + T_{path}(R) = T_0 + 0.05R \tag{14}$$

where $T_0 = \frac{1}{2 f_a(M)}$ is the source duration (Boatwright and Choy (1992)). f_a is the first corner frequency of the 2-corner frequency source spectra model and depends on earthquake magnitude. From data on source duration, Atkinson, 1993 found

that $\log(f_a) = 2.181 - 0.496M$. $T_{path}(R) = 0.05R$ is the path duration function used by Atkinson and Silva (2000) in simulation of ground motion. The distance R is in kilometer to obtain duration in second.

From considerations of oscillator response and numerical experiments with time-domain simulations, Boore and Joyner (1984) proposed the following equation for the time T_{rms} to be used in the computation of the variance:

$$T_{rms} = T_{gm} + T_r \left(\frac{\left(T_{gm} / T_r \right)^n}{\left(T_{gm} / T_r \right)^n + \alpha} \right) \tag{15}$$

where the equivalent stationary duration of the oscillator response is given by

$$T_r = \frac{1}{2\pi f_{st} \zeta}$$

From numerical experimentation, Boore and Joyner (1984) found that n=3 and α=1/3. More recently, Liu and Pezeshk (1999) proposed a more complex form for α. Comparisons between the Boore & Joyner (1984) and the Liu & Pezeshk (1999) modifications of random-vibration results for oscillator response show that the two methods are in good agreement (see Boore, 2003). Here, we use the earlier and simpler form α=1/3.

The durations above have been used to derive the acceleration response spectra *Sa* in Figure 2-25 to 2-31. Additional acceleration response spectra for different magnitudes, distances and soil conditions can be found in Appendix III.

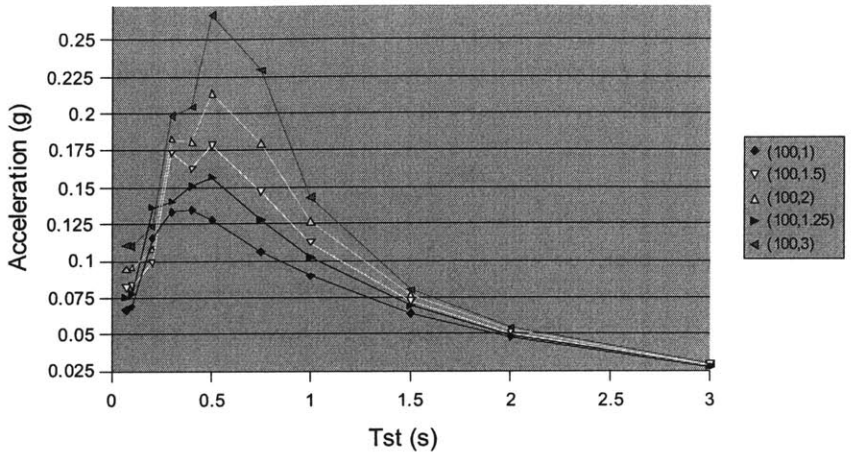

Figure 2-25 Acceleration response spectra: variation in soil condition modelled by variation in k, h=100m remains constant.

Figure 2-25 illustrates the effect of the impedance contrast k. As the impedance contrast k increases, the soil becomes softer, the amplification of the ground motion increases, and the resonance period also increases. The earthquake considered has magnitude 7 and an epicentral distance of 100km from the site.

Selected acceleration response spectra are shown in Figure 2-26, comparing our model (solid lines) with the empirical attenuations of Youngs, 1997 for inter-slab events (dotted lines). Note that in the long period range, the theoretical model using the modification from Boore no longer over-predicts the spectral acceleration.

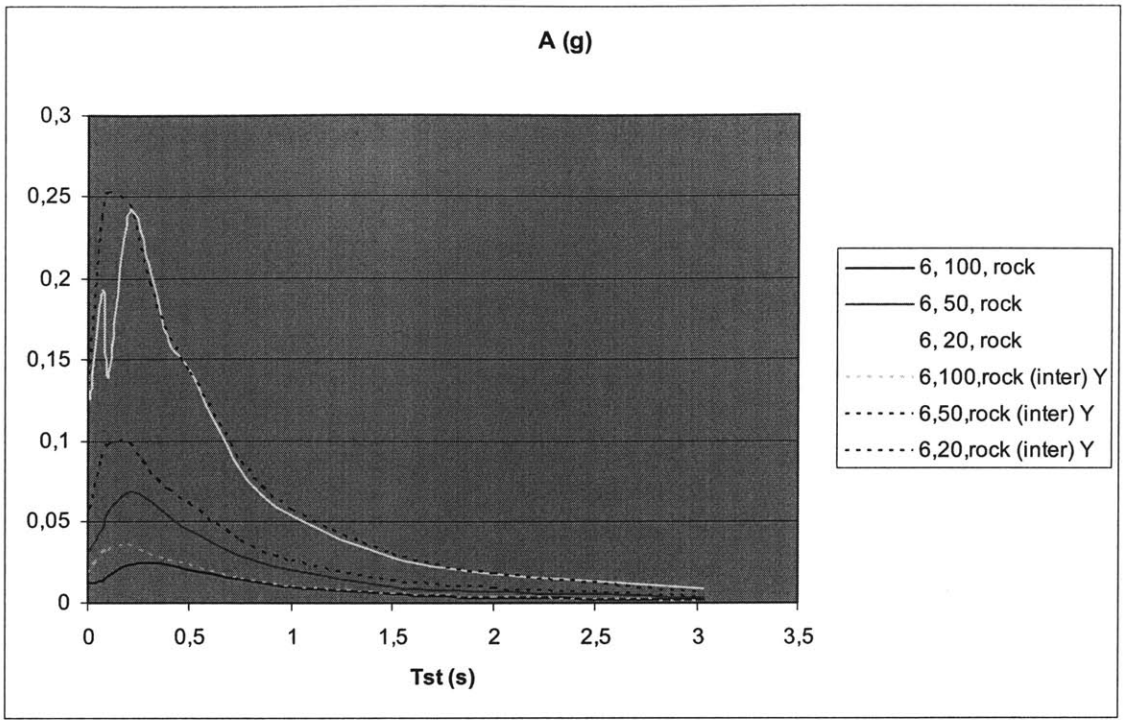

Figure 2-26 Acceleration response spectra, comparison between our model (solid lines) and the empirical relations of Youngs, 1997 (dotted lines)

The empirical relations of Youngs (1997) distinguish between two types of event: Intra-slab and inter-slab events. They have been shown to generate different accelerations. Figure 2-27 shows acceleration response spectra from our model (plain line) and inter and intra events from Youngs, 1997 (dotes lines). At the magnitude and distance considered in this example (7 and 50 km respectively), our model is closer to the empirical attenuation for inter-slab events. Nevertheless, this is not true for all magnitudes and distances.

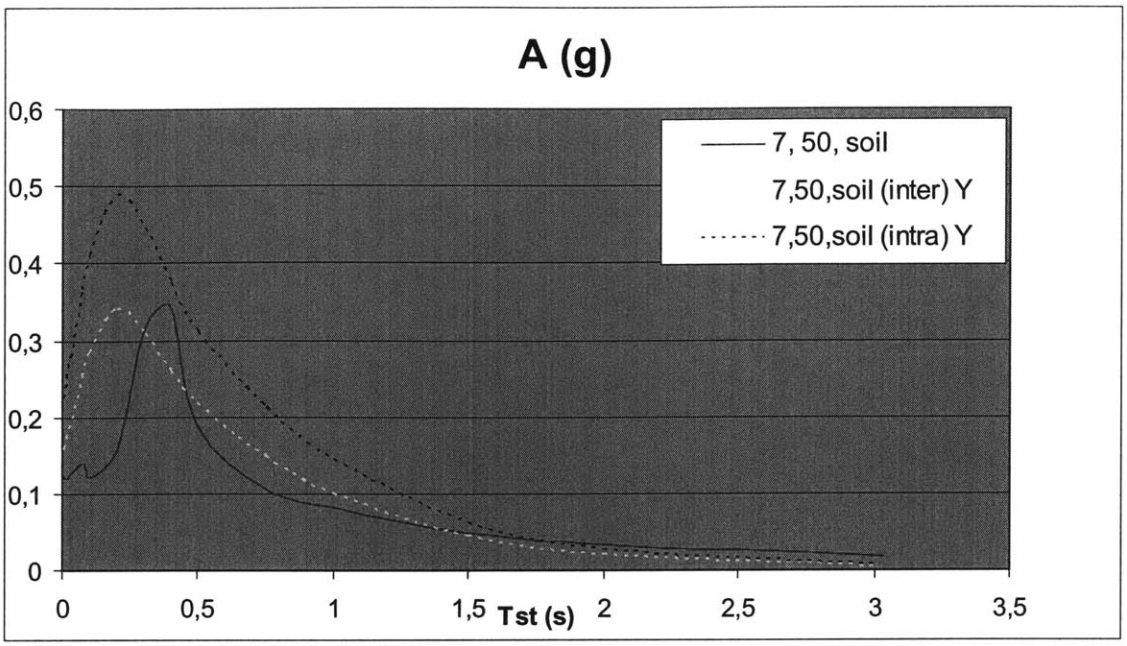

Figure 2-27 Acceleration response spectra, comparion between our model (solid line) and the empirical relations from Youngs, 1997 (dotted lines)

For example, Figure 2-28 shows that for large earthquakes, our model may be closer to the empirical relationships for intra-slab events. In any case, our model does not account for such differences.

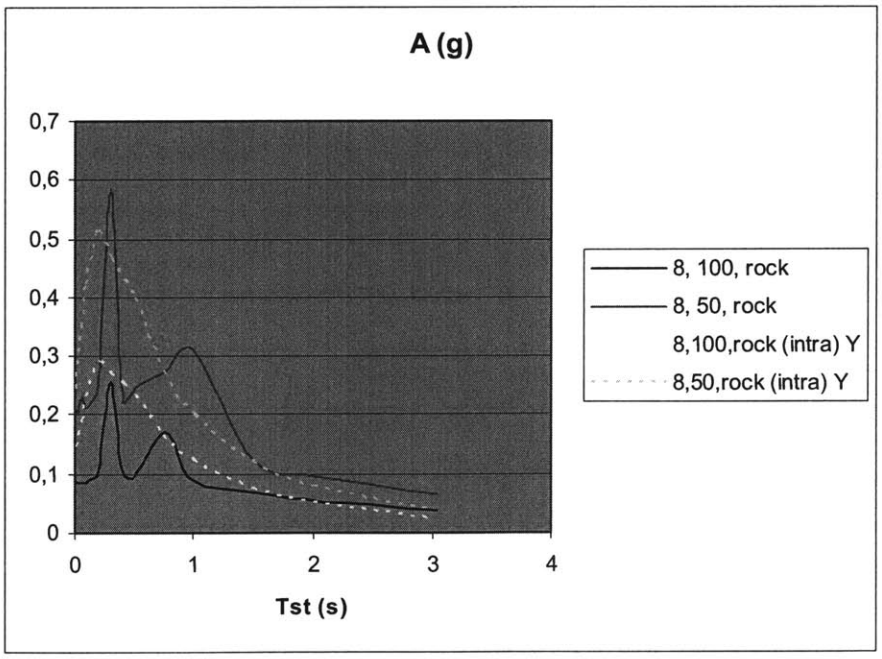

Figure 2-28 Acceleration response spectra, comparison between our model (solid lines) and the empirical relation from Youngs, 1997

The effect of soil conditions is shown in Figure 2-29. The peak acceleration at the resonance period for the soft soil considered is about 1.5 times higher than the acceleration at the reference rock site. For more flexible structures, $T_{st} \geq 1s$, the effect of soil is not noticeable. Additional comparison between the empirical relationship derived by Youngs (1997) for rock and soil, and the results of our model are presented in Appendix III.

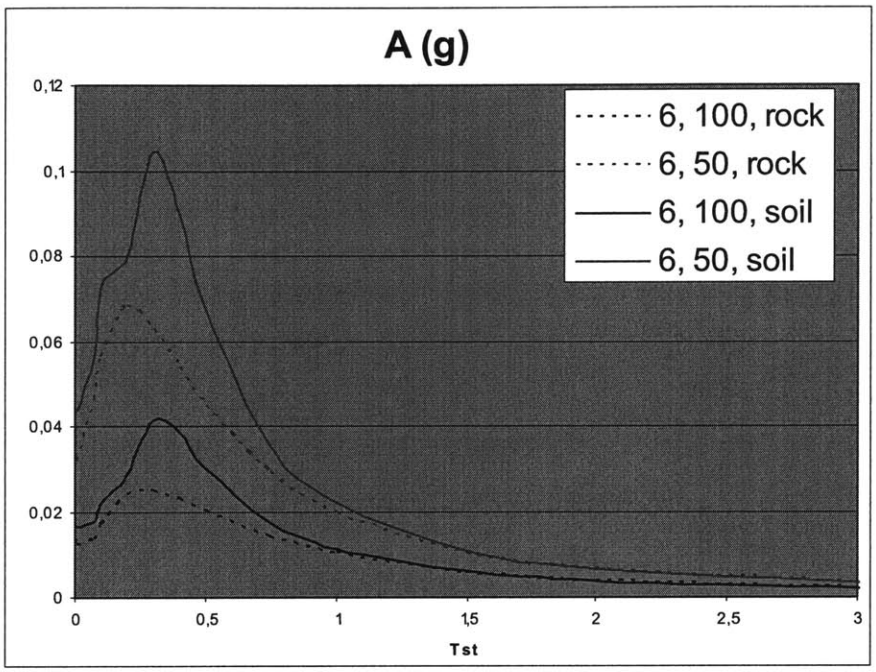

Figure 2-29 Acceleration response spectra for rock (dotted lines) and soft soil (solid lines)

The model is used to obtain the acceleration experienced by different structures given an earthquake scenario of magnitude M, a distance to the epicentre R and a specific soil condition. Different soil conditions can be selected since the model offers the flexibilities of a continuous model. For the examples in this study, 'soil' refers to a soil layer of 30m and a shear wave velocity of 350m/sec, classified as 'medium soil' in the literature. 'Rock' refers as a soil layer of 620m/s as defined by Boore and Joyner (1997).

Figure 2-30 shows the peak ground acceleration obtained with our model for Rock and Soil conditions for 4 different magnitudes (M=5, 6, 7 and 7.5) as a function of the

distance to the epicentre R (in Km). On average, the peak ground acceleration (PGA) on the soft soil considered is 1.4 times higher than the peak ground acceleration on rock site. For example, for an earthquake M=7.5 and at R=50km from the epicentre, the PGA on rock is 0.17g; whereas the PGA on soil is 0.24g.

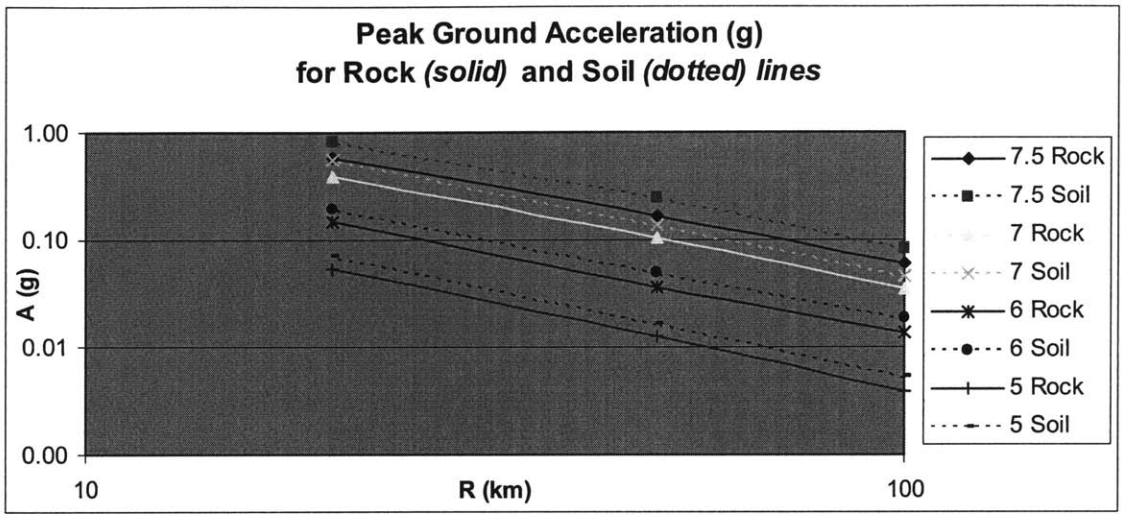

Figure 2-30 Peak Ground Acceleration (g) for Rock (solid lines) and Soil (dotted lines) as a function of distance from the source R (km) in log scale.

Figure 2-31 shows the peak acceleration obtained for a structure with natural period Tst=0.4s for both Rock and Soil conditions and for 3 different magnitudes (M=5, 6 and 7). The peak acceleration is plotted as a function of the distance to the epicentre R (in Km).

For structures with natural periods in the range 0.1-0.8 seconds, softer soils amplify the peak acceleration with factors of 2 or higher compared to 'rock'. For example, for an earthquake M=7 and at R=100km from the epicentre, the peak acceleration on rock is 0.06g; whereas it is 0.15g on soil.

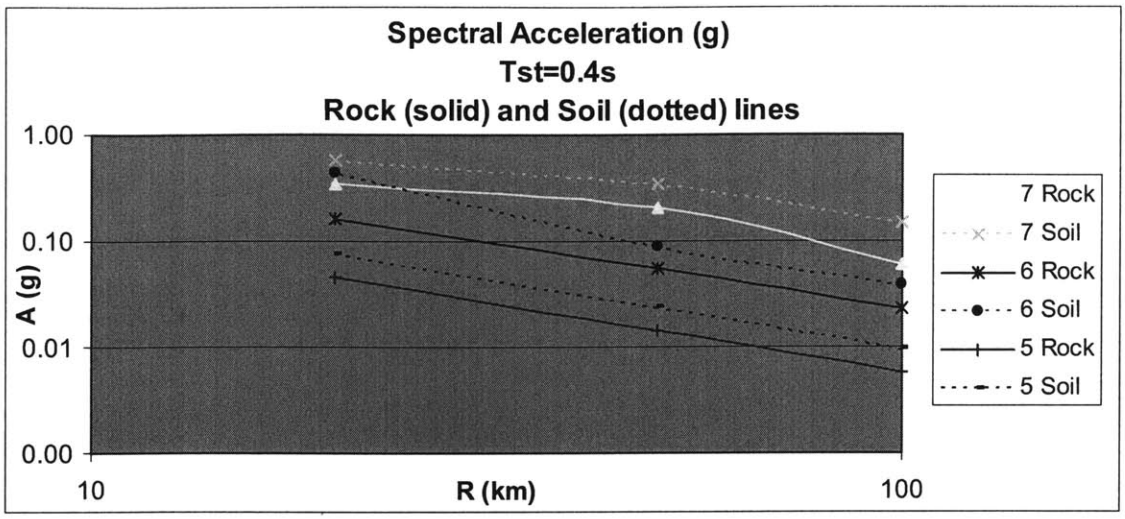

Figure 2-31 Spectral Acceleration (g) for Tst=0.4s for Rock (solid lines) and Soil (dotted lines) as a function of distance from the source R (km) in log scale.

Figure 2-32 shows the peak accelerations obtained for a structure with natural period Tst=1s for both Rock and Soil conditions for 4 different magnitudes (M=5, 6, 7 and 7.5) as a function of the distance to the epicentre R (in Km).

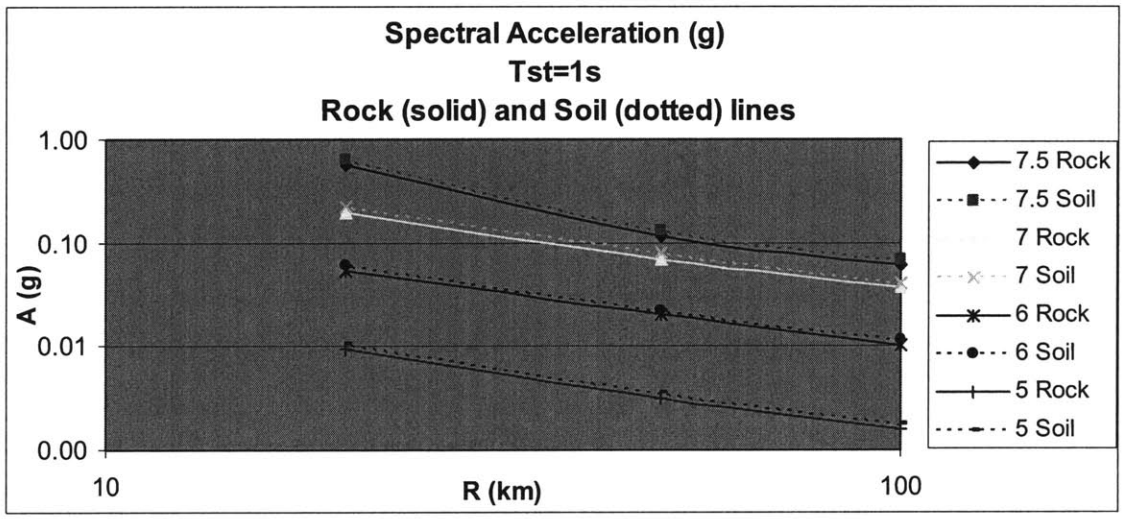

Figure 2-32 Spectral Acceleration (g) for Tst=1s for Rock (solid lines) and Soil (dotted lines) as a function of distance from the source R (km) in log scale.

As the structure becomes more flexible, the differences in the peak acceleration between rock and soil condition is less pronounced.

To use our model, one needs to estimate $V_{s\text{-}30}$ at the site, as well as the characteristics of the supporting structure in terms of its natural period T_{st} and its percentage of dampingξ.

- Tunnels have records of behaving particularly well during earthquake conditions. Peak ground accelerations in tunnels are generally lower than at the free surface. There is no free-surface effect, thus, the F factor in the Boore formulation that models the effect of free-surface amplification and taken as 2 in almost all applications, is set equal to 1.
- According to JR East simulations, the natural period of the viaduct in the JR East network varies between 0.4 and 0.9 seconds.
- The peak acceleration and displacement on embankments can be taken as the peak ground acceleration and peak ground displacement respectively.

Soil conditions are more difficult to assess. Currently, JREast classifies soils in 11 categories that are not directly related to the physical properties of the soil deposits. The National Earthquake Hazards Reduction Program (NEHRP) uses the average shear-wave velocity represented by parameter $V_{s\text{-}30}$, which is calculated as the ratio of 30 m to the vertical shear wave travel time through the upper 30 m of the site. The NEHRP classification is reported in Table 2-4. Studies by Borcherdt and Glassmoyer (1994), Borcherdt (1994) recommend $V_{s\text{-}30}$ as a means of classifying sites for building codes. The classification provides a first estimates to assess shear wave velocity of a soil layer.

NEHRP Category	Description	Mean Shear Wave Velocity to 30 m
A	Hard Rock	>1500 m/sec
B	Firm to hard rock	760-1500 m/sec
C	Dense soil, soft rock	360-760 m/sec
D	Stiff soil	180-360 m/sec
E	Soft clays	<180 m/sec
F	Special study soils, e.g., liquefiable soils, sensitive clays, organic soils, soft clays > 36 m thick	

Table 2-4 NEHRP classification for soils based on shear wave velocity

Stewart (2003) suggests using the correspondence between shear wave velocity and surface geology. Shear wave velocity has been found to be correlated with surface geology characteristics such as age, soil texture and fracture spacing for rock (Fumal, 1978). Quantitative estimates of this correlation have been derived by Wills and Silva (1998). The correlation between $V_{s\text{-}30}$ and surface geology characteristics can therefore be used to generate state-wide maps of $V_{s\text{-}30}$ by using current map of surface geology. This has already been done by Wills *et al.* (2000) for example.

Displacement Response Spectra

The model is also used to derive absolute displacement response spectra *Sd* and relative displacement response spectra. The absolute displacement response spectrum is derived directly from the auto power density spectrum for acceleration noting that $S_D(\omega) = \frac{1}{\omega^4} S_A(\omega)$, where $S_A(\omega)$ takes the form reported in Equation (12). Integration over the full range of frequency gives the variance of the displacement, and the peak absolute displacement is obtained assuming a relation between peak displacement and variance of the type:

$$Sd = 3\sqrt{\sigma_{D_{ii}}^2}$$

The relative displacement response spectrum is derived following the same methodology, but by considering the relative dynamic response of a single-degree-of-freedom system characterized by the transfer function: $\left|H(\omega|\omega_{st},\xi_{st})_{structure}-1\right|^2$

Where $H(\omega|\omega_{st},\xi_{st})_{structure}$ is the complex function $\frac{1+2i\xi_{st}(\omega/\omega_{st})}{1-(\omega/\omega_{st})^2+2i\xi_{st}(\omega/\omega_{st})}$.

The quantity of interest, peak ground displacement (PGD), is found at very short periods in the case of absolute response spectra or at sufficiently long periods in the case of relative displacement response spectra. The modifiers from Boore are not used because the parameters in the formulation are not calibrated for very short and very long periods. A peak-to-standard deviation ratio of 3 is therefore assumed.

Figure 2-33 to Figure 2-40 show absolute and relative displacement response spectra for different earthquake scenarios.

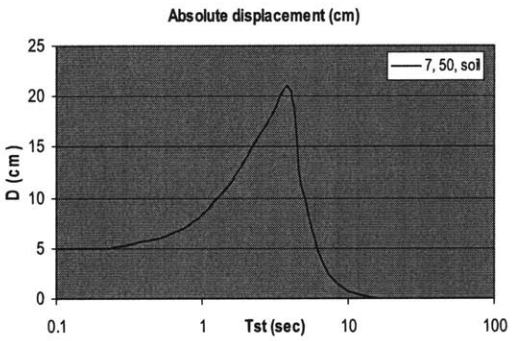

Figure 2-33 Absolute displacement response spectra for M=7 and R=50km (in cm)

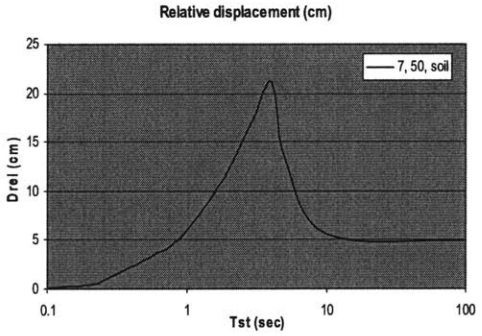

Figure 2-34 Relative displacement response spectra for M=7 and R=50km (in cm)

Figure 2-33 and Figure 2-34 show the absolute and the relative displacement response spectra for an earthquake scenario M=7 and R=50km. It is observed that in the range 0 – 1 second, the ground displacement dominates the relative displacement of the structure. The peak displacement is very close to the peak ground displacement in this range.

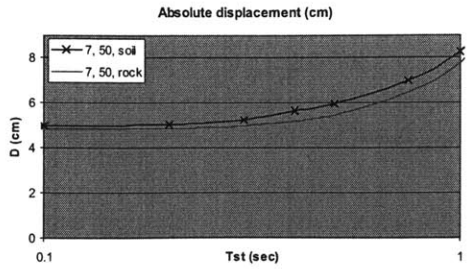

Figure 2-35 Absolute displacement response spectra for M=7 and R=50km for rock and soil (in cm)

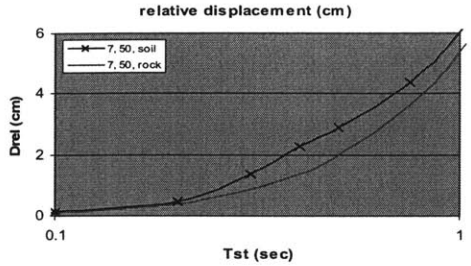

Figure 2-36 Relative displacement response spectra for M=7 and R=50km for rock and soil (in cm)

The effect of soil on the absolute and relative displacements is relatively small. Figure 2-35 and Figure 2-36 show the relative effect of soil. In the following response spectra, only one type of soil (soft) is shown.

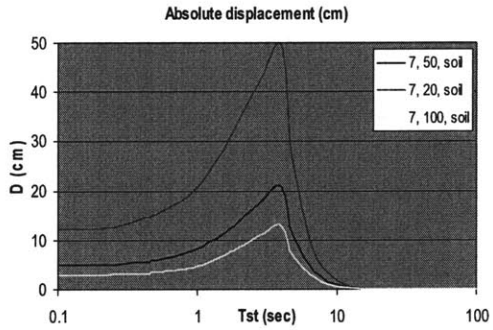

Figure 2-37 Absolute displacement response spectra for M=7 and R=100, 50 and 20km

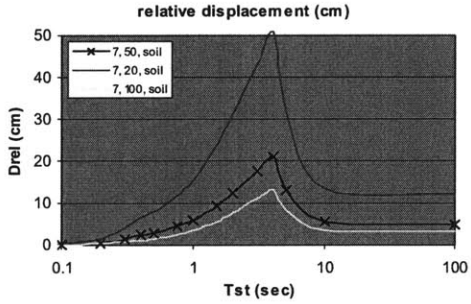

Figure 2-38 Relative displacement response spectra for M=7 and R=100, 50 and 20km

The effect of magnitude and distance on the absolute and relative displacement is shown in Figure 2-37, Figure 2-38, Figure 2-39 and Figure 2-40. In all cases, the PGD dominates the response in the range 0 – 1 second.

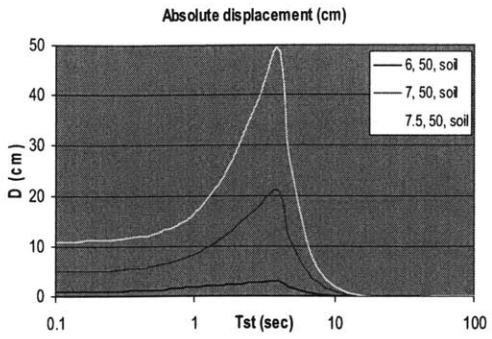

Figure 2-39 Absolute displacement response spectra for R=50 and M=6, 7 and 7.5

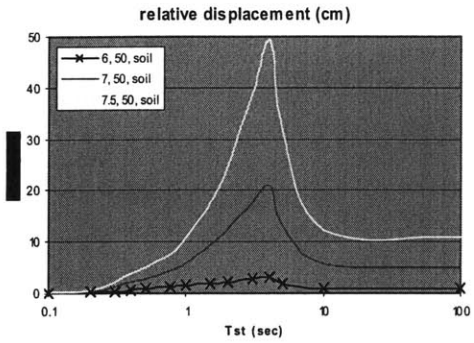

Figure 2-40 Relative displacement response spectra for R=50 and M=6, 7 and 7.5

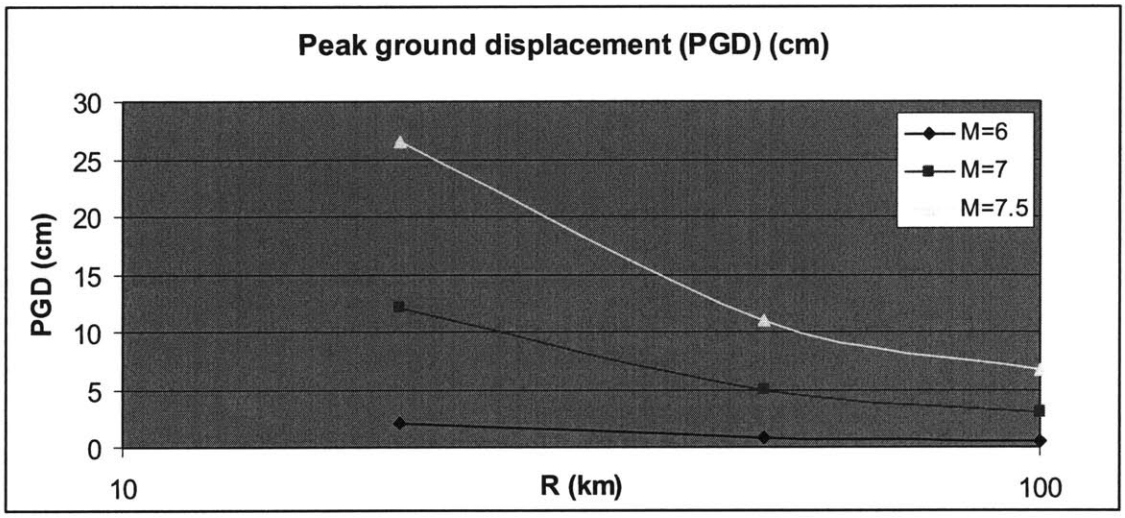

Figure 2-41 Peak ground displacement as a function of distance to the epicenter R (km) for M=6, 7 and 7.5

Figure 2-41 shows the peak ground displacement as a function of the distance to the epicenter for M=6, 7 and 7.5. For a train running on an embankment, the parameters of interest are PGA and PGD. For example, for an earthquake M=7.5 and at R=50km from the epicentre, the PGA on rock is 0.17g; whereas the PGD is 10.9cm. In this specific case, the displacement limit of 7cm is exceeded, whereas the acceleration limit of 0.3g is not reached.

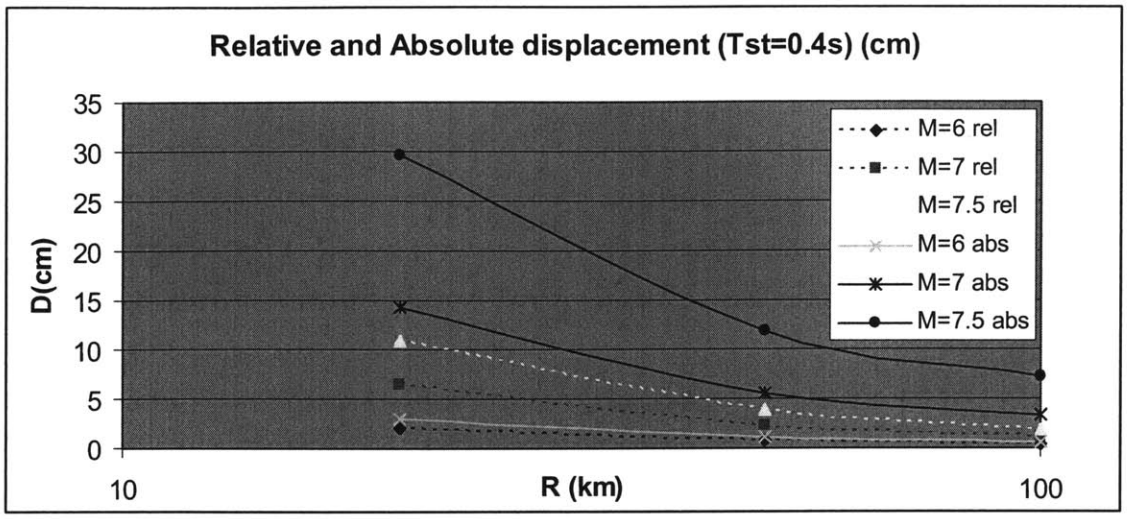

Figure 2-42 Absolute (solid lines) and Relative (dotted lines) displacement at Tst=0.4s, as a function of R, and for M=6, 7 and 7.5.

Figure 2-42 shows the comparison between the absolute and the relative displacement for a natural period of the structure of 0.4seconds. At this period, the PGD dominates the response.

The relative contribution of the ground displacement to the critical levels of shaking can be evaluated by comparing the relative displacement response spectra to the peak ground displacement (PGD). The relative displacement response spectrum is asymptotic to the PGD: The spectral deformation approach the peak ground displacement at sufficiently long periods. For example, for the 1940 El Centro earthquake, the processed peak values of ground acceleration (PGA) and displacement (PGD) are: PGA=0.348g and PGD=10.9cm respectively. The relative displacement response spectrum shows displacements over 40cm at the resonance period (Tst=10 seconds) (Mylonakis & Syngros, 2002). In the range 0-1second, the relative displacement is well below the PGD. Those orders of magnitude are observed in our model. Figure 2-43 and Figure 2-44 show the absolute and the relative displacement response spectra for an earthquake of magnitude M=7.5 and distance to the epicentre of 50km, derived from our model. Figure 2-45 shows the acceleration response spectra associated. The ground motion is such as PGA=0.24g and PGD=10.9cm. It is observed that the PGD dominates the response for periods in the range 0 – 1 second. A maximum relative displacement of 49cm is obtained at Tst=4s.

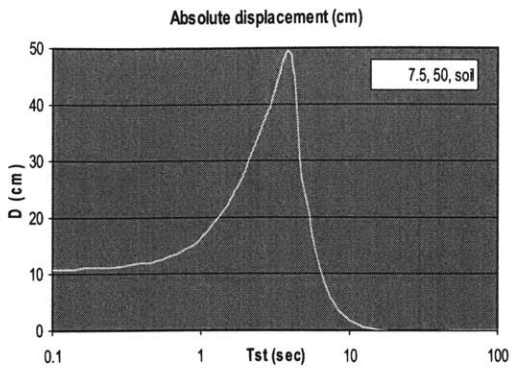

Figure 2-43 Absolute Displacement Response Spectra M=7.5, R=50km

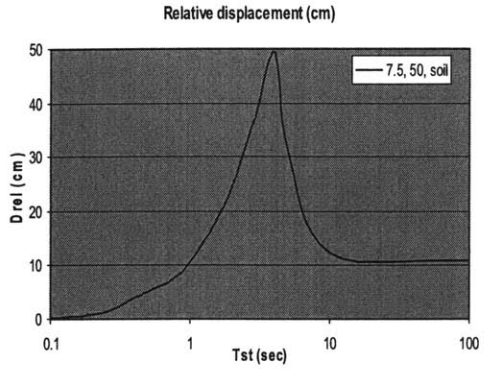

Figure 2-44 Relative Displacement Response Spectra M=7.5, R=50km

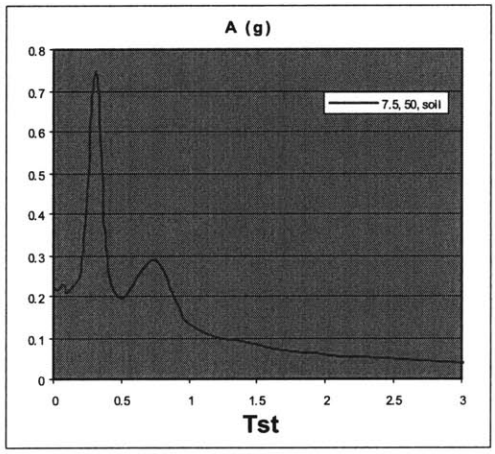

Figure 2-45 Acceleration response spectra for M=7.5, R=50km, on soft soil

Conclusion

In essence, we used the Fourier spectrum for ground motion acceleration compiled by Boore (2003) and others to relate *Sa* and *Sd* to earthquake magnitude, epicentral distance, site conditions and natural period of the structure. We slightly modified the model to obtain a continuous representation of the local soil conditions with parameters related to the soil physical properties such as the shear wave velocity $V_{s\text{-}30}$. In our model, the soil response is treated analytically by propagating the rock motion through a specified soil column. For small to medium size earthquakes ($M \leq 7.5$) and for distances from the epicenter from 10 to 100km, the model reproduces with accuracy the shape of the empirical response spectra. For large earthquakes ($M > 7.5$) and close distances to the

epicenter, the model over-predicts the peak acceleration at the resonance period. Sharp variations of the acceleration around the resonance period are observed in our model. The amplifications from rock to softer soils are in general in good agreement with empirical estimates.

In the next section, we assess the probability of derailment of a stationary train during the strong motion phase, given the natural period of the structure underlying the track and the soil conditions as given by the shear wave velocity $V_{s\text{-}30}$.

2.1.4 Probability of Derailment of a Stationary Train due to Vibratory Motion

In this section, we use the criteria for derailment derived in Section 2.1.2 to assess the probability of derailment by vibratory motion for a stationary train given an earthquake scenario. The analysis in Section 2.1.3 provides estimates of the peak acceleration *Sa* and the peak absolute displacement *Sd* given an earthquake scenario; and Section 2.1.2 provides the criteria for derailment in terms of *Sa* and *Sd*.

The conditions for derailment are $A_{limit} \geq 0.3g$ and $D_{limit} \geq 70mm$.

Based on a normal distribution of the natural logarithm of *Sa* with a corresponding standard deviation $\sigma_{\ln Sa} = 0.65$, and a normal distribution of the natural logarithm of *Sd* with a corresponding standard deviation $\sigma_{\ln Sd} = 0.75$, we assume that *Sa* and Sd are independent and the probability of derailment by vibratory motion is given by equation (3), reproduced below for convenience:

$$P[(Sa \geq 0.3g) \cap (Sd \geq 7cm)] = \Phi\left[-\frac{\ln 0.3g - m_{\ln Sa}}{\sigma_{\ln Sa}}\right] * \Phi\left[-\frac{\ln 7cm - m_{\ln Sd}}{\sigma_{\ln Sd}}\right]$$

From Equation (3) and the accelerations and displacement obtained from our model given an earthquake scenario, we evaluate the probability of derailment during the strong motion phase. Examples of results are presented below for magnitudes M=6, 7 and 7.5.

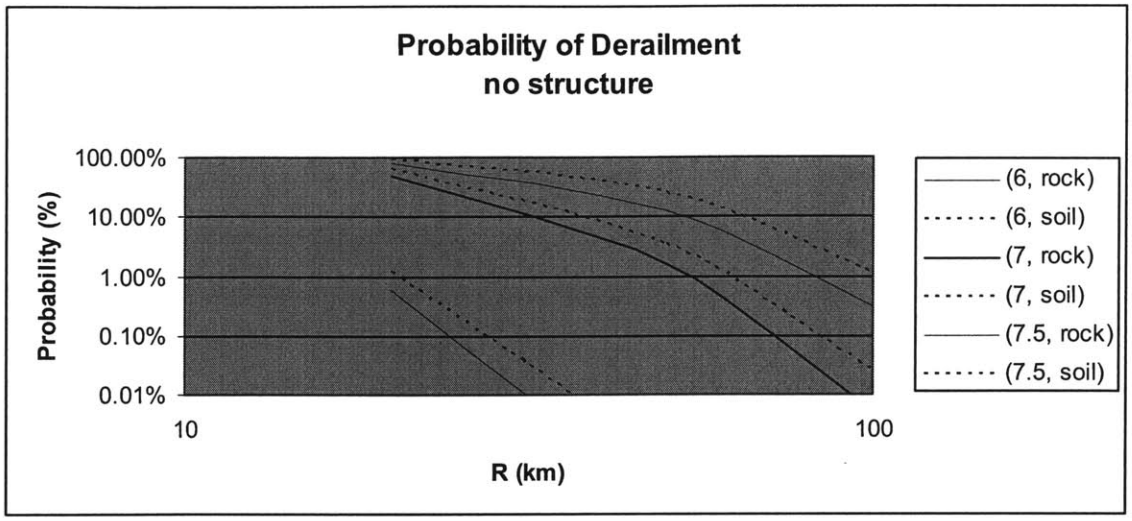

Figure 2-46 Probability of derailment by vibratory motion for the ground motion (no structure) for Rock (solid lines) and Soil (dotted lines) as a function of distance from the source R (km) in log scale.

Figure 2-46 shows the probability of derailment by vibratory motion given different earthquake scenarios at the ground level (no structure). It is the probability that the peak ground acceleration (PGA) exceeds 0.3g and that the peak ground motion exceeds 7cm. These probabilities may be applied to a train running on an embankment, for example.

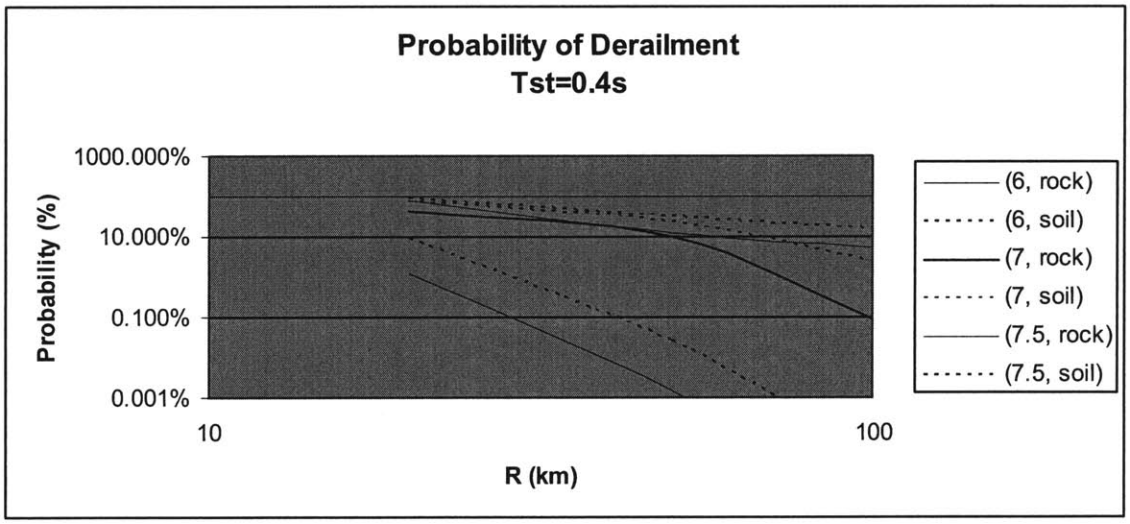

Figure 2-47 Probability of derailment by vibratory motion for Tst=0.4s for Rock (solid lines) and Soil (dotted lines) as a function of distance from the source R (km) in log scale.

Figure 2-47 shows the probability of derailment by vibratory motion for T_{st}=0.4s. It is the probability that *Sa* and *Sd* at Tst=0.4s exceeds 0.3g and 7cm respectively. These probabilities are to be applied to a train running on a structure with a natural period of 0.4s.

Figure 2-48 shows the probability of derailment by vibratory motion for a train running on a structure with natural period T_{st}=1s.

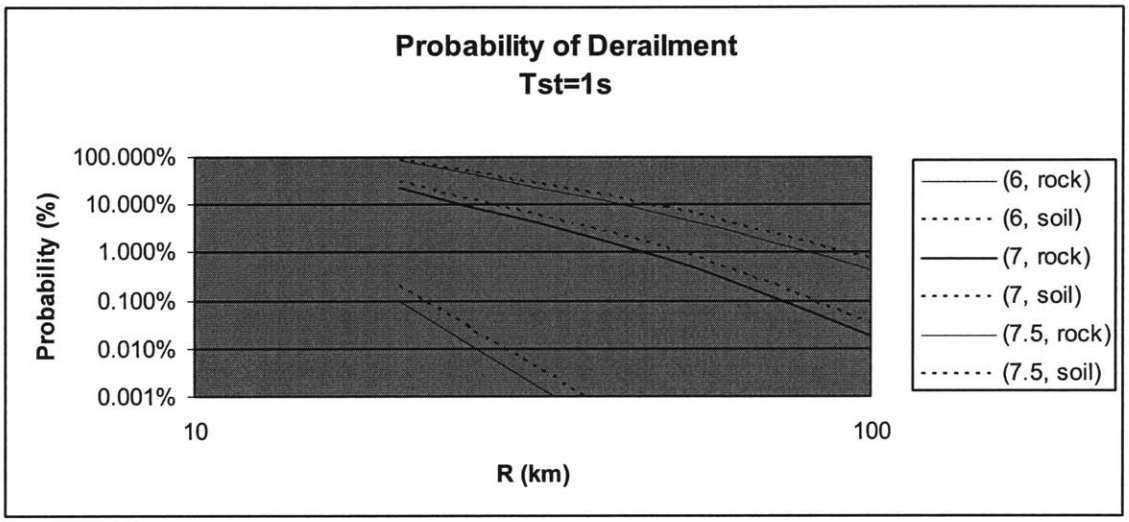

Figure 2-48 Probability of derailment by vibratory motion for Tst=1s for Rock (solid lines) and Soil (dotted lines) as a function of distance from the source R (km) in log scale.

Figure 2-46, Figure 2-47 and Figure 2-48 show the probabilities of derailment by vibratory motion of a stationary train, for different supporting structures (no structure, T_{st}=0.4 and 1sec respectively) and for different earthquake scenarios. The probability of derailment is higher for structures in the range $0.3s \leq T_{st} \leq 0.5s$. This is shown in Figure 2-51. Indeed, in this range, the spectral acceleration is amplified with respect to the peak ground acceleration (see Figure 2-49). For T_{st}=1s, the peak acceleration falls below the PGA, and the peak displacement is still close to the PGD (see Figure 2-50), thus leading to probabilities of derailment lower than in a case where there is no supporting structure.

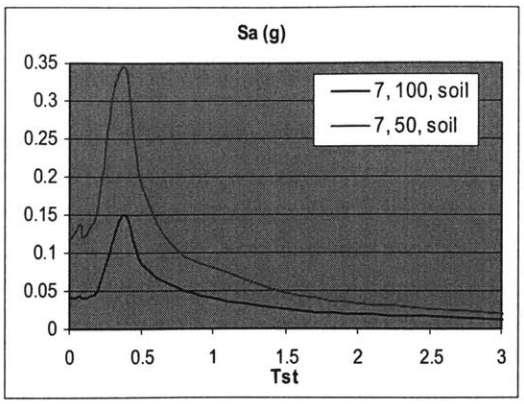

Figure 2-49 Acceleration response spectra for an earthquake M=7, and R=100 and 50km

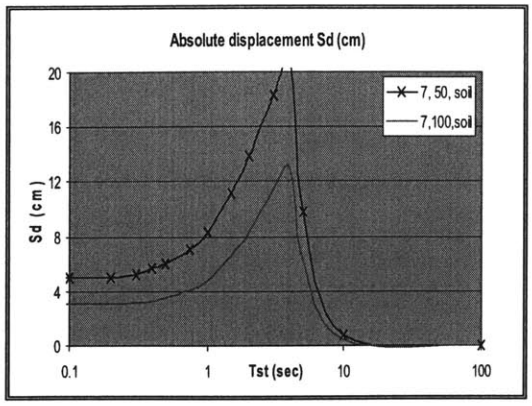

Figure 2-50 Displacement response spectra for an earthquake M=7, and R=100 and 50km

Figure 2-51 shows that the probability of derailment is statistically higher for structures with natural period around 0.4seconds, compared with a case where there is no structure (peak ground motion - PGM) or where the structure is more flexible (Tst=1sec).

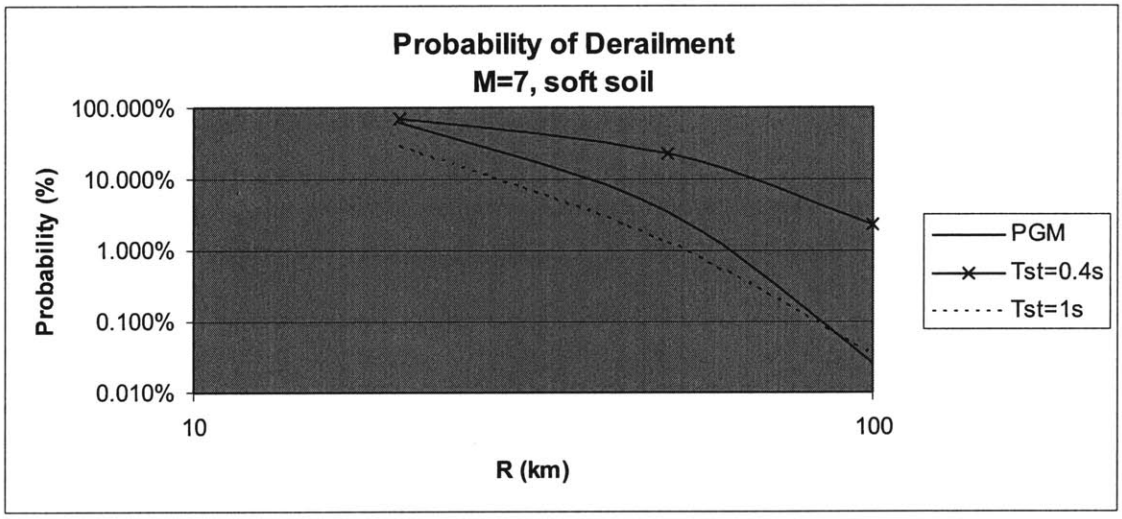

Figure 2-51 Probability of derailment by vibratory motion for the ground motion, Tst=0.4s and Tst=1s for an earthquake scenario M=7 on soft soil as a function of distance from the source R (km) in log scale.

The derailment probabilities reported above refer to a stationary train. One aspect that has been disregarded is the effect of speed. Speed has actually two effects: it may facilitate derailment under synchronous track motion and contribute to lateral acceleration and displacement under non-synchronous track motion. The later effect is considered in the next section (Section 2.2), whereas the former effect is being ignored.

Intuitively, one would expect that as the speed of train increases, the critical level of shaking for derailment decreases. To quantify this decrease, one should formulate a dynamic model of a moving train, which is behind the scope of the present work.

Case-Study: The Niigata Earthquake

During the magnitude 6.8 Niigata Chuetsu Earthquake of October 23, 2004, the Joetsu Shinkansen Toki No. 325 derailed. The train was located 10 km from the epicentre and was running at about 200km/h. The train was just out of a tunnel and entering a viaduct that presented sharp discontinuities in structural conditions. The peak-ground acceleration (PGA) at the location of the accident was about 0.6g.

Recordings of the ground motion near the location of the accident show a high frequency content near 0.8 second. Structures with natural period close to 0.8 second would therefore experience very strong motions.

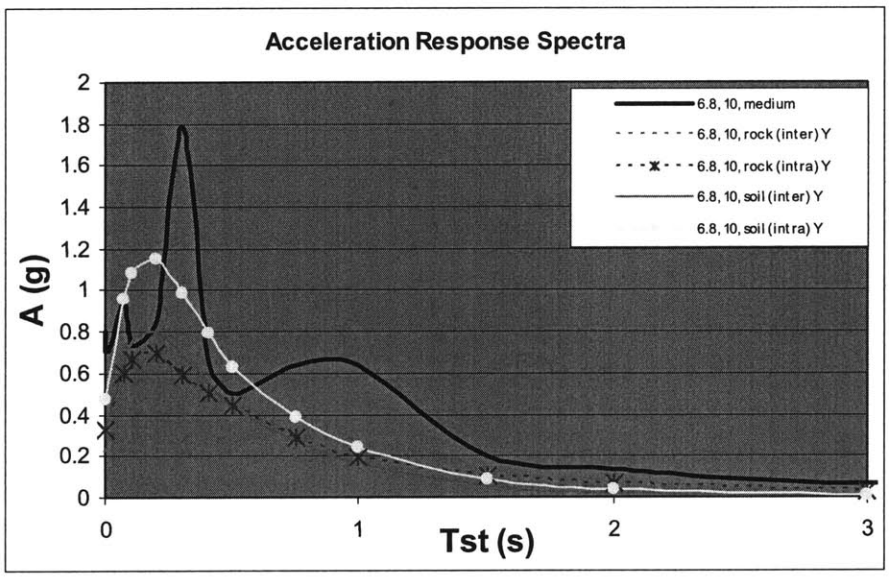

Figure 2-52 Acceleration response spectra - Niigata earthquake

Figure 2-52 shows different acceleration response spectra for an earthquake of magnitude 6.8 10km from the epicentre. The thick solid line is from our model, for medium soil. The remaining curves are from empirical attenuation relationships for rock and soil conditions and for inter-slab and intra-slab events (Youngs, 1997).

The PGA predicted for an earthquake of magnitude 6.8 and at a distance of 10km are 0.7g with our model and 0.5g with Youngs attenuation relationship for soil conditions and intra-slab event. Assuming the period of the viaduct to be 0.4s, our model predicts a peak acceleration of 0.9g and the empirical relation gives an acceleration of 0.8g. Hence, the two models predict similar structural responses. The PGA is also in agreement with what has been observed during the Niigata earthquake.

The absolute and relative displacement response spectra corresponding to the earthquake scenario M=6.8 and R=10 km are shown in Figure 2-52 and Figure 2-53 respectively. For Tst=0.4s, Sd=19 cm (and the relative displacement is 6.7 cm).

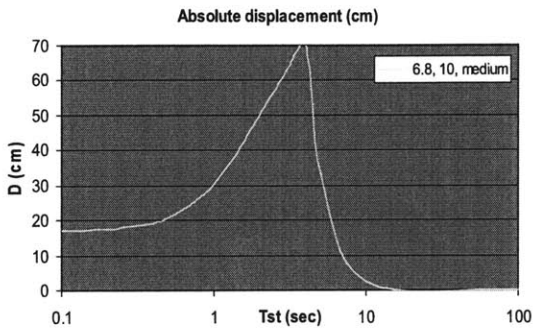

Figure 2-53 Absolute displacement response spectra for R=10 and M=6.8

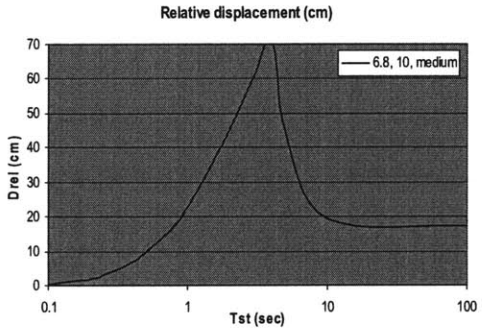

Figure 2-54 Relative displacement response spectra for R=10 and M=6.8

For an earthquake of magnitude 6.8, and at a distance of 10 km from the epicentre, the median peak acceleration is 0.9g and the median peak displacement is 19cm. Using our derailment criteria for a stationary train on a viaduct with a natural period of 0.4second, the probability that the acceleration exceeds 0.3g and the peak (absolute) displacement exceeds 7cm is:

$$P\left[(Sa \geq 0.3g) \cap (Sd \geq 7cm) \middle| M = 6.8, R = 10km\right] = 87\%$$

The corresponding probability of derailment under vibratory motion is relatively high: 87%. Thus, our criteria for derailment are in good agreement with what happened during the Niigata earthquake. Note that the two effects of speed aforementioned have not been considered yet and would give an even higher probability of derailment:

1) The train speed may have facilitated the derailment under synchronous track motion. At high speeds, the critical levels for derailment in Equation (2) should be lower; hence yielding a higher probability of derailment.

2) The train speed also contributes to lateral acceleration and displacement under non-synchronous track motion. The additional acceleration due to the passage of the train on wavy tracks (waviness induced by the relative displacement between two piers at the top of the structure) has not been taken into account. In the case of the Niigata earthquake, where the train was entering a more flexible structure with important changes in geometric and structural characteristics, the differences in support displacement may have played an important role. This phenomenon is considered next (Section 2.2), where a method to quantify the second component of lateral train acceleration Sa_d is presented.

The Niigata case is re-evaluated at the end of Section 2.2.

2.2 Derailment of a Moving Train under Heterogeneous Site Conditions

In the previous section, we have considered the derailment of stationary trains under vibratory motion. The critical acceleration under these conditions is denoted by Sa. As has been observed in the Niigata case, shifts in site conditions may induce differential structural responses sufficient to trigger derailment. Here we consider the effect of spatial non-homogeneities in soil and structural characteristics as well as the incoherence of the ground motion to obtain a second component of lateral train acceleration, Sa_d. This component is sensitive to train speed.

First, we present a method to quantify the differential response at different structural locations and derive Sa_d from the relative displacement of the track (Section 2.2.1). Second, we investigate in more detail the causes of differential ground motion and present a model to include spatial variability of ground motion (SVGM) through a coherency function (Section 2.2.2). Finally, we obtain the acceleration Sa_d (Section 2.2.3).

2.2.1 Modelling the Relative Displacement of the Track

Each location i along the track is characterized by a specific structure and a specific soil column, as shown in Figure 2-55.

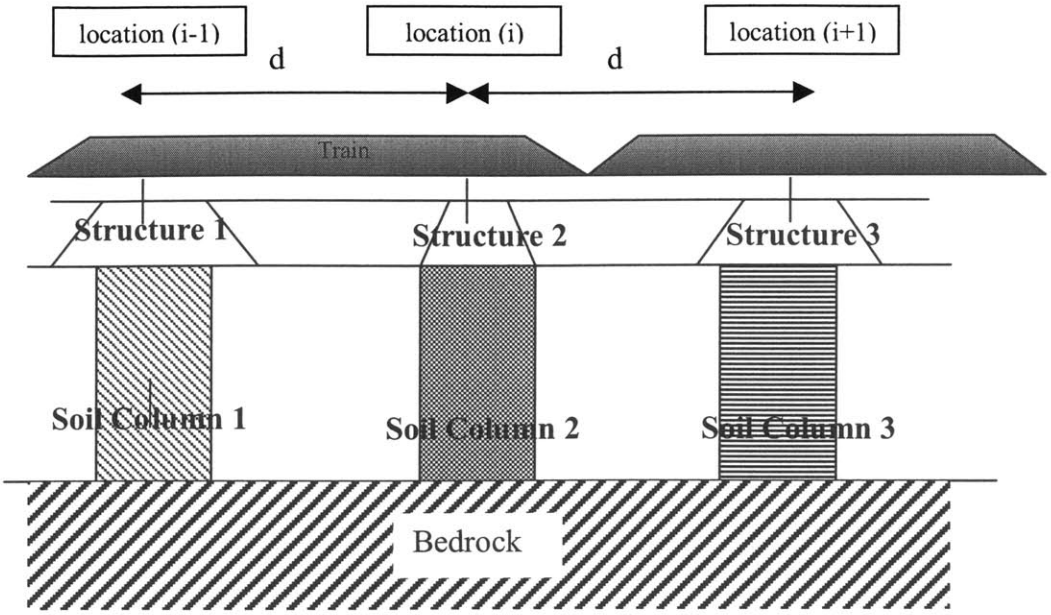

Figure 2-55 Discretization model for train acceleration

Three parameters are influential on the acceleration Sa_d :

1) The amplitude of the displacement $D_{train}(t_i)$, between the top and the bottom of the pier. This relative displacement depends mainly on magnitude M, epicentral distance R, and local soil and structural conditions.
2) The speed of the train, V; and
3) The spacing of the supports, d.

The evaluation of Sa_d will therefore depend on those three parameters. We denote the transversal train displacement by $D_{train}(t_i) = D_{track}(x(t_i), t_i)$. Technically, train and track displacements are not the same. Here, we are really evaluating D_{track} and we assume that the train follows the rails, with no slack, so that $D_{train} \approx D_{track}$. We can obtain $D_{train}(t_i)$ by using the power spectral density function of displacement. Then, if $D_{train}(t)$ is known at nearly equally spaced time t_i, the train acceleration Sa_d at time t_i may be evaluated as:

$$Sa_d(t_i) \approx \frac{D_{train}(t_{i-1}) - 2D_{train}(t_i) + D_{train}(t_{i+1})}{(\Delta t_i)^2} \tag{15}$$

where $\Delta t_i \approx \frac{t_{i+1} - t_{i-1}}{2}$ is the approximate time discretization step around t_i. The spacing of the supporting structure d and the train speed V are related to Δt_i through: $\Delta t_i \approx \frac{t_{i+1} - t_{i-1}}{2} = \frac{d}{V}$.

The variance of the train acceleration Sa_d, denoted $\sigma^2_{A_d}$, may be obtained as follow.

Consider the vector of transversal train displacements $\underline{D} = \begin{bmatrix} D_{train}(t_{i-1}) \\ D_{train}(t_i) \\ D_{train}(t_{i+1}) \end{bmatrix} \begin{matrix} 1 \\ 2 \\ 3 \end{matrix}$

The spectral density matrix of $\underline{D}$ is:

$$\underline{S_D} = \begin{bmatrix} S_{D_{11}} & S_{D_{12}} & S_{D_{13}} \\ & S_{D_{22}} & S_{D_{23}} \\ & & S_{D_{33}} \end{bmatrix} = \begin{bmatrix} \text{var}(D_1) & \text{cov}(D_1, D_2) & \text{cov}(D_1, D_3) \\ & \text{var}(D_2) & \text{cov}(D_2, D_3) \\ & & \text{var}(D_3) \end{bmatrix}$$

The spectral density matrix has components $S_{D_{i,j}} : S_{D_{i,j}}(\omega) = \frac{1}{\omega^4} S_{A_{i,j}}(\omega)$, which can be found directly from our model for spectral acceleration attenuation.

The train acceleration at time t_i is evaluated using the discrete formulation in Equation (15). It follows that:

$$\text{var}(A) = \frac{1}{\Delta t^4}\left[\text{var}(D_1) + 4\,\text{var}(D_2) + \text{var}(D_3) - 4\,\text{cov}(D_2, D_3) - 4\,\text{cov}(D_1, D_2) + 2\,\text{cov}(D_1, D_3)\right]$$

Hence, with respect to the power spectral density function for displacement $S_{D_{i,j}}$, $S_{A_d}(\omega)$ is obtained as:

$$S_{A_d}(\omega) = \frac{1}{(\Delta t_i)^4}\left\{S_{D_{11}}(\omega) + 4S_{D_{22}}(\omega) + S_{D_{33}}(\omega) - 4\,\text{Re}\left[S_{D_{12}}(\omega)\right] - 4\,\text{Re}\left[S_{D_{23}}(\omega)\right] + 2\,\text{Re}\left[S_{D_{13}}(\omega)\right]\right\} \quad (16)$$

The variance of the train acceleration, $\sigma^2_{A_d}$, is obtained by integrating $S_{A_d}(\omega)$ over the full range of frequency, and the acceleration Sa_d is obtained by multiplying the standard deviation by the peak-to-standard deviation ratio described earlier in this study.

The power spectral density functions for acceleration $S_{A_{i,j}}$ are needed to derive the power spectral density functions for displacement $S_{D_{i,j}}$ in Equation (16). Therefore, a presentation of the functional form of $S_{A_{i,j}}$ is presented below based on the analysis of derailment of a stationary train.

Spatial variability is described by means of a stationary, zero-mean Gaussian random field in space-time. The field is completely described by the matrix of spectral density functions for acceleration $S_A(\omega)$:

$$S_A(\omega) = \begin{bmatrix} S_{A_{11}}(\omega) & S_{A_{12}}(\omega) & S_{A_{1n}}(\omega) \\ & S_{A_{22}}(\omega) & S_{A_{2n}}(\omega) \\ & & \\ & & S_{A_{nn}}(\omega) \end{bmatrix}$$ where n is the number of spatial location or 'stations'.

The diagonal terms (the auto-power spectral density functions $S_{ii}(\omega)$) describe the process at each single station i. It can be shown that there is at least one function $H_i(\omega)$ that satisfies $S_{ii}(\omega) = |H_i(\omega)|^2$. In the earlier assessment of derailment for a stationary train, we used the following form for the mean auto power spectral density for acceleration (Equation 12):

$S_A(\omega) = S_{A_{ii}}(\omega) = |H(\omega|M,R)|^2_{rock} |H(\omega|soil)|^2_{soil} |H(\omega|\omega_{st},\xi_{st})|^2_{structure}$. Only the functional form of $S_{A_{ii}}(\omega) = |H_i(\omega)|^2$ was needed, since it describe completely the process at a single location i. The off-diagonal terms (the cross-power spectral density functions $S_{A_{ij}}(\omega)$) measure the dependence of the processes at station i and j. Denoting by $H_i(\omega)$ the function $H_i(\omega) = H(\omega|M,R)_{rock}\ H(\omega|soil)_{soil}\ H(\omega|\omega_{st},\xi_{st})_{structure}$ at station i, then $S_{A_{ii}}(\omega) = |H_i(\omega)|^2$ and $S_{A_{ij}}(\omega) = H_i(\omega)H_j(-\omega)$.

Consequently, the functional forms of the auto- and cross- power spectral density functions for displacement $S_{D_{i,j}}$ are obtain using:

$$S_{D_{i,j}}(\omega) = \frac{1}{\omega^4}\left[H(\omega)_{rock}\right]^2 \left[H(\omega)_{soil\,i} H^*(\omega)_{soil\,j}\right]\left[H(\omega)_{structure\,i} H^*(\omega)_{structure\,j}\right]\left[\gamma_{ij}(\omega)\right]\left[\exp\left[i\omega(t_i - t_j)\right]\right] \quad (17)$$

Where H_{rock}, H_{soil} and $H_{structure}$ are the Fourier spectrum for acceleration modelling the effect of source and propagation, soil amplification and track support structure response respectively; as defined in equation (12); H^* is the conjugate of H. γ_{ij} is the coherency function whose functional form is derived in the next section (Section 2.2.2). $\exp\left[i\omega(t_i - t_j)\right]$ is the shift in phasing due to the fact that the train is moving at a speed V and therefore reaches station j at time t_j with a time lag $\Delta t_i = t_i - t_j$ of $\frac{d}{V}$ after having reached station i, d being the distance separating station i and j. This shift is different from the lagged time for the arrival of the waves, included in the coherency function γ_{ij}. For the case of the auto-power spectral density functions, we have the simplified form:

$$S_{D_{i,i}}(\omega) = \frac{1}{\omega^4} S_{ii}(\omega) = \frac{1}{\omega^4} \left[H_{boore}(\omega)\right]^2 \left[H_{soil\,i}(\omega)\right]^2 \left[H_{structure\,i}(\omega)\right]^2$$

The motion between i and i is fully coherent, therefore $\gamma_{ij} = 1$, and there is no lagged time due to the traveling of the train from i to i. For the case of the cross-power spectral density functions, we have to refer to Equation (17).

The functional form of the coherency function γ_{ij} is derived next.

2.2.2 Causes of Spatial Variability

To obtain the second component of lateral train acceleration Sa_d, we consider the different causes of spatial variation in support motion. Spatial variation may result from: 1) The heterogeneity of soil or structural characteristics at different locations along the track, and 2) The lack of spatial coherence of the bedrock ground motion.

a. Spatial Variability of Site Conditions

Also for perfectly coherent waves and identical motion at all bedrock locations, the local soil and structural conditions can vary and produce differential motion. Figure 2-56 illustrates the variability of site conditions. The parameters reported in the figure

are: for the soil, its type modeled through the shear wave velocity v_s and the depth of the soil layer h, and for the structure, the type (viaduct, bridge, embankment, tunnel...) and the specific characteristics of each type (e.g. for a viaduct, the natural period and damping, and the spacing of the supports).

Changes in soil and structural properties along the track may be gradual or sudden.

Spatial Variability of Site Conditions

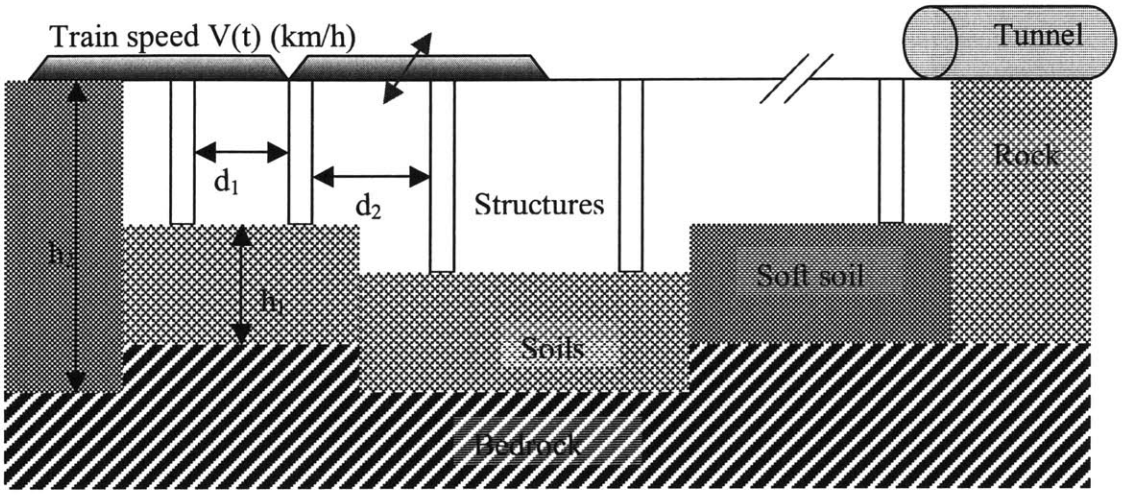

Figure 2-56 Spatial variability of site condition

b. Spatial Variability of Bedrock Ground Motion

Also in the case of spatially uniform soil and structural conditions, different points along the track experience different ground motions. This phenomenon is modeled through a coherency function. A functional form for the coherency function is derived, based on reviews of what is known concerning the spatial variability of ground motion (SVGM).

During ground motion, spatially extended structures such as viaducts and embankments experience excitations that vary along the structure in terms of arrival time, amplitude, phase and frequency content (e.g., Sextos et.al, 2003). Four distinct phenomena contribute to the spatial variation of earthquake ground motion (e.g., Der Kiureghian,1992 and 1996; Harichandran, 1999; or Lupoi et al., 2005):

1) The loss of correlation – referred to as the *incoherence effect* – between the motions at separate points. Spatial incoherence arises from two phenomena: The scattering of the waves as they propagate through the heterogeneous medium of the ground produce random reflections and refractions as the waves travel. Second, the differential superpositioning of the waves when arriving from extended sources amplifies the loss of coherency. These two components are denoted collectively as the 'incoherence effect'.
2) The difference in arrival times of the seismic waves at different stations commonly referred to as the *wave-passage effect.*
3) The *attenuation effect* which is the gradual decay of ground motion amplitude (especially at the high frequencies) due to geometric spreading and energy dissipation; and
4) The *site-response effect* due to spatially varying soil profiles.

In the context of a stationary representation, the spatial variation of ground motion can be characterized through $S_{ij}(\omega)$, the *cross*-power spectral density function of ground acceleration at point i and j. The coherency function $\gamma_{ij}(\omega)$ is a normalized version of this function, defined as:

$$\gamma_{ij}(\omega) = \frac{S_{ij}(\omega)}{\sqrt{S_{ii}(\omega)S_{ij}(\omega)}} \tag{18}$$

The coherency has a bounded modulus, $|\gamma_{ij}(\omega)| \leq 1$, and is a measure of linear dependence between the two ground motions at the two locations. $\gamma_{ij}(\omega) = 1$ implies identical synchronous motions whereas $\gamma_{ij}(\omega) = 0$ denotes complete lack of correlation.

Der Kiureghian (1996) presents a theoretical model of the coherency function. It incorporates incoherence, wave-passage, and site-response effects.

By expressing the coherency function in the form:

$$\gamma_{ij}(\omega) = |\gamma_{ij}(\omega)| \exp[i\theta_{ij}(\omega)] \tag{19}$$

Der Kiureghian shows that the two factors in Equation (19) characterize distinct aspects of spatial variability:

- The modulus $|\gamma_{ij}(\omega)|$ describes the **incoherence** effect (variation in space) due to the scattering and the superpositioning of the waves at each location.
- The frequency-shift in the phasing of the two processes, $\exp[i\theta_{ij}(\omega)]$, is due to the two remaining effects: **wave-passage** (variation in time) and **site response**.

The nature and the magnitude of the variation in space (incoherence effect) and time (wave passage effects) have been studied based on actual records in region where the soil conditions are more or less uniform (e.g., Harichandran and Vanmarcke, 1986). Abrahamson, Schneider and Stepp (1991) proposed empirical spatial coherency functions. Variations in both space and time have been shown to increase with distance between the stations and with increasing frequency ω. The attenuation effect is insignificant for typical sizes of structures and has little influence on the coherency function (Der Kiureghian, 1996). Attenuation is included in the power spectral density function $S_{ij}(\omega)$ but not in the coherency function.

The most popular form of coherency function (e.g., Der Kiureghian and Neuenhofer 1992, Monti et al. 1996, Der Kiureghian 1996, Lupoi et al. 2005) is:

$$\gamma_{ij} = \exp\left[-\left(\frac{(2\pi f)\ a * d}{v_s}\right)^2\right] * \exp\left[i\frac{(2\pi f)\ d^L}{v_{app}}\right] * \exp\left[i\theta_{ij}^{soil}(\omega)\right] \qquad (20)$$

- The first term of Equation (20) is real-valued and models reflection/refraction effects. In this term, v_s is the shear-wave velocity of the waves (bedrock), d the distance between i and j and a is a parameter. Typically, one uses $\frac{v_s}{a} = 300m/s$ (e.g., Lupoi et al., 2005). This choice of v_s/a produces rather low values of $|\gamma_{ij}(\omega)|$. $\frac{v_s}{a} = \infty$ implies fully coherent waves.

- The second term in Equation (20) models the wave passage effect through a phase shift associated with the time lag τ_{ij} for the arrival of the waves at station j after

their arrival at station i. If v_{app} is the apparent surface wave velocity and d^L is the projected distance d along the direction of wave propagation then $\tau_{ij} = \frac{d^L}{v_{app}}$. Hence $v_{app} \to \infty$ models full coherence in time; and v_{app}=300m/s is usually considered in application (e.g., Lupoi et al., 2005).

- The Theoretical form of θ_{ij}^{soil} in Equation (20), which models the incoherence induced by soil variations, is $\theta_{ij}^{soil} = \tan^{-1}\frac{\mathrm{Im}\left[H_{soil\_i}(\omega)H_{soil\_j}(-\omega)\right]}{\mathrm{Re}\left[H_{soil\_i}(\omega)H_{soil\_j}(-\omega)\right]}$ where $H_{soil}(\omega)$ is the linear transfer function for soil (e.g., see Equation 11). The phase shift caused by the soil columns does not depend on the power spectral density of the bedrock motion or the distance between the two stations, but only on the characteristics of the two soil columns.

The vast majority of recent studies concerning the effect of spatial variation of ground motion on structural response finds that spatial variation in ground motion influence negatively the response of structures and should therefore be included in seismic design evaluations. The relative displacements between two piers are statistically larger when spatial variation of ground motion is considered than when it is assumed that all points experience the same ground motion (Sextos et al., 2003). The commonly adopted synchronous input procedure is not conservative when soil conditions differ along the structure (e.g., Shinozuka et al., 2000). Sextos et al. (2003) present a parametric study where results are expressed in terms of maximum relative pier top displacements (displacement between pier tops). Scenarios that include spatial variation of ground motion are normalized with respect to the synchronous-input base case. The vast majority of the ratios of the relative displacements are in the range 1 to 2. Hence, the relative displacements between pier tops are statistically larger when spatial variation of ground motion is considered than in the synchronous case. When loss of coherence and wave-passage are considered alone (no sites effect) the detrimental effect is not pronounced, and in some cases lightly favourable. But when sites effects are added, it is clearly observed that spatial variation of ground motion increases the relative

displacement between two piers by a factor of 1.5 to 2 with respect to the uniform base case. By taking into account inelastic behaviour, the response is amplified by factors ranging from 1 to 3 with respect to the uniform inelastic base case. The presence of non-homogeneous soil profile under the supports dominates over other sources of spatial variation (loss of coherence and wave-passage). This result is first reported by Monti and Pinto (1998), and confirmed by Shinozuka et al. (2000); Sextos et al. (2003) and Lupio et al. (2005). The different scenarios involving loss of coherence and wave-passage effects produce relatively small differences in the response; whereas when soil conditions differ, the magnitude of the response increases significantly (e.g., Shinozuka et al., 2000). It is suggested to set to one the third factor of the coherency function modelling site conditions (third factor of Equation 20). The problem of variation in site condition can be dealt with by using correlated ground motions that have specific response spectra appropriate to each site condition. This possibility is validated by Monti & Pinto, 1998; and in accordance with the findings of Shinozuka et al., 2000. As a result, in our model, where the variation of site condition is taken into account by using specific response spectra representative of the soil column at each location, the site conditions are included in the power spectral density function $S_{ij}(\omega)$ and will not appear in the coherency function.

In what follows, the coherency function γ_{ij} takes the simpler form:

$$\gamma_{ij}(\omega) = \exp\left[-\left(\frac{a*\omega*d}{v_s}\right)^2\right] * \exp\left[i\frac{\omega\, d^L}{v_{app}}\right] \tag{21}$$

2.2.3 Sensitivity Analysis

Due to the complexity of the problem, we have performed a series of analyses to estimate the effect and relative importance of each parameter or set of parameters. Specifically, we have considered

1) The variation in site conditions alone,

2) The spatial variation in ground motion, which adds incoherence and wave-passage effects to site variations,

3) The effect of train speed, support spacing, and earthquake characteristics (M, R).

As a reference, Table 2-5 gives the peak track acceleration Sa experienced by a stationary train for the two earthquake scenarios and for the two soil conditions that will be used in the analysis of Sa_d.

Sa (g)	7, 100km		7, 50km	
	PGA	Tst=0.4s	PGA	Tst=0.4s
Rock	0.04	0.06	0.1	0.18
Soil	*0.08*	*0.15*	*0.12*	*0.30*

Table 2-5 Peak Acceleration for a stationary train (in g)

One should compare Sa_d to Sa to assess the extent to which the acceleration due to track deformation increases the base acceleration. The resulting acceleration Sa_{tot} may be estimated by combining Sa_d and Sa as follow:

$$Sa_{tot} = \sqrt{Sa^2 + Sa_d^2} \tag{22}$$

a. Variation in Site Conditions alone

In order to appreciate the effect of varying site conditions (soil and structure) relative to incoherence and wave-passage, we start by evaluating Sa_d for the case of fully coherent waves ($\gamma_{ij} = 1$). The shift in phase due to the fact that the train reaches station j $\frac{d}{V}$ seconds after having reached station i is nevertheless kept. Two scenarios are presented: One assumes the same structural characteristics at the 3 supports, but considers variation in the soil columns (Figure 2-57). The second one models variation in structural conditions, but with identical soil conditions at all locations (Figure 2-58).

It should be noted that the acceleration Sa_d is zero when both the soil and the structure are identical along the track.

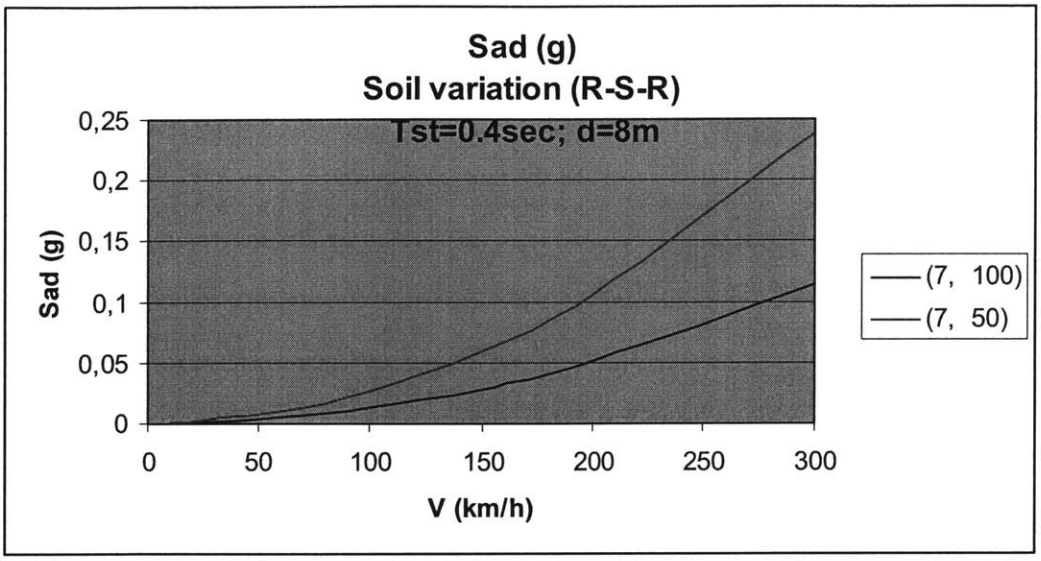

Figure 2-57 Acceleration due to track deformation - variation in soil conditions

Figure 2-57 gives Sa_d as a function of train speed for an earthquake of magnitude 7 at epicentral distance of 50 or 100 km. Results are for a natural period of the structure of 0.4 sec at all locations. The soil condition at locations 1 and 3 is rock ($v_{s30} = 620m/s$), and soft at location 2 ($v_{s30} = 350m/s$). The spacing of the support is set to 8m (typical distance between span in the JR East network).

Note that for (M, R) = (7, 100km), the peak ground acceleration (PGA) on soil is about 0.08g. A structure with natural period of 0.4s amplifies this base acceleration to $Sa(T_{st} = 0.4s) = 0.15g$. In the (M, R) = (7, 50km) case, PGA $\approx$ 0.12g on rock and the response of a structure with natural period of 0.4s amplifies this base acceleration to 0.3g (see Table 2-5).

Note that Sa_d varies proportionally to $\frac{1}{\left(d/V\right)^2}$ and is zero for a stationary train ($V = 0$).

Track deformation has small effects at ordinary speeds: for example, at 200km/h, and for the earthquake scenario (7, 100), Sa_d =0.05g. Combination with the base acceleration of 0.15g gives a total peak acceleration $Sa_{tot} = \sqrt{Sa^2 + Sa_d^2} = \sqrt{0.15^2 + 0.05^2} = 0.16g$, which is not significantly different from Sa. For (M, R)=(7, 50), Sa_d =0.1g. Compared with the base acceleration

of 0.3g, we obtain $Sa_{tot} = \sqrt{Sa^2 + Sa_d^2} = \sqrt{0.3^2 + 0.1^2} = 0.31g$, leading to the same conclusion. Nevertheless, as speed increases, the effect of varying soil conditions is more pronounced. For V=300km/h and for the earthquake scenario (7, 100), Sa_d=0.12g. This gives a total peak acceleration $Sa_{tot} = \sqrt{Sa^2 + Sa_d^2} = \sqrt{0.15^2 + 0.12^2} = 0.19g$. It is a 26% increase in the peak acceleration from the uniform case.

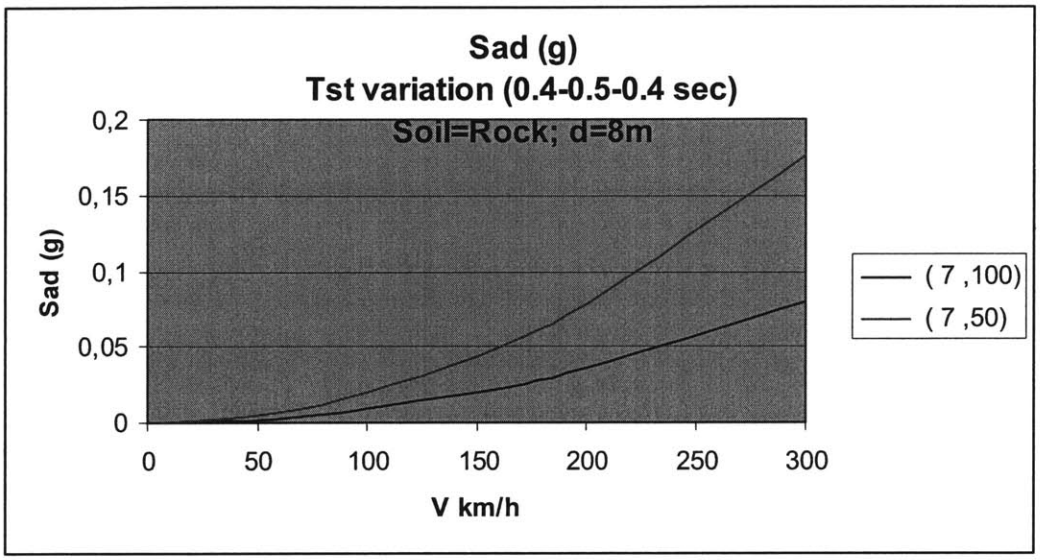

Figure 2-58 Acceleration due to track deformation - variation in structural characteristics

Similar results are obtained when the soil is uniform (rock), and the structural characteristics vary. As an example, Figure 2-58 shows results for a natural period of the structure of 0.4 sec at stations 1 and 3, and 0.5sec at station 2, on rock. In this specific case, at 300km/h and for the earthquake scenario (7, 100), Sa_d=0.08g. Combination with the base acceleration of 0.09g (Tst=0.4s, on rock) gives a total peak acceleration $Sa_{tot} = \sqrt{Sa^2 + Sa_d^2} = \sqrt{0.09^2 + 0.08^2} = 0.12g$, which is a 34% increase compared with the uniform case.

The effect of varying the spacing of the supports is presented in Figure 2-59. Sa_d is plotted for a given earthquake scenario and a given variability in structural conditions.

Two different spaces between supports are considered. In general, all over conditions being the same, Sa_d depends on support spacing d and train speed V as $\frac{1}{\left(d/V\right)^2}$.

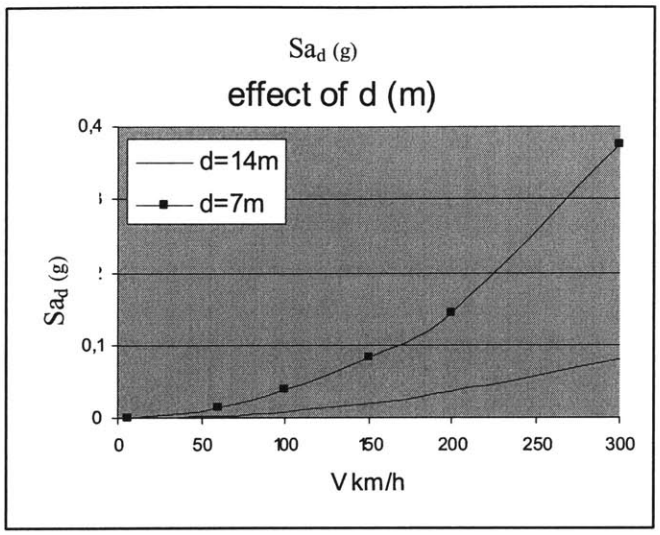

Figure 2-59 Acceleration due to track deformation - variation in the spacing of the support

From this first model, it is inferred that the acceleration due to track deformation Sa_d has small effects at ordinary speed but that it would become noticeable as the speed increases. We are interested in speed in a range from zero up to 400km/h. Along the Sanyo line in Japan, trains operate at a top speed of 300km/h since 1997.

Concerning the support spacing, the effect will be emphasized and noticeable for closely spaced supports. In this case, the train has to negotiate the waviness within a smaller distance, making it therefore more challenging than if the same amount of displacements were spread on a longer distance. JR East estimates an average of 8m between span. Based on this first series of analyses, for an average distance between span of 8m, Sa_d becomes noticeable at speed of 300km/h and higher.

The importance of the acceleration due to track deformation Sa_d relatively to the base acceleration Sa is analysed with more detail later on, after adding the coherency function.

b. Introduction of spatial variation of ground motion

We now include the effect of lack of ground motion coherency (Equation 21). Incoherence and wave-passage effects are considered in addition to site variations.

Figure 2-60 and Figure 2-61 show Sa_d when considering only spatially varying soil or structural conditions and when in addition the loss of bedrock motion coherency is included. Both figures are for M=7 and R=50km and for a support spacing d of 8m. Figure 2-60 shows results for variation in soil conditions; whereas Figure 2-61 analyses a case with variable structural characteristics.

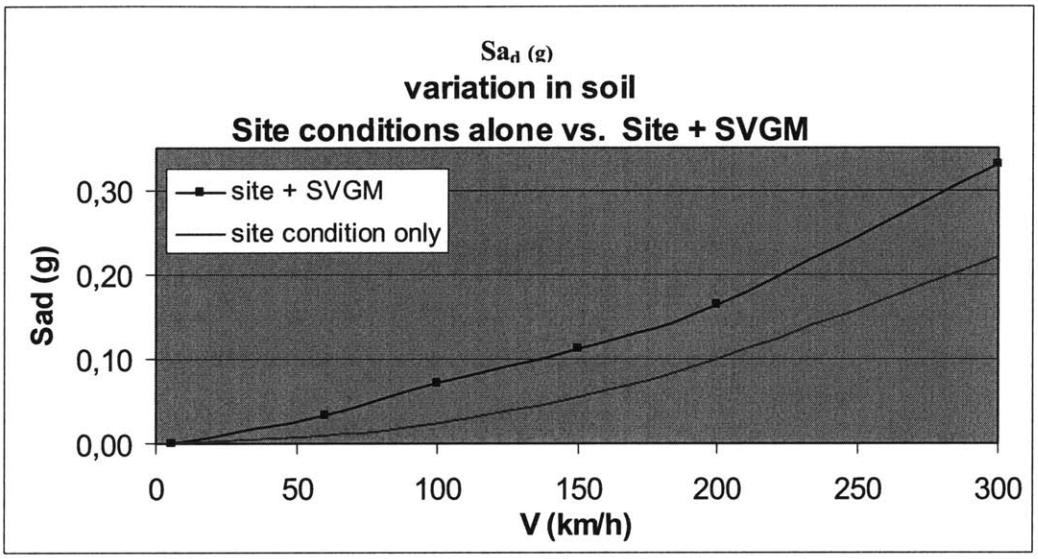

Figure 2-60 Acceleration due to track deformation - variation in soil conditions vs. soil conditions and SVGM

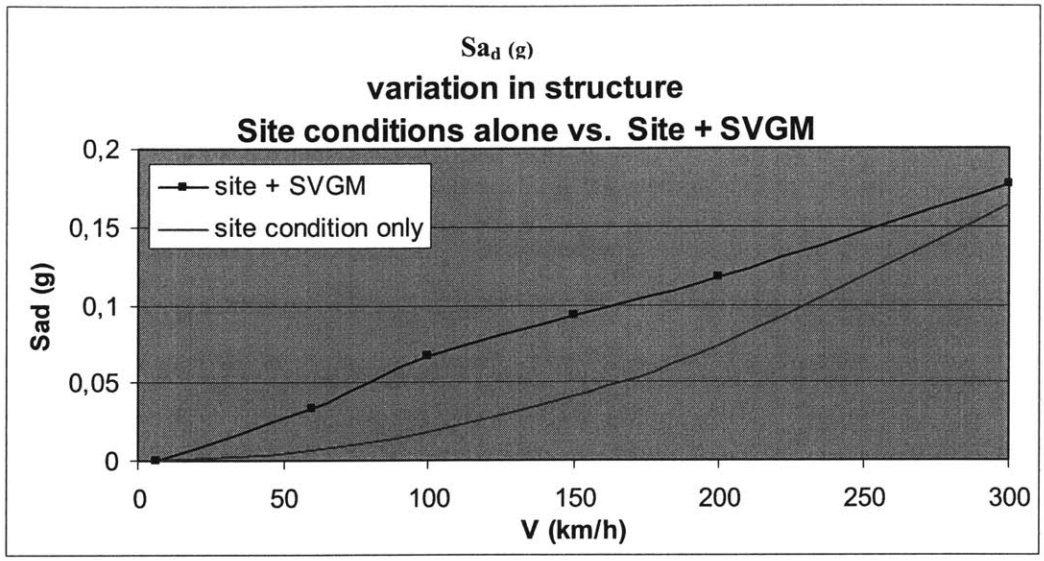

Figure 2-61 Acceleration due to track deformation - variation in structural characteristics vs. structural characteristics and SVGM

Notice that adding spatial variation of ground motion through the coherency function increases the acceleration due to track deformation.

Figure 2-62 re-investigates the dependence in the spacing of the support, for an earthquake of magnitude 7 and distances to the epicentre of 50km.

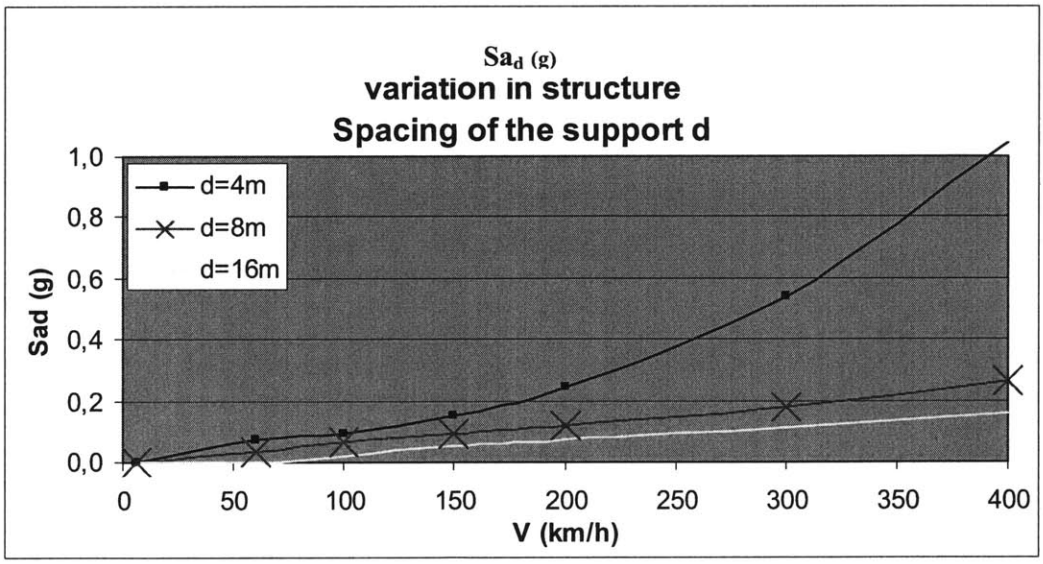

Figure 2-62 Acceleration due to track deformation – effect of the spacing of the support

Figure 2-63 presents the relative effect of soil and structural variations, for two earthquake scenarios. For each earthquake scenario, two types of variation are shown:

One assumes the same structural characteristics at the 3 supports (natural period of the structure set to 0.4s), but considers variation in the soil columns: rock condition, as defined by $v_{s_{30}} = 620m/s$, at stations 1 and 3, and soft soil, with $v_{s_{30}} = 320m/s$, at station 2. The second one models variation in structural conditions (Tst=0.4s at stations 1 and 3, and Tst=0.5s at station 2), but with identical soil conditions at all locations (rock). In this specific case, with the parameters used to model structural and soil variation, the soil variations dominate over the structure variations. Nevertheless, no general statement can be drawn from this specific example.

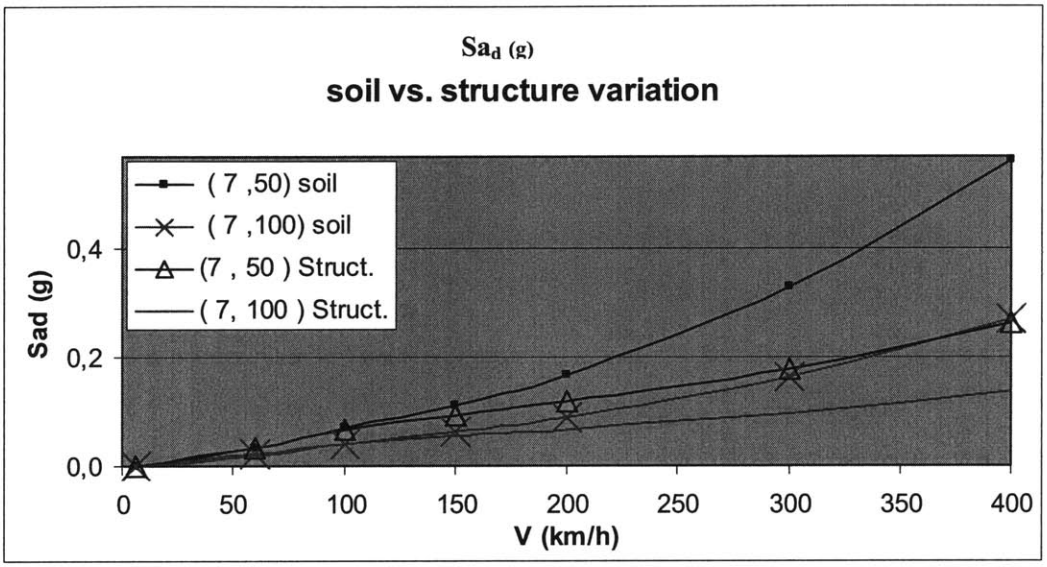

Figure 2-63 Acceleration due to track deformation – soil vs. structural variation

The total accelerations in Table 2-6 and Table 2-7 are obtained by combining Sa_d and Sa as: $Sa_{tot} = \sqrt{Sa^2 + Sa_d^2}$. The percentage increase is relative to the base acceleration Sa. The acceleration due to track deformation has small effects at ordinary speed: Table 2-6 shows the effect of Sa_d for a train speed of 100km/h. The effect of Sa_d is not noticeable. It becomes noticeable as the speed increases: in Table 2-7, the percentage increase in Sa due to Sa_d is of about 50% for a train speed of 300km/h.

Accelerations (g)	variation in soil		variation in structure	
	(7, 100)	(7, 50)	(7, 100)	(7, 50)
Sa	0.15	0.3	0.06	0.18
Sa_d (v=100km/h)	0.042	0.072	0.041	0.068
Sa_{tot}	0.16	0.31	0.07	0.19
% increase	**4%**	**3%**	**21%**	**7%**

Table 2-6 Relative importance of Sad compared to Sa at V=100km/h

Accelerations (g)	variation in soil		variation in structure	
	(7, 100)	(7, 50)	(7, 100)	(7, 50)
Sa	0.15	0.3	0.06	0.18
Sa_d (v=300km/h)	0.16	0.33	0.097	0.18
Sa_{tot}	0.22	0.45	0.11	0.25
% increase	**46%**	**49%**	**90%**	**41%**

Table 2-7 Relative importance of Sad compared to Sa at V=300km/h

Figure 2-64 and Figure 2-65 show the comparison between the probability of derailment of a stationary train and the probability of derailment of a moving train on wavy tracks. Figure 2-64 shows the results for varying structural condition, whereas Figure 2-65 shows the results obtained for varying soil conditions. For v=100km/s, the increase is very small, for v=300km/h, the increase in the probability of derailment is of importance.

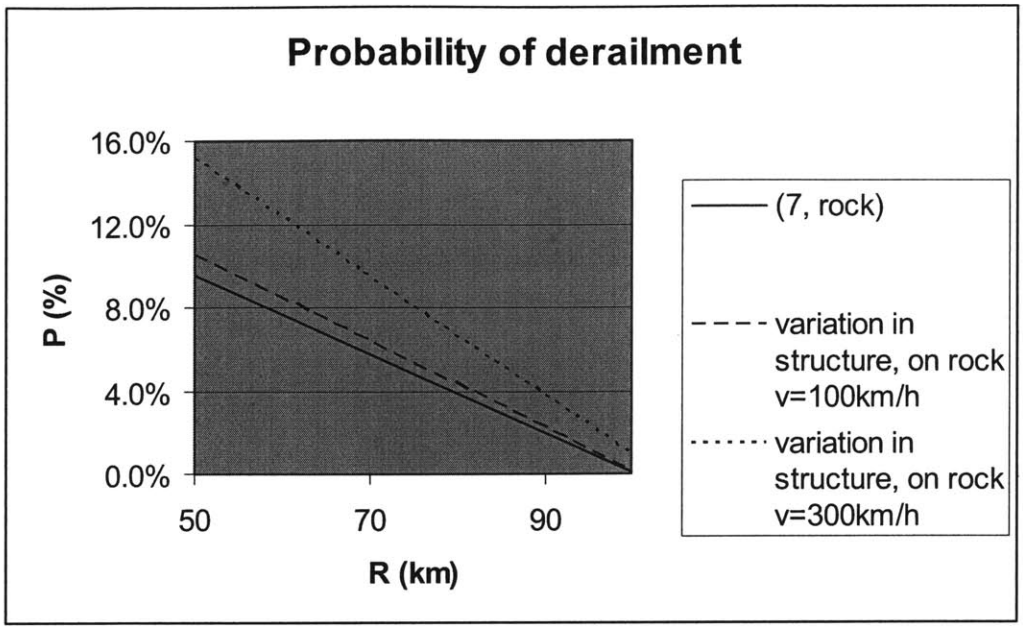

Figure 2-64 Comparison between derailment of a stationary train and derailment of a moving train on wavy tracks for M=7 on rock, and for varying structural characteristics

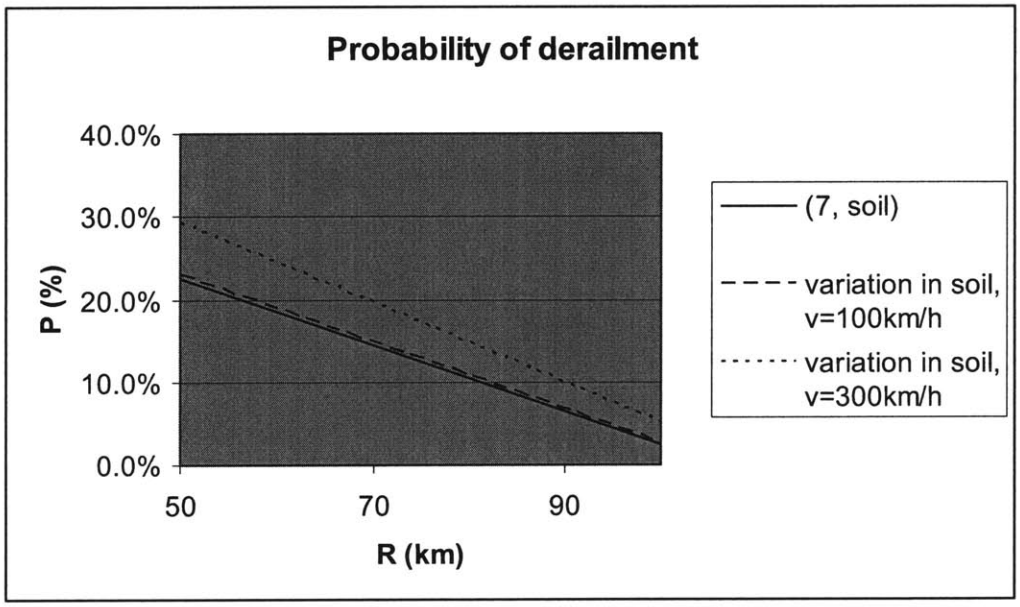

Figure 2-65 Comparison between derailment of a stationary train and derailment of a moving train on wavy tracks for M=7 and for varying soil conditions at Tst=0.4s.

Based on this analysis, the peak acceleration of a stationary train Sa is expected to increase by a factor between 1 and 2 when considering a moving train on varying site conditions. The number of cases analyzed in this study is not sufficient to draw more

specific conclusions concerning the ratio $\frac{Sa_{tot}}{Sa}$. Nevertheless, this section provides a general framework that can be used for parametric studies of the ratio $\frac{Sa_{tot}}{Sa}$ for different scenarios of variation in soil and structural characteristics. From this analysis, it can be concluded that the acceleration due to track deformation Sa_d has small effects at ordinary speed but that it becomes noticeable as the speed increases. Concerning the support spacing, the effect will be emphasized and noticeable for closely spaced supports. As a first reference, for an average of 8m between supports, Sa_d becomes noticeable at speed of 300km/h and higher and may increase the peak acceleration by a factor of 1.5 in some cases.

Re-Evaluation of the Niigata Case:

In the Niigata case, sudden shifts in site conditions may have induced differential structural responses. The train was just out of a tunnel and entering a viaduct that presented sharp discontinuities in structural conditions. In light of the results concerning spatial variability of ground motion, the base acceleration due to track motion at a single location Sa=0.9g may be increased by a factor of 1.5; thus, in the Niigata case, one can consider that the total acceleration was Sa_{tot}=1.35g. This yield a probability of derailment $P[Derailment|Sd = 19cm, Sa = 1.35g] = 90\%$.

Already, without taking into account the discontinuities in site conditions, the situation was rather precarious: the probability of derailment under vibratory motion for a stationary train was 87%. When the discontinuities in site conditions are considered, the situation is worst, for the probability of derailment under vibratory motion for a moving train becomes 90%.

3 Inelastic Analysis

In the previous chapter, we assumed linear dynamic behavior of the soil and the structure. In this section, nonlinearities in the structural response and permanent deformations are included.

In linear analysis, the acceleration response spectra were obtained by filtering the bedrock ground motion through a linear soil filter and a linear structural filter. Considering that most structures behave inelastically in a major earthquake, this linear approach may not be appropriate to describe seismic demands. Parameters that describe the inelastic behaviour of a structure under seismic conditions are the ductility demand μ, which measures the imposed post-elastic deformation on a member; and the inelastic strength demand which is the yield strength required to limit the ductility ratio μ to a given value.

In Section 3.1, we re-evaluate derailment due to vibratory motion by considering inelastic behaviour of the structure. The soil is assumed to remain linear elastic, and the structure is assumed to behave like an elasto-plastic SDOF system. In Section 3.2, permanent deformations are included, and derailment due to running on damaged tracks is considered. A method based on residual displacement is presented. In this approach, derailment of the second type occurs when the residual displacement of the track exceeds a displacement limit $D_{\lim it}$. Also in this analysis we assume that the soil is linear elastic and the structure elasto-plastic. Spatial dependence of damage is considered, including train speed in the model.

3.1 Derailment during Ground Motion

In this section, we re-consider derailment by vibratory motion under the assumption that the soil behaves linearly whereas the structure has elasto-plastic behaviour. If the linear elastic acceleration demand $Sa_{el}(\omega_{st})$ is less than the acceleration at yielding Sa_{yield}, the elastic analysis presented in the previous chapter is adequate: both the peak acceleration and the peak displacement remain unchanged. When $Sa_{el}(\omega_{st})$

exceeds Sa_{yield}, the acceleration demand equals to $Sa_{yield}(\omega_{st})$. In this case, non-linear behaviour in the structure reduces the peak elastic acceleration to the acceleration at yielding, but it also increases the peak relative displacement. Criteria for derailment are in terms of both peak acceleration and peak absolute displacement. Therefore, one must consider the trade-off between the increase in displacement and the decrease in acceleration. Specifically, we determine whether the increase in relative displacement may increase sufficiently the absolute displacement to augment the probability of derailment with respect to the elastic case. A brief review of the demand parameters when considering inelastic behaviour is presented first. Then, a method to evaluate the probability of derailment is presented.

One effect produced by nonlinear behavior in the structure is the reduction in lateral strength demand Sa. Another effect is an increase in displacement demand. The parameters that describe these effects are the strength ratio R, and the ductility demand μ. They are described next.

The relative elastic lateral strength is measured by the relative elastic strength ratio R. It is defined as:

$$R = \frac{Sa_{el}}{Sa_{yield}}$$

where Sa_{yield} is the lateral acceleration at yielding, and Sa_{el} represent the lateral strength required to maintain the system elastic. It is the absolute acceleration of the elastic system, sometimes referred to as the elastic strength demand.

The ductility inelastic displacement ratio μ measures the imposed post-elastic deformation on a member and is defined as the ratio of the maximum lateral inelastic displacement $D_{inelastic}$ to the yield displacement D_{yield}:

$$\mu = \frac{D_{inelastic}}{D_{yield}}$$

Note that the displacements are relative to the ground. These parameters are summarized in Figure 3-1.

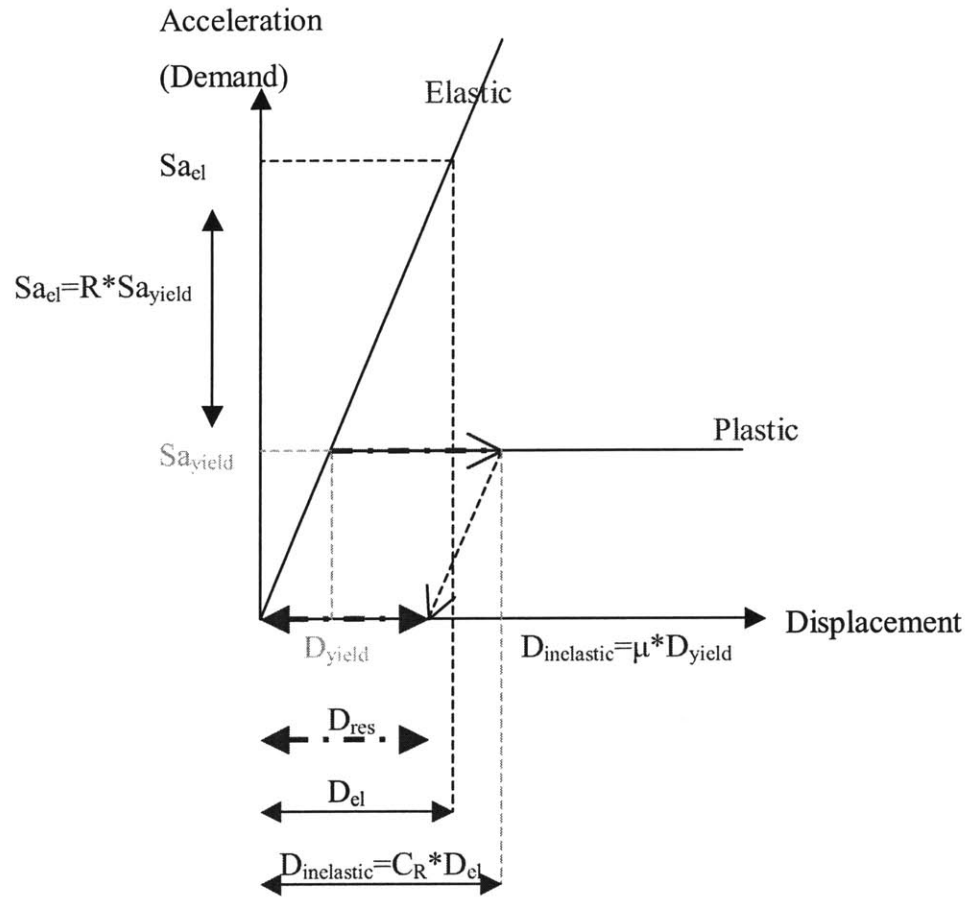

Figure 3-1 Demand parameters when considering inelastic behaviour (elasto-plastic system)

The inelastic displacement ratio C_R is defined as the maximum lateral inelastic displacement demand $D_{inelastic}$ divided by the maximum lateral elastic displacement demand D_{el} on systems with the same mass and initial stiffness (i.e. same period of vibration) when subjected to the same earthquake (i.e. constant relative strength):

$$C_R = \frac{D_{inelastic}}{D_{el}} \tag{23}$$

with $C_R = 1$ in the elastic range ($R \leq 1$) and C_R tends to be greater than one when inelastic behaviour are considered. Displacements are relative to the ground.

Ruiz-Garcia and Miranda (2003) studied how C_R depends on the natural period of the structure T_{st} for different values of the relative elastic strength R. In this investigation non-linear regression analyses on C_R yield to the following equation:

$$C_R = 1 + \left[\frac{1}{a\left(T_{st}/T_s\right)^b} - \frac{1}{c} \right](R-1) \tag{24}$$

Where T_{st} is the natural period of the structure, T_s is a characteristic period at the site and a, b and c are constants that depend on site condition. The effect of soil type on C_R is small and in what follows we use the ratio averaged over the different soil types. Equation (24) provides estimates of C_R as a function of R and T_{st}.

For $R \leq 1$, the structure behaves elastically, and the inelastic displacement ratio $C_R = 1$. The values of the peak acceleration and the peak displacement remain unchanged.
For $R > 1$, the peak acceleration decreases: $Sa_{inelastic} = Sa_{yield}$, and the inelastic displacement ratio $C_R > 1$ implies that the peak relative displacement increases: $D_{inelastic} = C_R * D_{el}$.

Given R, the ductility demand μ can be computed with the constant relative strength inelastic displacement ratios C_R. The relationship between R and the expected value of μ can be expressed in terms of the expected value of the inelastic displacement ratio C_R as follows (Ruiz-Garcia and Miranda, 2003):

$$E[\mu] = R * E[C_R]$$

Therefore, the constant relative strength ratio C_R like those reported by Ruiz-Garcia and Miranda (2003) can be used to obtain the maximum inelastic displacement when R is know for a given ground motion.

The absolute acceleration *Sd* may be estimated as:

$$Sd = \sqrt{PGD^2 + D_{inelastic}^2} \tag{25}$$

Figure 3-2 shows the expected value of C_R for R=2, 4 and 6; using Equation (24) with $T_s = 0.85s$.

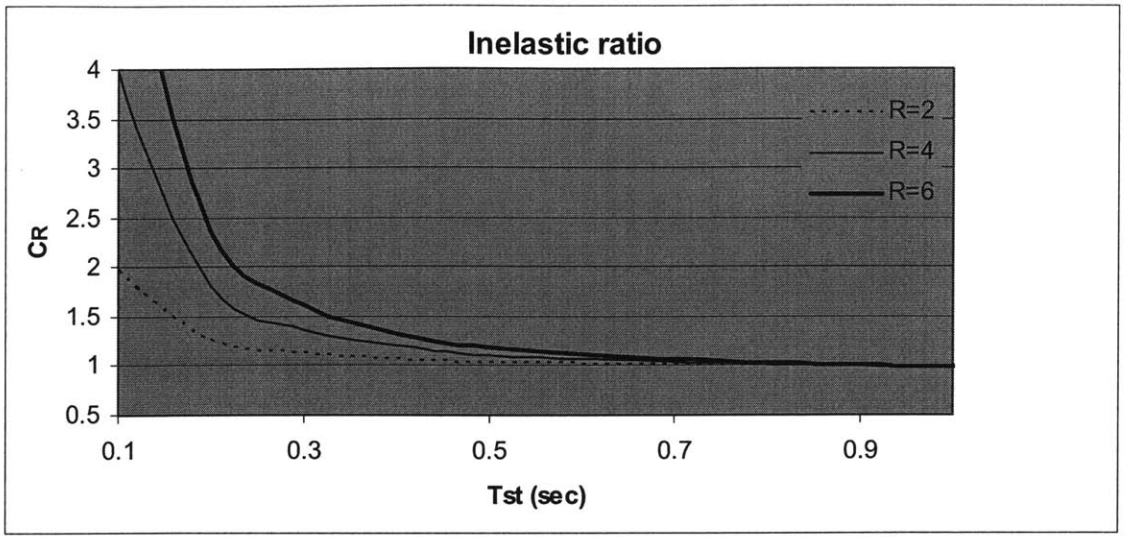

Figure 3-2 Inelastic displacement ratio C_R as a function of the natural period of the structure Tst, for relative strength R=2, 4 and 6 (Miranda, 2003)

Clearly, for flexible structures ($T_{st} \geq 0.7$s) the inelastic displacement equals the elastic displacement; and thus even for large values of R. Therefore, for structures with natural period greater than 0.7 seconds, the elastic analysis is only conservative: in this range, nonlinear behavior in the structure produces only a reduction in the lateral acceleration; the increase in relative displacement being not noticeable, the increase in absolute displacement *Sd* as reported in Equation (25) is even more negligible. The elastic analysis for $T_{st} \geq 0.7$s yields conservative results when *Sa* exceeds Sa_{yield}. Sa_{yield} for flexible structures ($T_{st} \geq 0.7$s) are low so it is likely that *Sa* exceeds Sa_{yield}. For example, in the case of a natural period of T_{st}=1sec, the peak acceleration exceeds Sa_{yield} in one scenario, for M=7.5 and R=20km.

For stiffer structures (T_{st} <0.7s), there is a more pronounced increase in the displacement produced by nonlinear behavior in the structure. Note that this increase is in the relative displacement. This range is of particular interest and investigated next.

Figure 3-3 shows C_R as a function of the relative strength R for natural periods of the structure Tst=0.3, 0.4 and 0.5s.

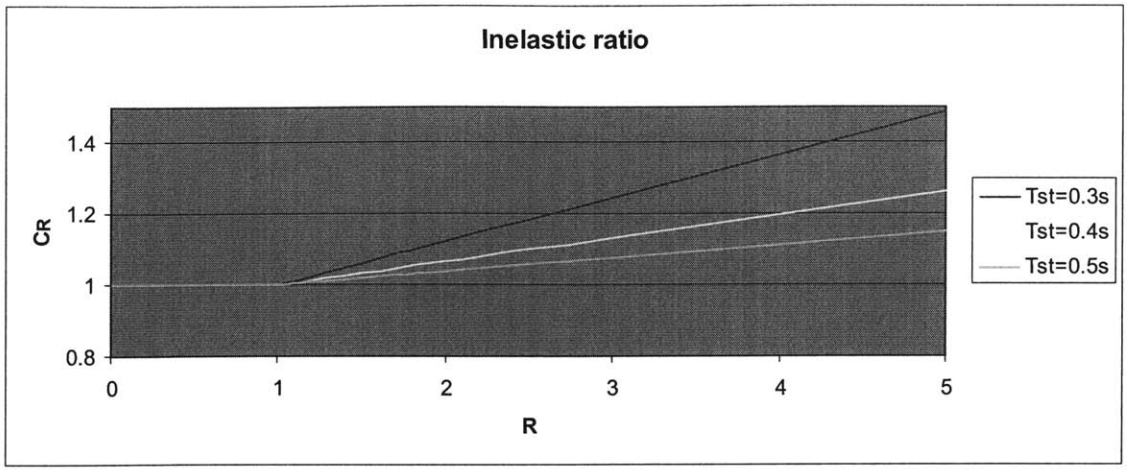

Figure 3-3 Inelastic displacement ratio C_R as a function of the relative strength R for natural period of the structure Tst=0.3, 0.4 and 0.5s (Miranda, 2003)

The amplitude of C_R increases as the natural period of the structure decreases. The peak relative displacement increases for stiffer structures. Figure 3-4 summarizes the different cases. In zone 1, the elastic analysis is adequate. In zone 2, the elastic analysis is conservative. In zone 3, there is a trade-off between the increase in Sd and the decrease in Sa.

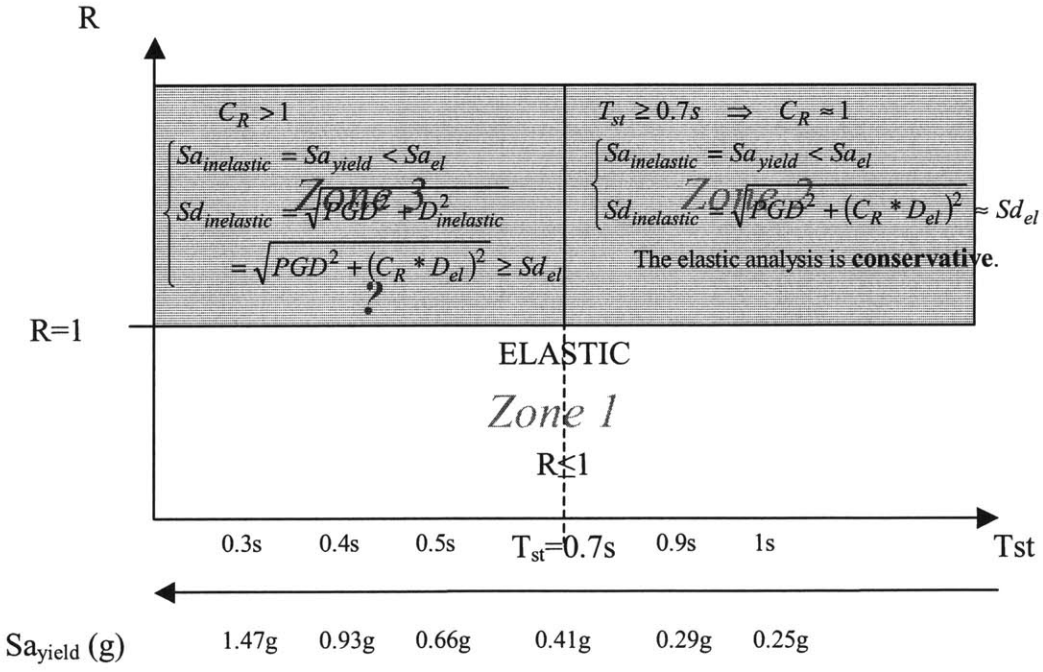

Figure 3-4 Trade-off between increase in Sd and decrease in Sa

As shown in Figure 3-4, the trade-off between the increase in Sa and the decrease in Sd is to be considered when T_{st}<0.7s. Nevertheless, three observations lead us to consider that the elastic analysis remains conservative even in Zone 3:

1) In this range, for structures with natural periods T_{st}>0.3s, and for low-level of lateral strength ratio (R<2), C_R<1.13 (see Figure 3-3). Thus the increase in relative displacement due to the non-linear behaviour remains small. For example, for R=2, the spectral acceleration decreases by a factor of 2 whereas the relative displacement increases by less than 13%.

2) In addition, For T_{st}<1s, the peak ground displacement dominates the absolute displacement: the relative displacement is thus small compared with the peak ground displacement. Therefore, the increase in the absolute displacement must not be noticeable. Equation (24) gives: $Sd_{inelastic} = \sqrt{PGD^2 + D_{inelastic}^2} = \sqrt{PGD^2 + (C_R * D_{el})^2}$. For T_{st}=0.3s, $D_{el} < PGD/3$, hence, a 13% increase in D_{el} only yields a 1.6% increases in absolute displacement. By comparison, *Sa* decreases by a factor of 2 in this example.

3) Finally, Sa_{yield} increases as the natural period of the structure decreases. Thus C_R is high when the acceleration at yielding is high (see Figure 3-4). Table 3-1 shows the displacements and accelerations at yielding D_{yield} and A_{yield}; and the displacements D_{max} that cause the ductility capacity of the viaduct to be exceeded. D_{yield} and D_{max} are from JR East assessments of viaduct damages through simulations; A_{yield} is computed using $A_{yield} = \omega_{st}^2 D_{yield}$.

Tst	Dyield	Ayielding	Dmax
0.3s	3.29cm	1.47g	11.10cm
0.4s	3.71cm	0.93g	12.80cm
0.5s	4.13cm	0.66g	14.50cm
0.75s	5.17cm	0.37g	18.75cm
1s	6.22cm	0.25g	23.00cm

Table 3-1 Displacements (cm) and Accelerations (g) at yielding and before failure (JR East viaduct damage assessment)

As a result, two observations are made:

1) When considering very flexible structures (T_{st}>0.7s) , the elastic criteria are conservative compared with results that could be obtained by allowing inelastic behaviours. Inelastic behaviour produces a decrease in the peak acceleration, the increase in the peak displacement for T_{st}>0.7s being not noticeable. Since Sa_{yield} for flexible structures are low, the elastic analysis may be quite conservative.

2) For stiffer structures, the peak ground displacement largely dominates the relative displacement. Hence, as a first approximation, one can assume that the increase in absolute displacement is negligible and that the elastic analysis is still conservative.

In what follows, we re-evaluate the probability of derailment under vibratory motion for the 3 scenarios presented in the elastic case: no structure (criteria for derailment in terms of PGA PGD), and for a natural period of the structure of T_{st}=0.4s and T_{st}=1s (see Figure 2-46, Figure 2-47 and Figure 2-48 in the elastic case).

When there is no structure, the elastic case remains unchanged.

For T_{st}=0.4s, and for the 3 earthquake scenarios considered previously (M=6, 7 and 7.5 and R=20, 50 and 100km), the expected value of Sa_{el} never exceeds Sa_{yield}=0.94g. To obtain the probability of derailment, one must consider the probability that Sa_{el} exceeds Sa_{yield}.

For T_{st}=1s, and for the 3 earthquake scenarios aforementioned, Sa_{el} exceeds Sa_{yield}=0.25g once, in the case M=7.5 and R=20. In the elastic case, the probabilities of derailment in this scenario were 82.7% and 86.6% for rock and soil respectively. They fall to 38.5% and 38.6% when considering the reduction in *Sa* in the inelastic case.

As a conclusion, the elastic criteria are in most cases conservative compared with results that are obtained by allowing inelastic behaviours. The order of magnitude of the demand parameters at stake when considering seismic loads (peak displacement and peak acceleration) are in most cases within the elastic range for stiff structures and an elastic analysis may be considered adequate. For more flexible structure, as Sa_{yield} takes

lower values, the decrease in *Sa* is of importance and may yield to lower probability of derailment when considering inelastic behaviours.

Next, we consider the second cause of derailment due to permanent deformations of the track.

3.2 Derailment after the Ground Motion due to Track Damage

The cause of derailment considered so far has been excessive track vibration and deformation during the ground motion. Now we consider the second cause of derailment, which is permanent track deformation after the ground motion as ended. Structural damages are primarily the result of lateral deformations (Garcia and Miranda, 2005). Section 3.2.1 reviews studies where derailment is related to the peak displacement demands on the supporting structure. However, excessive residual deformation appears as a more pertinent criterion for derailment due to running on damaged tracks. A method based on residual displacements is presented in Section 3.2.2.

3.2.1 Previous Studies of Derailment due to Permanent Track Deformation

Papadimitriou (1995) presented an evaluation of the probability of train derailment due to permanent track damage. JR East Research Laboratory developed its own evaluation using semi-empirical results of viaduct failures based on simulations. These two methods relate derailment due to track damage to peak deformation demand.

Papadimitriou (1995) assumed that a train does not derail unless the viaduct structure it runs on has exceeded its ductility capacity estimated to be 4 for a typical Shinkansen viaduct. For a viaduct height of 10m designed under normal soil conditions, the viaduct top displacement at yielding $Sd_{yielding}$ was estimated to be between 3.1 and 3.4cm. Hence, the maximum peak displacement demand at failure is assessed to be between 12.4 and 13.6cm. The median spectral accelerations at yielding for different natural periods were estimated assuming $Sa_{yield} = \omega_{st}^2 Sd_{yield}$. The median spectral acceleration Sa_{limit} that causes the ductility capacity of the viaduct to be exceeded are obtained through the strength reduction factor $R(\mu) = {}^{S_{a\,\lim}}\!/_{S_{a\ yielding}}$ by which the median resistance relative to first yielding $S_{a\ yielding}$ is increased to obtain Sa_{limit}. Table 3-2 summarizes the values of Sa_{yield}, R and Sa_{limit} for different natural periods of the structure.

Tst (sec)	$Sa_{yielding}$ range (in g)	$R(\mu = 4)$	Sa_{limit} (in g)
0.3	1.36 – 1.49	2.2	2.99 – 3.28
0.4	0.76 – 0.84	2.3	1.75 – 1.93
0.5	0.49 – 0.54	2.4	1.18 – 1.30

Table 3-2 Median spectral acceleration at yielding

It is assumed that the structural resistance of the structure in terms of S_a follows a log-normal distribution (NIBS Technical Manual, 1994). The median resistance of the structure is Sa_{limit} and the value of the logarithm standard deviation $\sigma_{\ln R}$ is based on results on literature on the seismic fragility of framed reinforced concrete structures and set at $\sigma_{\ln R} = 0.4$. The median values of Sa_{limit} shown in Table 3-2 are used to evaluate the probability of structural damage in Figure 3-5.

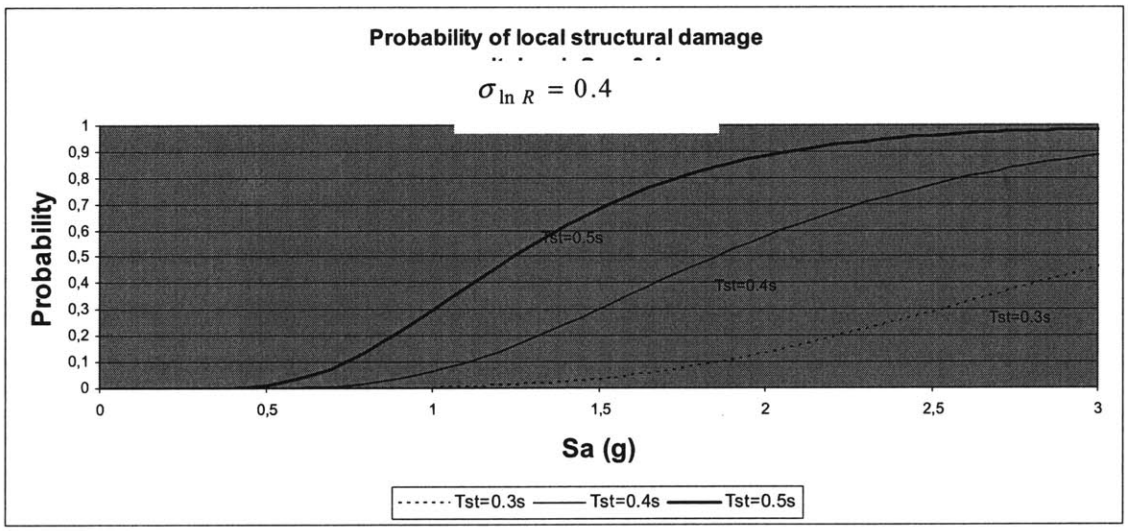

Figure 3-5 Probability of local structural damage for normal soil condition and for Tst=0.3, 0.4 and 0.5s

Estimates of the probability of local structural damage given *Sa* as reported by Papadimitriou (1995) are listed in Table 3-3. In addition, it shows the corresponding probability of derailment by vibratory motion, from our study. Derailment by vibratory motion dominates.

Sa (g)	0.1g	0.3g	0.5g	1g	1.5g
Probability of derailment by track damage (papadimitriou, 1995)	0.0000%	0.0002%	0.0367%	5.01%	26.43%
Sd_{rel} (cm)	0.40	1.19	1.99	3.98	5.97
PGD (cm)	5.17	10.99	15.60	25.10	33.16
Sd_{abs} (cm)	**5.19**	**11.06**	**15.73**	**25.42**	**33.69**
Probability of derailment (%) by vibration (our study)	1.57%	36.45%	67.42%	92.66%	97.54%

Table 3-3 Probability of derailment by track damage (Papadimitriou, 1995) and by vibratory motion (our study).

Figure 3-6 shows the comparison between the two modes of derailment. Clearly, derailment by local track damage does not dominate.

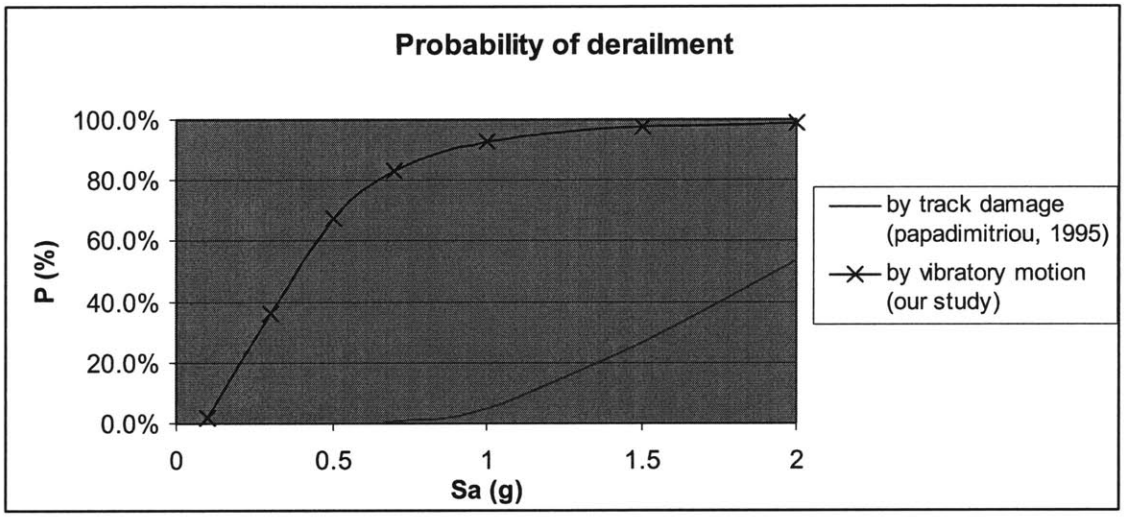

Figure 3-6 Comparison between derailment by track damage (papadimitriou) and by vibratory motion.

JR East research laboratory developed its own evaluation of damaged spans using semi-empirical results based on simulations. In Papadimitriou (1995) work, one level of damage was considered. In JR East work, the resistance performance is evaluated for 4 different levels: shear failure, yielding, maximum moment and ultimate bending moment (see Figure 3-7 below). First, the 4 displacement magnitude limits D_{limit} corresponding to the 4 damage levels are evaluated for different structures; then, the maximum response displacement magnitude D_{max} are calculated as a function of earthquake intensity (SI).

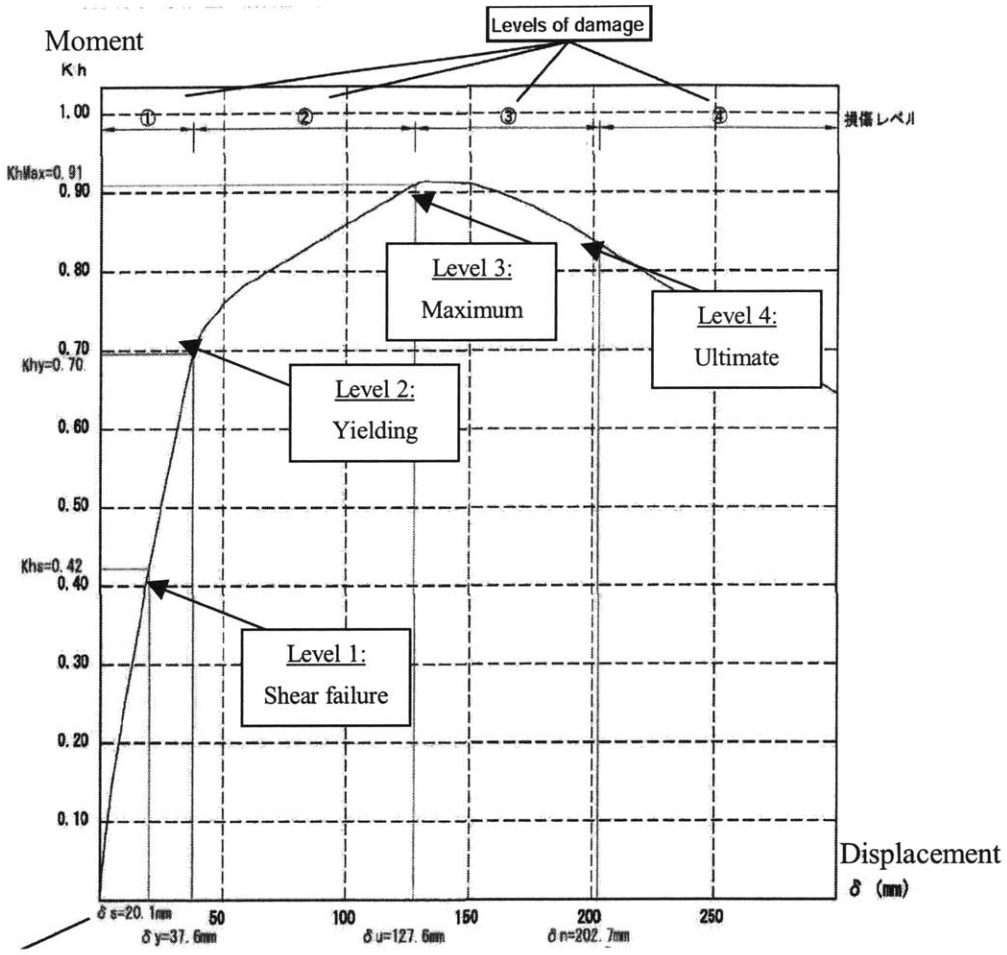

Figure 3-7 Levels of damage - Moment as function of displacement (JR East, 2005)

First, six types of representative viaducts were selected, each characterized by different foundations, upper structure shapes, height of columns, shearing resistance ratios, etc. Static non-linear analyses in the rail direction and at right angle to the rails were conducted to evaluate the earthquake resistance performance of the structures in terms of the displacement magnitude limit D_{limit} for each damage level. Table 3-4 shows an example of D_{limit} values obtained for a particular viaduct (Tst=0.5sec).

D_{limit} (cm) of a specific viaduct for different damage levels			
Level 1 shear failure	Level 2 yielding	Level 3 maximum	Level 4 ultimate
2,49cm	4,99cm	22,99cm	31,24cm

Table 3-4: Example of D_{limit} for a specific viaduct and for different level of damages

Figure 3-8 shows the displacement limits as function of the natural period of the structure Tst. The relationships are obtained by linear regressions on the simulation results.

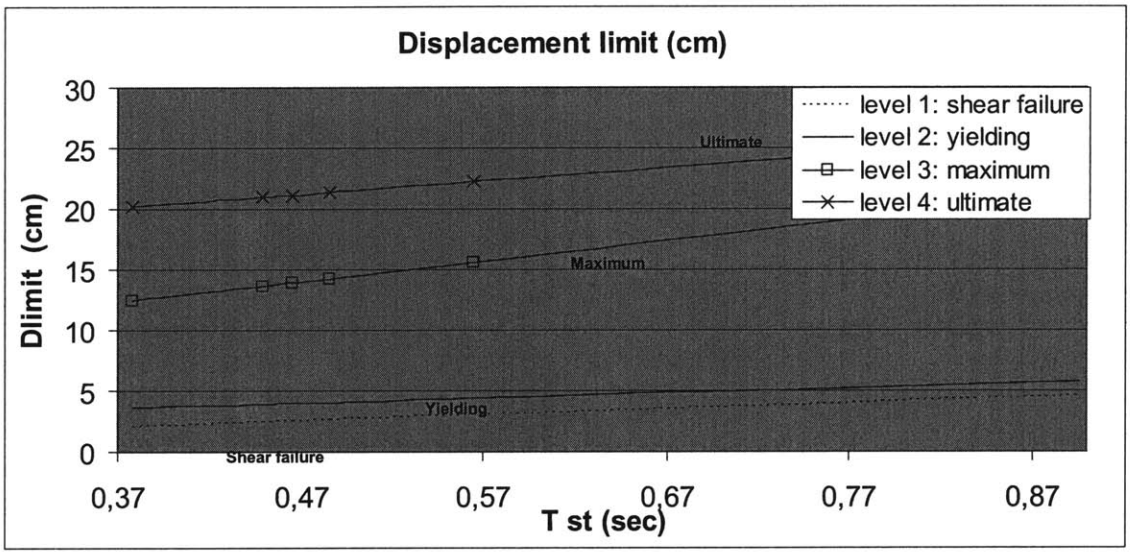

Figure 3-8 Displacement limits as a function of the natural period of the structure (JR East simulation)

Second, the relationship between ground motion intensity – measured in SI value – and peak displacement D_{max} was assessed by conducting dynamic response analysis using numerical models for the frameworks of the viaducts and ground motion time history as vibratory inputs.

Table 3-5 shows examples of D_{max} values for a specific viaduct (same viaduct as in table Table 3-4) as a function of earthquake intensity (SI).

Mean of D_{max}(cm) as function of SI(cm/s) for T_{st}=0.5sec									
SI(cm/s)	20	30	40	50	60	70	80	90	100
D_{max}(cm)	2.3cm	3.4cm	4.8cm	9.0cm	11.9cm	18.6cm	19.8cm	20.8cm	23.6cm
σ_{lnD}	0.23	0.20	0.24	0.56	0.47	0.44	0.37	0.35	0.27

Table 3-5: Example of D_{max} for a specific viaduct (Tst=0.5sec), as a function of SI (cm/s).

It is then assumed that the logarithm displacement ratio $\ln\left(\frac{D_{\max}}{D_{\lim it}}\right)$ follows a normal distribution. The standard deviations of the lognormal distribution are in the range 0.25 and 0.45. The damage probability for each damage level was calculated as the probability that the logarithmic displacement ratio would be positive. Figure 3-9 shows an example of fragility curves for viaduct damage for T_{st}=0.5s.

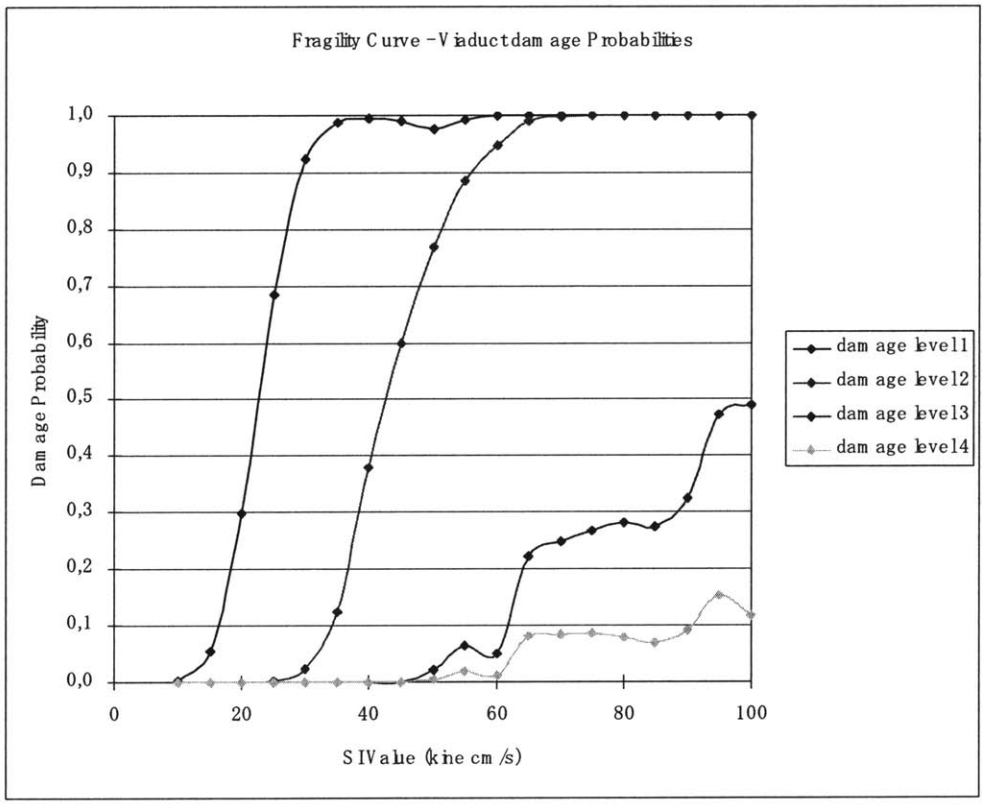

Figure 3-9: Example of a fragility curve for Tst=0.5s.

In Papadimitriou (1995), $3.1cm \le Sd_{yielding} \le 3.4cm$. JR East's estimates of displacement at yielding, as shown in Figure 3-8, are of about 4cm for T_{st}= 0.4sec. The two models are in good agreement. Failure in Papadimitriou's model occurs when the

displacement exceeds the ductility capacity. This corresponds to a damage level of 3 with the JR East notations. To evaluate the probability of derailment by track damage with the methodology used by JR East, one should consider damage level 3.

Results for the first mode of derailment (by vibration during the ground motion) are compared to the results for the second mode (derailment by damaged tracks with level 3 as the critical level); according to JR east simulations. Figure 3-10 shows the comparison between derailment by vibratory motion and derailment by track damage for Tst=0.4s; whereas Figure 3-11 shows the comparison between the two modes for Tst=1s.

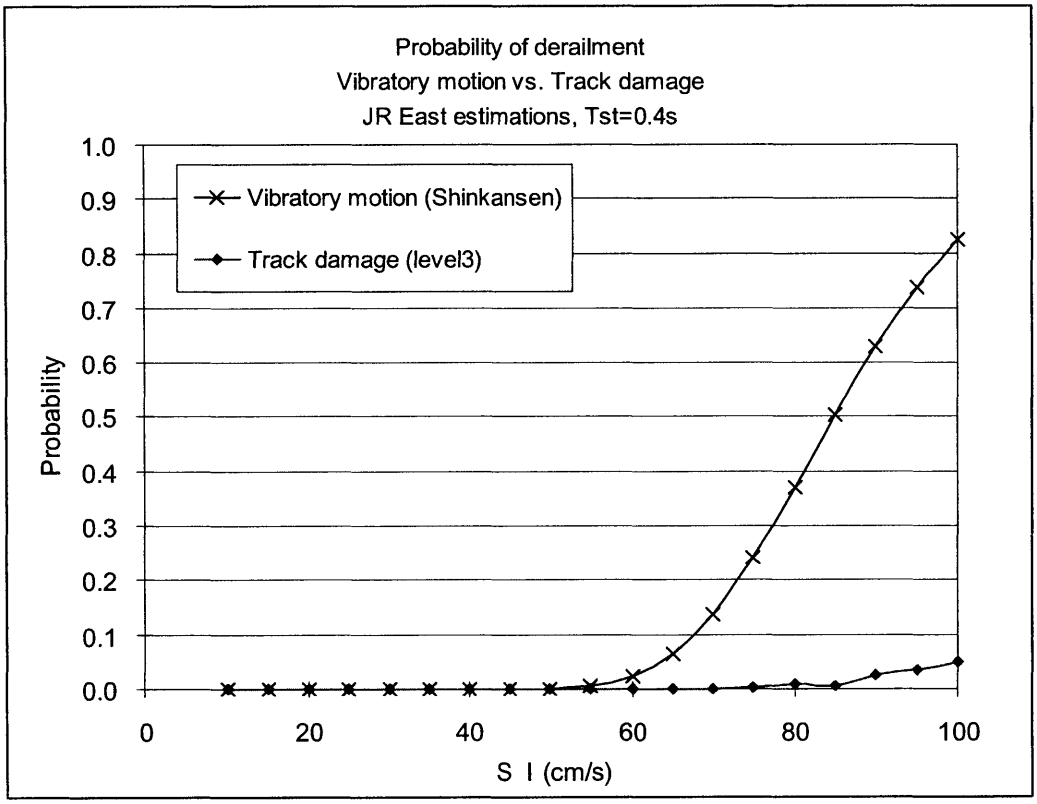

Figure 3-10 Comparison between derailment by vibratory motion vs. derailment by track damage for Tst=0.4s, JR East simulations

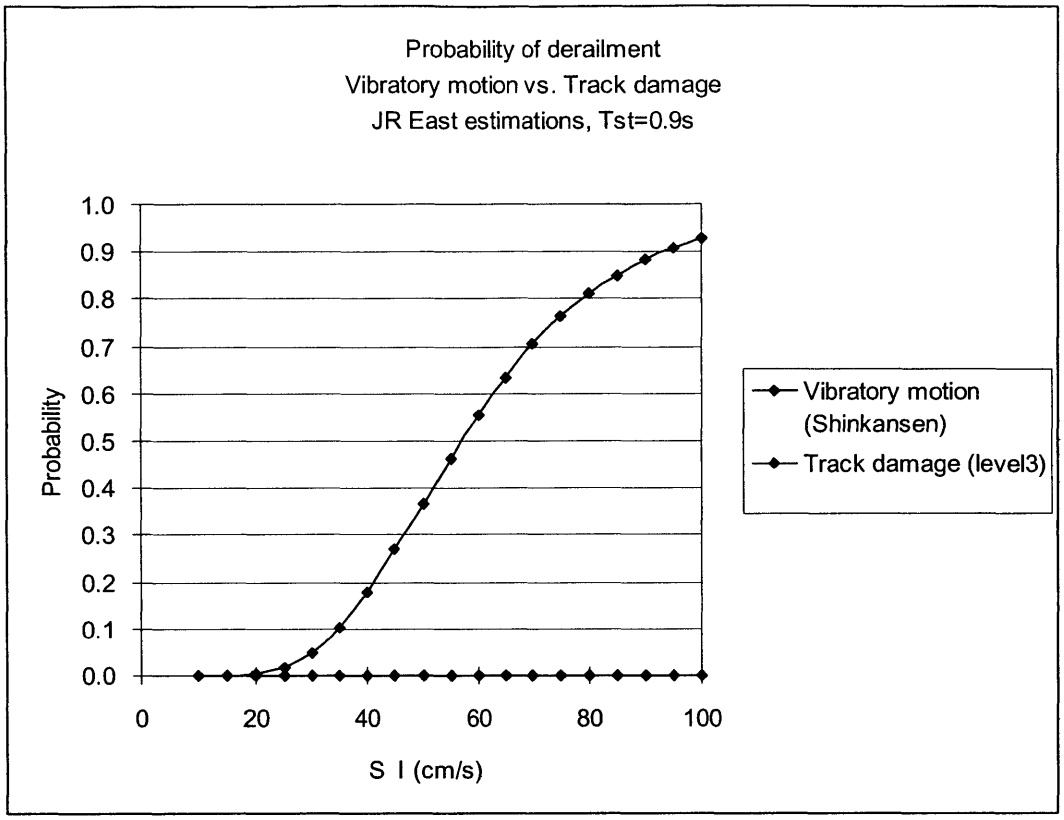

Figure 3-11 Comparison between derailment by vibratory motion vs. derailment by track damage for Tst=1s, JR East simulations

Clearly, when considering level 3 as the critical level for derailment by track damage, this mode of derailment is not dominant.

When considering derailment of a moving train running on damaged track, a more pertinent parameter is the residual displacement. During the ground motion phase, our model assumes that derailment does not occur until the relative displacement between wheel and rail exceeds 70mm. After the ground motion phase, the same derailment criteria must apply, and derailment should not occur until those criteria are met. Next, a method based on residual displacement is presented.

3.2.2 Residual Displacement

The amplitude of the residual deformation appears as a more relevant parameter when determining whether a train running on damaged tracks will manage to negotiate the deformed tracks.

The criteria for derailment derived earlier are (Equation 2):

$$\begin{cases} A \geq 0.3g \\ \quad and \\ D \geq 70mm \end{cases}$$

If these two parameters are sufficient to trigger derailment during the ground motion, then, it is expected that the same criteria must apply after the ground motion. After the ground motion ended, only one parameter is considered: the permanent displacement D_{res}. In what follows, it is assumed that a permanent displacement of $d_{\lim} = 7cm$ after the ground motion is by itself sufficient to trigger the derailment of a moving train running on damaged tracks. The acceleration is not considered after the ground motion ends. This second constraint would yield even lower probability of derailment by track damage.

The second step is to evaluate the amplitude of the residual displacement as a function of the peak elastic acceleration Sa_{el}. Given the acceleration Sa_{el} and a natural period of the structure T_{st}, we can obtain the probability that the residual displacement D_{res} exceeds $d_{\lim} = 7cm$. This is done by deriving the probability density function $f_{\ln Dres}(\ln d)$ as a function of Sa_{el} and T_{st}. The probability that $D_{res} > d_{\lim}$ is:

$$P(\ln D_{res} > \ln d_{\lim}) = \int_{\ln d_{\lim}}^{+\infty} f_{\ln Dres}(\ln d) d \ln d$$

A brief review on residual displacement is presented first, followed by the derivation of $f_{\ln Dres}$.

The evaluation of residual displacement demands has been generally oriented to a constant-ductility approach (e.g., Kawashima et. al, 1998), when the displacement ductility resistance of the system is known. However, Miranda (2001) and Ruiz-Garcia and Miranda (2003) note that the displacement ductility demand is in general not known and therefore a more appropriate procedure is to evaluate deformation demands from known properties of the system such as the period of vibration T_{st} and the lateral strength R. Ruiz-Garcia and Miranda (2005) have studied the residual displacement ratio C_r:

$$C_r = \frac{D_{res}}{D_{el}}$$

C_r is the ratio between the residual displacement D_{res} and the peak relative elastic displacement D_{el}. The ratios C_r were computed using single degree of freedom (SDOF) systems with specific lateral strength ratio R. The lateral strength ratio R is given by:

$$R = Sa_{el} / Sa_{yielding}$$

where Sa_{el} is the peak elastic acceleration and $Sa_{yielding}$ is the lateral yield strength capacity of the system.

The residual displacement ratios C_r were computed for elastoplastic, bilinear and stiffness-degrading SDOF systems with lateral strength ratio R=1.5, 2, 3, 4, 5 and 6. Systems with positive post-yield stiffness and stiffness-degrading systems produce smaller residual displacement ratios than elastoplastic systems. Hence, elastoplastic results are conservative.

The following simplified form for C_r is proposed by Ruiz-Garcia and Miranda (2005):

$$C_r = a\left[\frac{1}{b} + \frac{1}{41T_{st}^c}\right]\left[1 - \exp\left[-d(R-1)^e\right]\right]$$

where T_{st} is the natural period of the structure, R the lateral strength ratio and a, b, c, d and e are coefficients that depend on site condition.

Figure 3-12 and Figure 3-13 show the amplitude of the residual displacement ratios for elastoplastic systems and for R=2 and R=4 respectively. The different curves in each figure are for different soil conditions (denoted AB, C and D). The effect of soil type on C_r is small and in what follows, we use the ratio averaged over the three soil types (denoted ABCD).

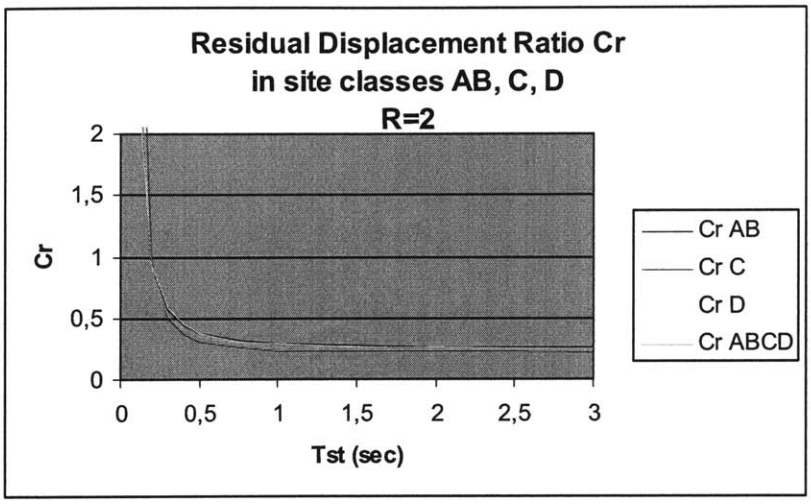

Figure 3-12 Residual displacement ratio for R=2; Ruiz-Garcia and Miranda (2005)

For example, for R=2, a structure with T_{st}=0.4s is expected to experience a terminal permanent deformation equal to about 50% of the maximum displacement of a linear elastic structure.

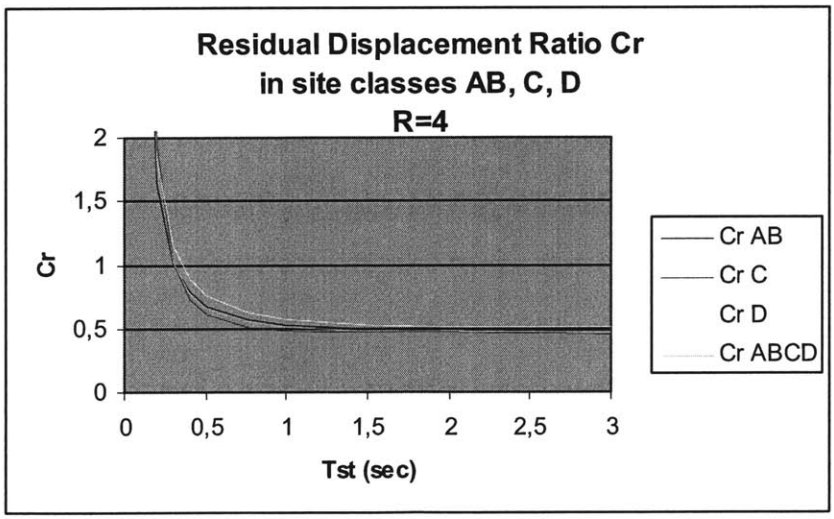

Figure 3-13 Residual displacement ratio for R=4; Ruiz-Garcia and Miranda (2005)

C_r displays a large record-to-record variability. The coefficient of variation of Cr ranges from 1.6 for periods smaller than 0.3s to 0.8 for longer periods (T>0.5s) (see Table 3-6). This variability is significant and must be taken into account. For example, for systems with period of vibration smaller than 1s, the residual displacement can vary from being less than 10% of peak elastic displacement to being larger than the elastic deformation (Ruiz-Garcia and Miranda, 2005).

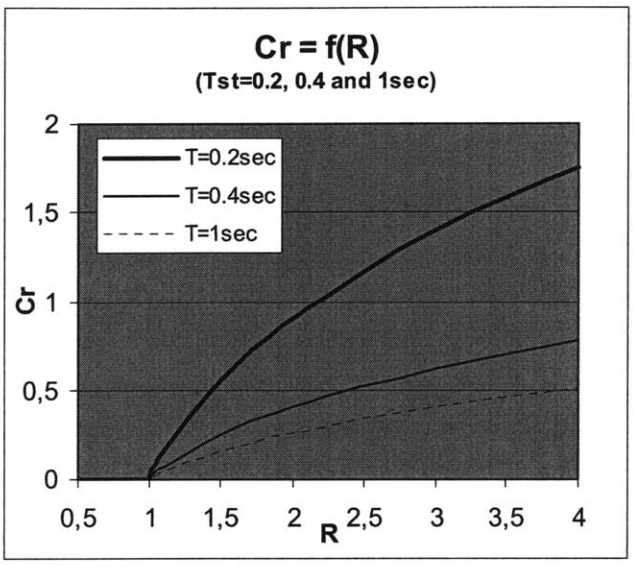

Figure 3-14 Residual displacement ratio as a function of the relative lateral strength R

When $R \leq 1$, the structure responds elastically and there is no residual displacement: C_r=0 (see Figure 3-14). Nevertheless, even if R is expected to be less than 1, there is still a probability that R exceeds 1, yielding non zero residual displacements.

The probability density function $f_{\ln Dres}(\ln d)$ is calculated as follows.

Given the acceleration demand Sa_{el} for a structure with natural period T_{st}, the median lateral strength ratio R is: $R = {Sa_{el}}/{Sa_{yielding}(T_{st})}$. The standard deviation of the lognormal distribution of R is 0.4 (see Section 3.2.1).

Assuming a relation between acceleration Sa and relative displacement D of the form $Sa = \omega_{st}^2 D$, the ratio of the relative displacements equals the ratio of the accelerations:

$$\frac{D_{el}(M, R\_km)}{D_{yield}} \approx \frac{Sa_{el}(M, R\_km)}{Sa_{yield}} = R$$

Given R, the residual displacement ratio $C_{r|R}$ can therefore be written as:

$$C_{r|R} = \frac{D_{res}}{D_{el}} = \frac{D_{res}}{R * D_{yield}}$$

It follows that: $D_{res} \approx C_{r|R} * D_{yield} * R$ or: $\ln(D_{res}) \approx \ln(C_{r|R}) + \ln(D_{yield}) + \ln(R)$

The ratio $C_{r|R}$ may be taken as having a log-normal distribution with standard deviations evaluated from the coefficients of variation of $C_{r|R}$ given by Ruiz-Garcia and Miranda (2005). When R≤1, the structure responds elastically and there is no residual displacement C_r=0. Therefore, the log-normal distribution of $C_{r|R}$ is truncated and for R≤1, C_r=0.

The probability density function of the residual displacement is obtained as:

$$f_{\ln Dres}(\ln d) = \int_0^\infty f_{\ln R}(\ln r) * f_{\ln C_{r|r}}(\ln d - \ln Dy - \ln r) \quad d\ln r$$

Where

$$f_{\ln R}(\ln r) = \frac{1}{\sigma_{\ln R}\sqrt{2\pi}} \exp\left[-\frac{1}{2}\left(\frac{\ln r - m_{\ln R}}{\sigma_{\ln R}}\right)^2\right]$$

$$f_{\ln C_{r|r}}(\ln c_r) = \frac{1}{\sigma_{\ln C_{r|r}}\sqrt{2\pi}} \exp\left[-\frac{1}{2}\left(\frac{\ln d - \ln Dy - \ln r - m_{\ln C_{r|r}}}{\sigma_{\ln C_{r|r}}}\right)^2\right]$$

The following values of the displacement at yielding are from JR East and refer to viaduct structures. The coefficients of variation of C_r are from Ruiz-Garcia and Miranda, 2005.

Tst (sec)	Dy (cm)	COV C_r
0.3	3.3	1.2
0.4	3.7	1.1
0.5	4.1	1
0.9	5.8	0.8

Table 3-6 Displacement at yielding and coefficient of variation of C_r as a funtion of the natural period of the structure T_{st}

The probability that the residual displacement D_{res} exceeds a residual displacement limit $d_{\lim}$ of 7cm given the lateral strength ratio R is presented in Figure 3-15.

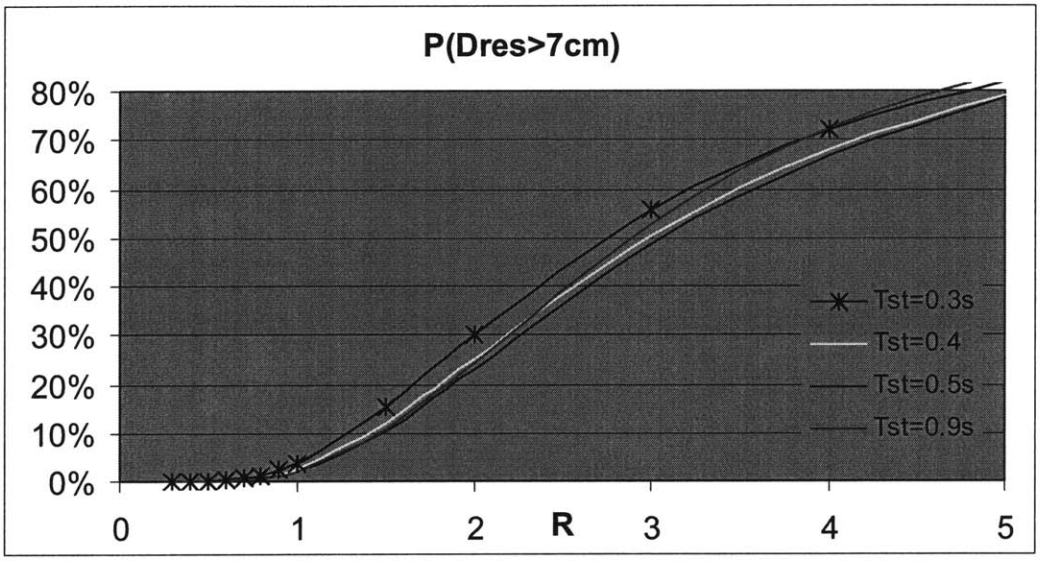

Figure 3-15 Probability of exceeding a residual displacement of 7cm given R

Interest is mostly in lateral strength ratios smaller than 1 (Figure 3-16). For example, for a structure with natural period T_{st}=0.4s, Sa_{yield}=0.93g. For an earthquake of magnitude M=7 at 50 km of the epicentre, Sa_{el}=0.3g (soft soil). This excitation yields an expected lateral strength ratio R of 0.33. Given R=0.33, the probability that the residual displacement exceed 7cm is 0,0003%.

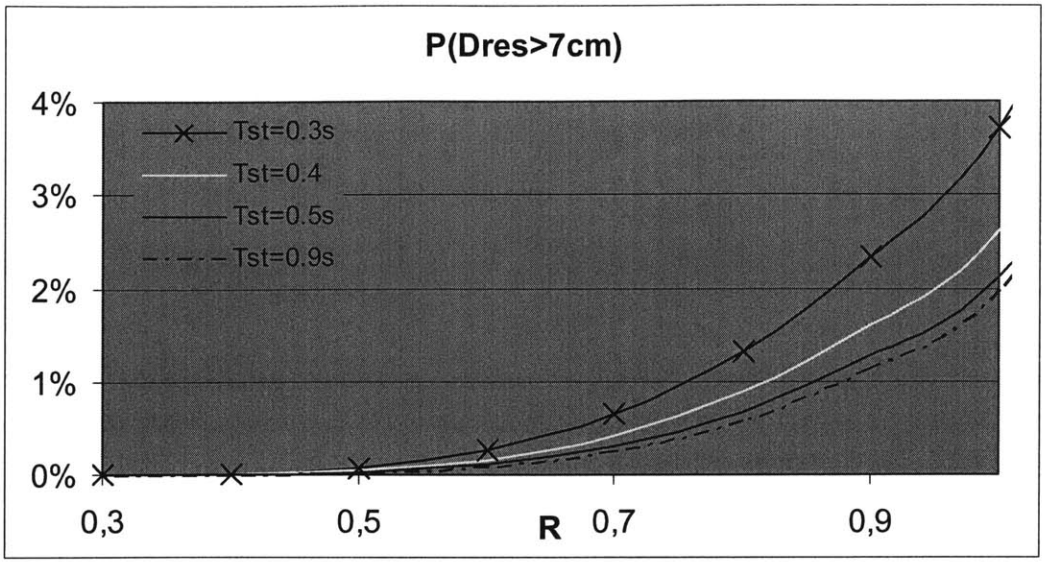

Figure 3-16 Probability of exceeding a residual displacement of 7cm given R

Sensitivity analysis concerning the residual displacement limit has been conducted for 3 different levels of d_{lim} : 5, 7 and 9 cm. They are reported in Figure 3-17.

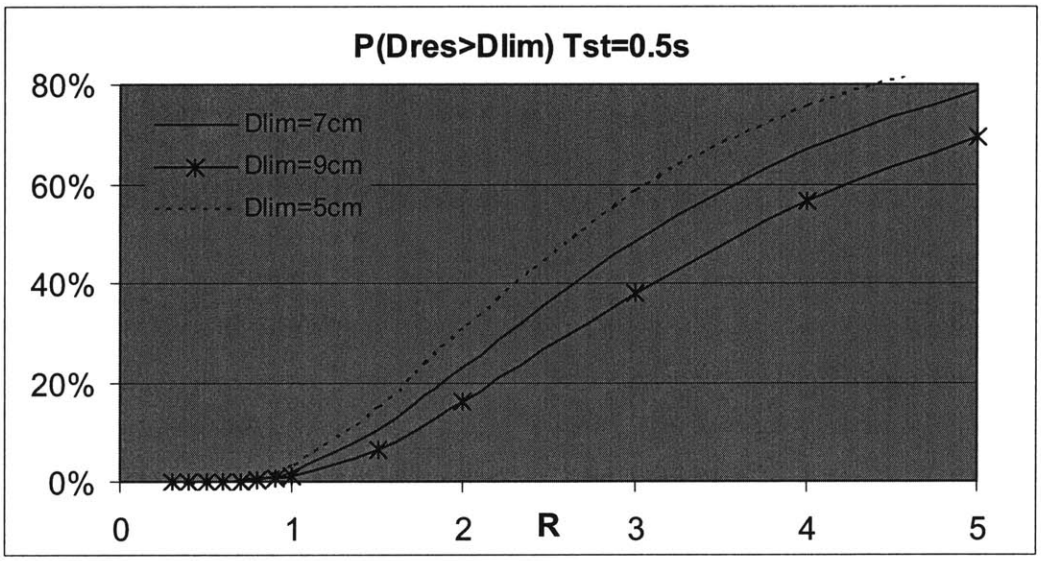

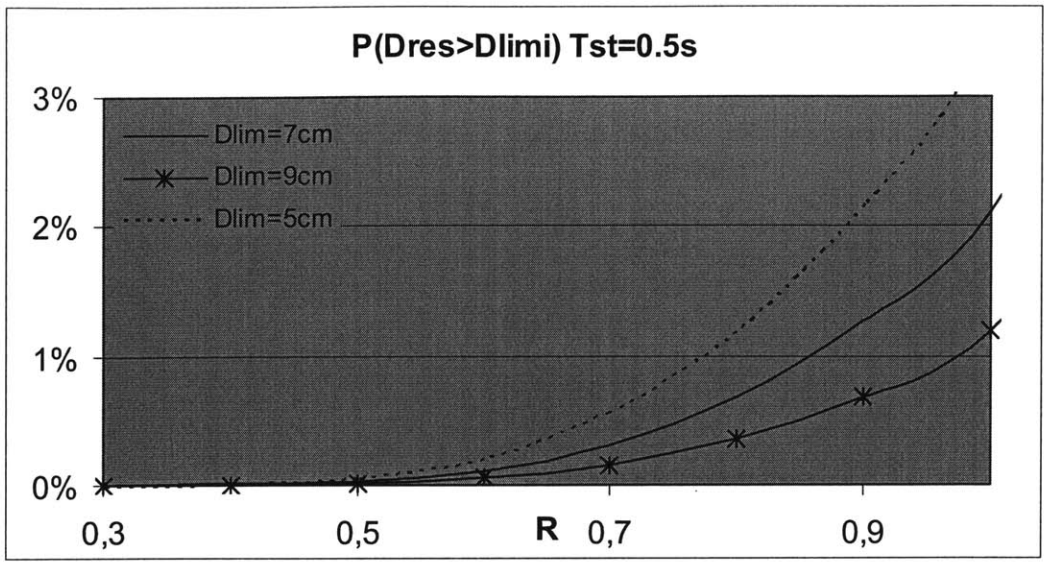

Figure 3-17 Probability of exceeding a residual displacement of 5, 7 and 9 cm given R; for T_{st}=0.5s

Given a lateral strength ratio of R=0.5, and for a natural period T_{st}=0.5s, the probability that the residual displacement exceed 5cm is 0,06%. It becomes 0,03% when $d_{\lim}$ is set equal to 7cm; and 0,01% when $d_{\lim}$ =9cm.

In what follows, we evaluate the probability of derailment due to running on damaged tracks for two of the earthquake scenarios presented in the elastic case: for T_{st}=0.4s and T_{st}=1s (see Figure 2-47 and Figure 2-48 in the elastic case) and for M=6, 7 and 7.5. The probability that D_{res} exceeds 7cm in these scenarios is shown in Figure 3-18 for T_{st}=1s; and in Figure 3-19 for T_{st}=0.4s.

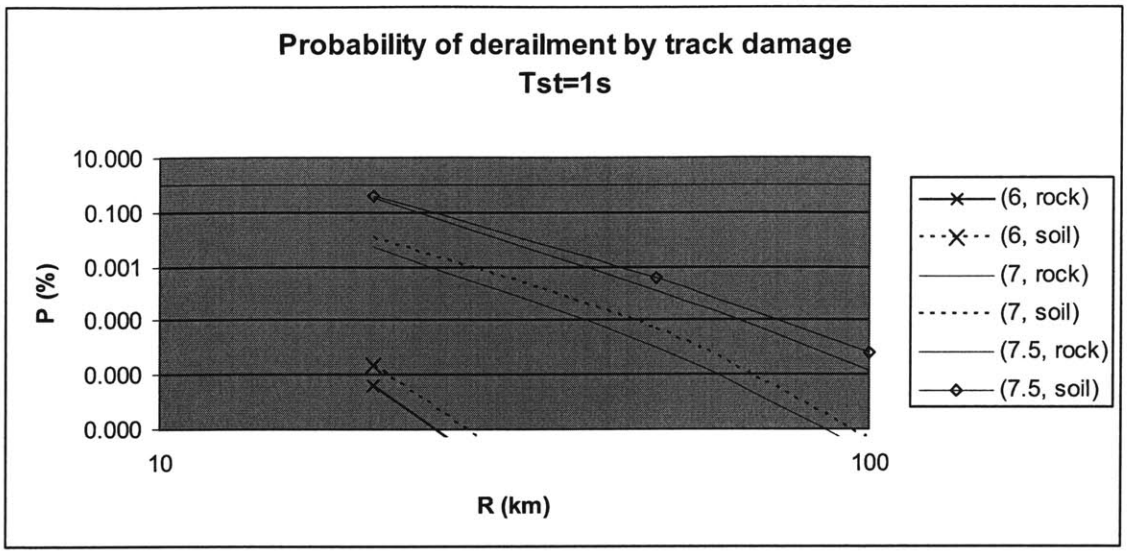

Figure 3-18 Probability of derailment by local track damage for Tst=1s

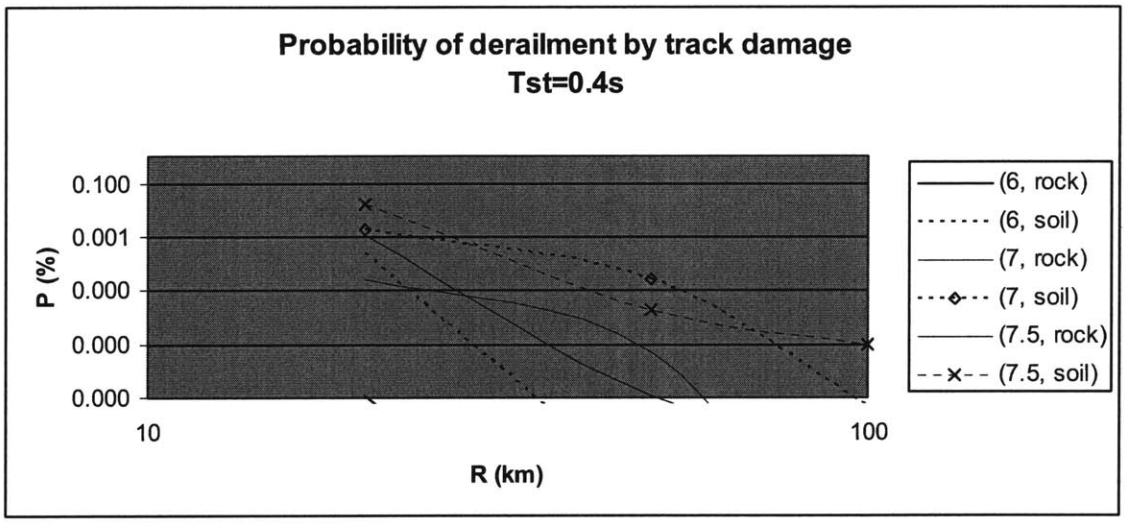

Figure 3-19 Probability of derailment by local track damage for Tst=0.4s

The probabilities obtained are relatively low: In Figure 3-20, the probability of derailment by local track damage (solid line) is compared to the probability of derailment by vibratory motion (dotted line) for an earthquake of magnitude 7. When considering the same earthquake scenario and the same site conditions, the probability of derailment by vibratory motion dominates.

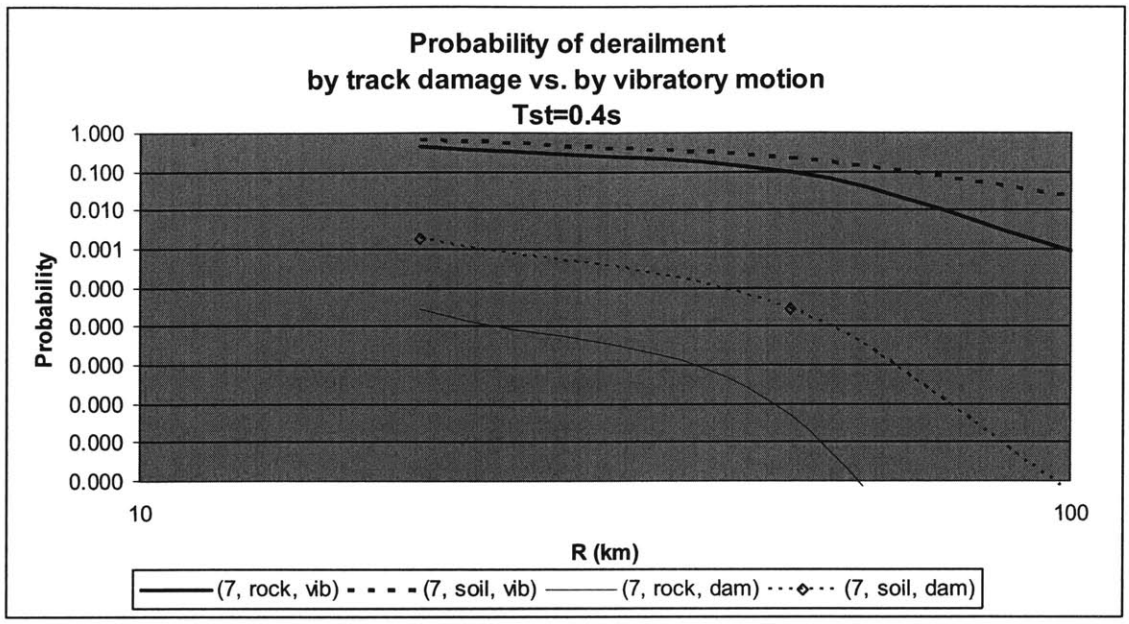

Figure 3-20 Comparison between derailment by vibratory motion and by track damage

Clearly, any permanent deformation at the end of the ground motion would be equaled or exceeded during the motion itself. Based on this consideration, derailment by track damage is not dominant, at it is shown in Figure 3-20. Papadimitriou (1995) and JR East simulations (2005) also come to the same conclusion.

Spatial dependence of damage

The probability of derailment by local track damage is further investigated by taking into account the spatial dependence of damage. Equation (26) formulates the phenomenon of clustering of earthquake damage:

$$P_d = 1 - \exp[-A * P] \tag{26}$$

where A is the number of spans that a train runs through until it stops. P is the probability of local damage as estimated in this section and P_d is the probability of derailment by track damage that takes into consideration the phenomenon of clustering of damage. In this formulation, the train speed is included, for A will increase as the speed increases. The probability of derailment by track damage increases as the number of spans that a train runs through until it stops increases, as seen in Figure 3-21.

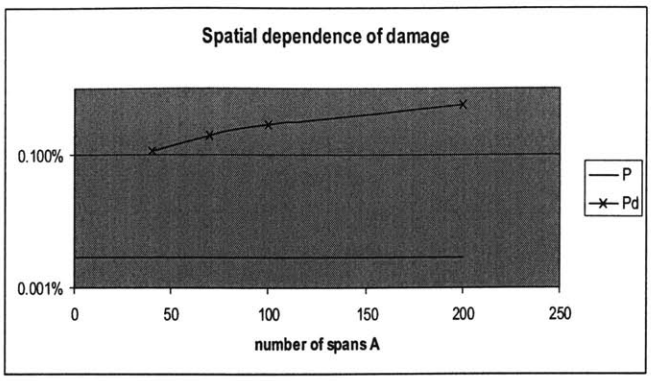

Figure 3-21 Spatial dependence of damage

In order to compare the results under the same conditions, it is assumed that the train runs at the highest speed, 275 km/h, and stars the brake when the wave arrives at the site. Under these assumptions, the number of spans A is 78 (JR East estimations, personal communication). The probability of derailment by track damage with spatial dependence of damage is presented in Figure 3-22 for an earthquake scenario M=7 on soft soil, for T_{st}=0.4s. The probability of derailment by track damage without spatial dependence of damage is plotted in solid line; whereas the probability of derailment by track damage with spatial dependence of damage is plotted in dotted lines for A=78 and A=140.

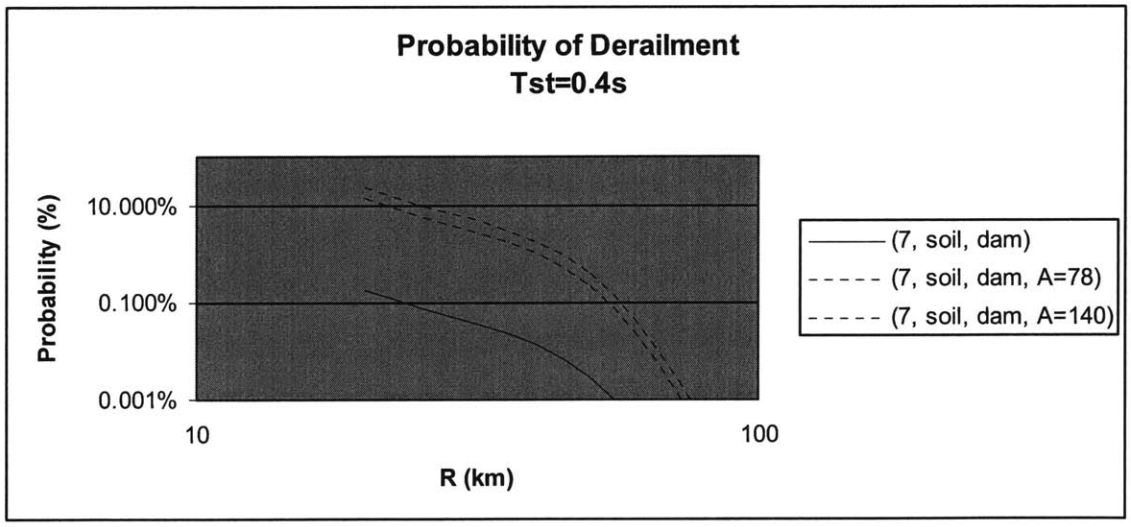

Figure 3-22 Probability of derailment by track damage with spatial dependence of damage

Spatial dependence of damage increases significantly the probability of derailment by track damage. The sensitivity to A is relatively minor.

In Figure 3-23, the probability of derailment by track damage with spatial dependence of damage is compared with the probability of derailment by vibratory motion. The probability of derailment by vibratory motion is plotted in dotted line; whereas the probability of derailment by track damage with spatial dependence of damage is plotted in solid lines for A=78 and A=140.

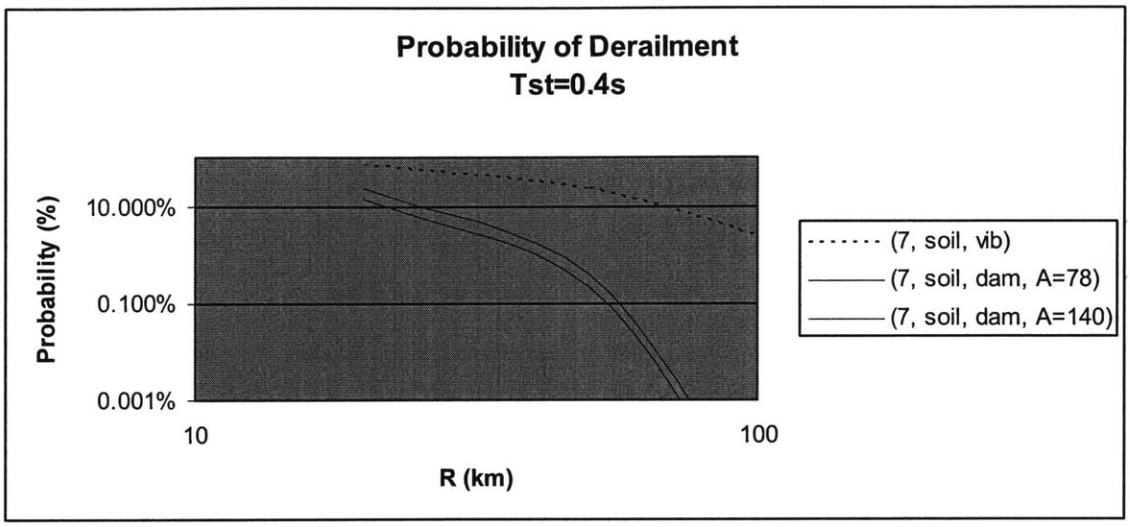

Figure 3-23 Probability of derailment by track damage with spatial dependence of damage compared with the probability of derailment by vibratory motion

Also in the case of spatial dependence of damage, derailment by vibratory motion dominates. If the derailment criteria are not met during the vibratory motion phase, it is possible but unlikely that they are met after the ground motion ended. Any permanent deformation at the end of the ground motion would be equaled or exceeded during the motion itself. Hence, we find that the first mode of derailment by vibratory motion dominates over the second mode, and the same result is obtained when spatial dependence of damage and train speed is considered. Spatial dependence of damage increases significantly the probability of derailment by track damage but not sufficiently to exceed the probability by vibratory motion under the same conditions.

The acceleration criterion has not been considered after the ground motion ends. In any case, adding a second constraint to the probability of derailment by track damage would

have yield lower probabilities for this mode of derailment. Hence, by considering only the displacement criterion, one is being conservative.

4 Conclusions

General criteria for derailment under earthquake conditions have been derived in terms of peak transversal acceleration and peak transversal displacement of the train.
It has been concluded that a train derails if:

$$\begin{cases} A \geq 0.3g \\ \quad and \\ D \geq 70mm \end{cases} \tag{2}$$

These criteria reproduce JR East's results very accurately for high-speed trains (Shinkansen). For commuter trains, the agreement is not as good. The criteria are in terms of absolute acceleration and absolute displacement, thus accounting for the contribution of the ground motion to the critical level of shaking. The vertical component of the acceleration is not considered and is usually disregarded in derailment risk analysis. However, to quantify the contribution of the vertical component, one should conduct simulations similar to those performed by JR East, using a dynamic train model with input excitations vertical to the track direction.

The derailment criteria should be expressed in probabilistic terms. Here, we considered sharp boundaries between the safe and unsafe regions. In reality, it is stochastic: There is a non-zero probability that a train derails in the safe region; as well as a non-zero probability that a train does not derail in the unsafe region. It is assumed that this second type of uncertainty is small relative to the uncertainty on $\{(D,A)|M,R\}$, thus the analysis that considers only the uncertainty on $\{(D,A)|M,R\}$ is adequate. Although the uncertainty in the derailment criteria is a second order uncertainty compared to the uncertainty in displacement and acceleration given M and R, it could be analysed in future work.

Two modes of derailment have been considered. First, during the ground motion, derailment may occur due to excessive track vibration and deformation. Second, after the ground motion has ended, derailment may occur due to excessive permanent track deformation. The criteria in equation (2) refer to both modes of derailment. If the

derailment criteria are not met during the vibratory motion phase, it is possible but unlikely that they are met after the ground motion ended. Any permanent deformation at the end of the ground motion would be equaled or exceeded during the motion itself. Hence, we find that the first mode of derailment by vibratory motion dominates over the second mode. This result holds when spatial dependence of damage is considered, and train speed included in the assessment of the probability of derailment by track damage. However, the relation between the probability of derailment by local damage and the probability of derailment by track damage that considers the spatial dependence of damage needs to be further investigated.

Train speed has been considered only in part in the assessment of the first mode of derailment. Speed has actually two effects: 1) It may facilitate derailment under synchronous track motion and 2) It contributes to lateral acceleration and displacement under non-synchronous track motion. The latter effect is considered in the estimation of the second component of train acceleration, whereas the former effect has been ignored. Intuitively, one would expect that as the speed of train increases, the critical level of shaking for derailment decreases. To quantify this decrease, one should formulate a dynamic model of a moving train, which is behind the scope of the present work. The decrease in the critical level induced by train speed will increase the probability of derailment by vibratory motion.

An elastic analysis is considered adequate to assess the probability of derailment under earthquake conditions. One effect produced by nonlinear behavior in the structure is a reduction in lateral acceleration. Another effect is an increase in relative displacement. In theory, one should consider the trade-off between the increase in displacement and the decrease in acceleration. However, it is concluded that the increase in relative displacement is not sufficient to yield a significant increase in the absolute displacement. Hence, only the decrease in acceleration is considered of importance. The elastic criteria are therefore conservative compared with results that are obtained by allowing inelastic behaviours. When the period of the structure is greater than 1 second, the yielding accelerations are low, and the elastic analysis is quite conservative. However, such periods are not common. The order of magnitude of the demand

parameters at stake when considering seismic loads (peak lateral displacement and peak lateral acceleration) are in most cases within the elastic range for stiffer structure. An elastic analysis is therefore considered adequate.

Under linear elastic conditions, a method to obtain the power spectral density function for ground acceleration is presented and used to obtain acceleration response spectra for the train. This model includes non-homogeneous site conditions when dealing with derailment of a moving train. Two components of the total lateral motion of the train are obtained. One is the track motion at a fixed location and the other is the motion as the train travels on deformed tracks. The latter component includes the effect of spatial variations in soil and structural characteristics as well as the effect of the incoherence of ground motion. It is found that the train motion due to track deformation has small effects at ordinary speeds but becomes noticeable as the speed increases and the support spacing decreases. For example, for a spacing of 8m between supports, the second component of train motion becomes important at speeds of 300km/h or higher and in some cases may increase the peak acceleration due to track motion at a single location by a factor of 2. In the Niigata case, sudden shifts in site conditions may have induced differential structural responses. In light of the results concerning spatial variability of ground motion, the base acceleration due to track motion at a single location *Sa* may be increased by a factor of 1.5. Already, without taking into account the discontinuities in site conditions, the situation was rather precarious: the probability of derailment under vibratory motion for a stationary train was 87%. When the discontinuities in site conditions are considered, the situation is worst, for the probability of derailment under vibratory motion for a moving train becomes 90%.

The model used in this study to obtain theoretical acceleration response spectra has parameters whose effects on the shape of the response spectra need to be further discussed. In particular, a more complete sensitivity analysis on the parameters of the power spectral density function for acceleration is needed. The effect of the shear wave velocity $v_{s\,30}$, the depth of the soil column h and the percentage of damping ξ should be further investigated.

Appendix I: The Sliding Block Model

A simple theoretical model – the sliding block model – is used to verify the trends observed in the simulations. As a first approximation, the sliding-block model is used to model the dynamic behavior of a train subject to seismic ground acceleration. The simulations conducted by JR East research laboratory derive the relationship between the period of the input motion and the critical acceleration yielding to a limiting displacement of 70mm. They are interpreted as the base acceleration required to overcome transversal resistance and initiate derailment. In earthquake engineering, the sliding-block model is used for Newmark analysis to model the dynamic behavior of landslides.

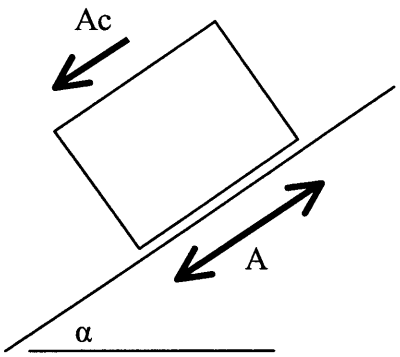

Sliding-block model used for Newmark analysis

It has been shown (e.g., Wilson and Keefer (1983)) that using Newmark's method to model the dynamic behavior of landslides on natural slopes yields reasonable and useful results. As summarized by Jibson et al (1998), Newmark's method models a landslide as a rigid block that slides on an inclined plane. The block has a known critical (or yield) acceleration, Ac, which is the threshold base acceleration required to overcome shear resistance and initiate sliding. The block is subjected to a base acceleration representing the earthquake shaking. The analysis calculates the cumulative permanent displacement of the block relative to its base as it is subjected to the effects of an earthquake acceleration-time history. In the figure below, an acceleration-time history of interest is selected, and the critical acceleration of the slope to be modeled is superimposed. Accelerations below this level (in the figure, Ac is chosen equal to 0.3g) cause no

permanent displacement of the block. As soon as Ac is reached, a permanent displacement occurs.

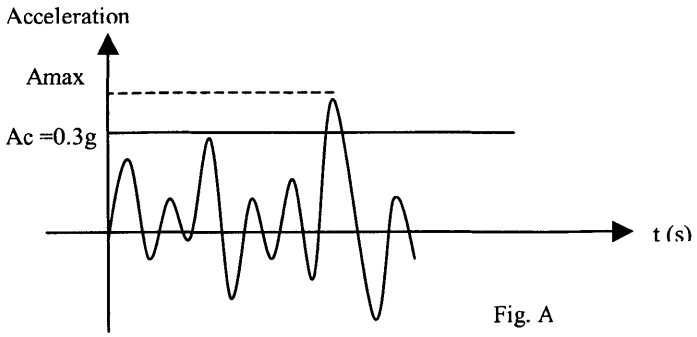

Fig. A

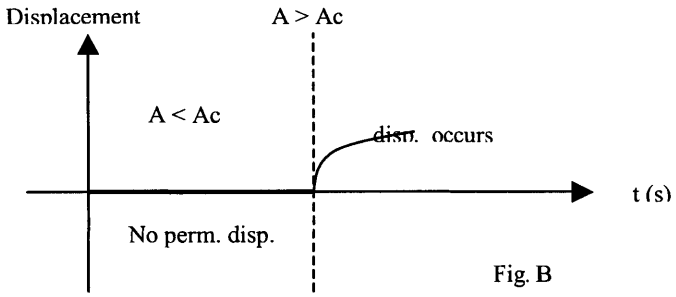

Fig. B

Newmark-analysis algorithm in picture, adapted from Wilson and Keefer (1983)

Various equations have been proposed to assess the normalized residual displacement D as a function of the normalized transmittable acceleration N. Equations proposed by Newmark (1965), Richards-Elms (1979) and Igarashi are reproduced below. The following notations have been used: S is the residual displacement of the bloc; V the peak velocity; A the peak ground acceleration; and D defined as $\frac{V^2}{A} = D$ is the peak displacement of the ground. The ratio $\frac{S}{V^2/A}$ is the normalized residual displacement; Ac is the transmittable block acceleration; and finally $N = \frac{Ac}{A}$ is the normalized transmittable acceleration.

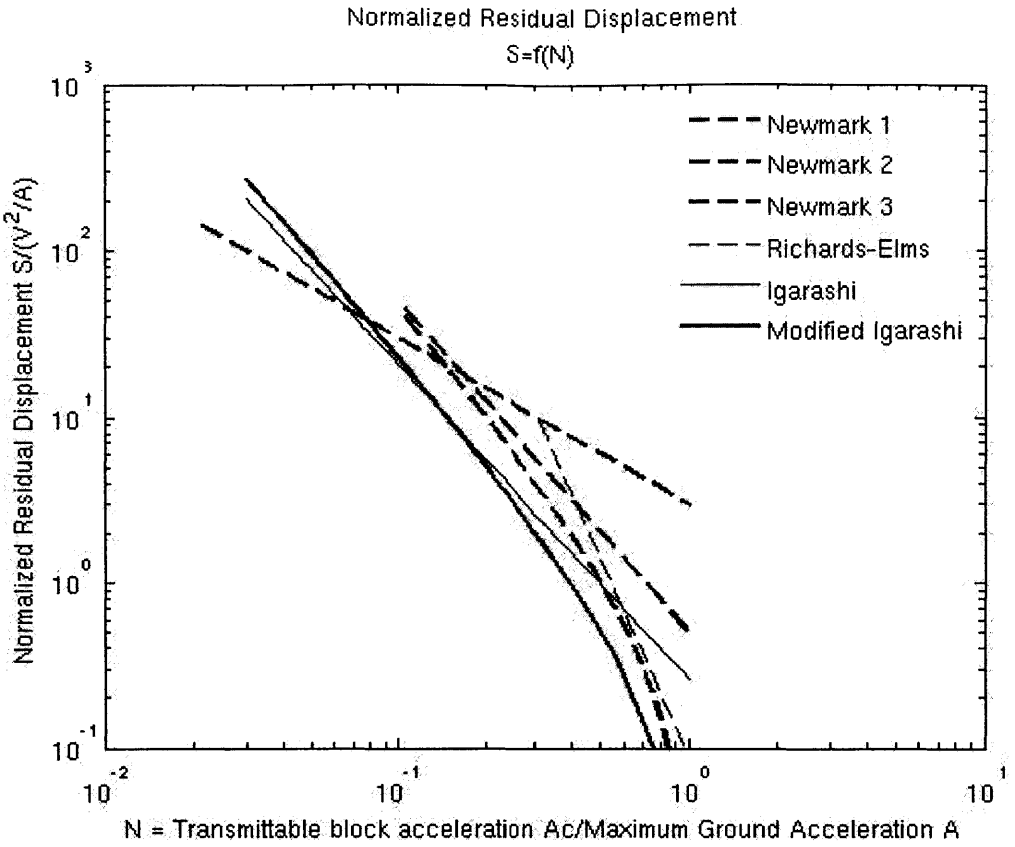

Regression against Peak velocity and Acceleration reproduced after Igarashi (1986) and Whitman and Liao (1985)

Most of the previous equations of siding block model are upper bound predictions of residual displacement. Igarashi's equation provides the less conservative results and will be used in our study. We modified Igarashi's equation to obtain no residual displacement when the maximum ground acceleration A is less or equal to Ac. It is also reproduced in the figure above and referred to as the Modified Igarashi's equation.

In our study, this analysis will model a train as a rigid block that slides on an inclined plane (the rails). The block has a known critical (or yield) acceleration, Ac, which is the threshold base acceleration required to overcome transverse resistance and initiate derailment. The block/train is subjected to a base acceleration (A) representing the earthquake shaking. Ground motions below the critical levels (A_c and S_c) cause no derailment.

In order to compare the modified Igarashi equation with the results obtained by simulations, we converted the modified Igarashi's equation from a regression of peak displacement against peak acceleration into a regression of peak displacement against frequency.

S_c and A_c being the critical displacement and acceleration of the train before derailment respectively, we Assume the following critical acceleration and displacement:

$$\begin{cases} A_c = 0.3g = 3000mm/s^2 \\ S_c = 70mm \end{cases}$$

We obtain an equation of D_c as a function of f plotted in yellow in the figure below with the simulations results.

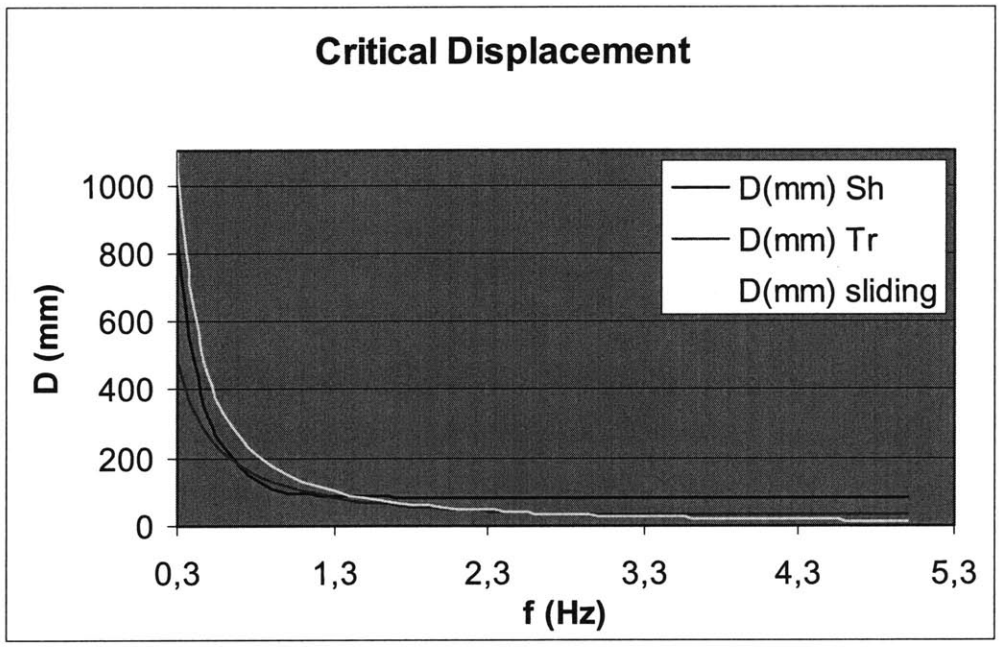

Critical displacement as a function of frequency. From dynamic modeling (JREast model: D-Sh and D-Tr) and from the slinding-block model (Igarashi's modified equation D-sliding).

It appears that the sliding block approximation to model dynamic train derailment subject to earthquake-induced ground motion yields results in terms of critical displacement that are in general agreement with those observed in the JREast simulations. Although the same trends are observed, the numerical values are not identical: the sliding-block model is a simple model.

Critical Accelerations before derailment (in g)			
Tst (s)	Shinkansen	Regular train	Sliding Block
0,3	3,57	1,53	1,17
0,4	2,01	0,96	0,99
0,5	1,29	0,80	0,87

Critical Accelerations before derailment. Comparison between simulations (Shinkansen and Regular train) vs. the sliding-block model.

This table presents some values of critical acceleration for selected natural periods (0.3-0.5 sec). The sliding block model is conservative. A train is more stable than a block sliding in only one direction on a slope. But the trends observed are in general agreement with the simulation.

Appendix II: The Modified Kanai-Tajimi Spectrum

The approach considers the dynamic properties of the soil through a linear transfer function. To describe the soil layer at station i, a popular functional form for the auto spectral density function is the modified Kanai-Tajimi Spectrum (MKT) for ground acceleration (Clough and Penzien, 1975), expressed as:

$$\left|H(\omega|\omega_i,\xi_i)\right|^2_{soil\ i} = \frac{1+4\zeta_i^2\left(\omega/\omega_i\right)^2}{\left[1-\left(\omega/\omega_i\right)^2\right]^2+4\zeta_i^2\left(\omega/\omega_i\right)^2} * \frac{\left(\omega/\omega_f\right)^4}{\left[1-\left(\omega/\omega_f\right)^2\right]^2+4\zeta_f^2\left(\omega/\omega_f\right)^2}$$

Ground acceleration histories can be directly generated from the *modified* Kanai-Tajimi power spectral density function - eg. Der Kiureghian and Neuenhofer (1992), Monti et al. (1996). This model idealizes the soil layer as a single-degree-of-freedom oscillator of frequency ω_i and damping ratio ζ_i. The first term on the RHS of the equation is the Kanai-Tajimi spectrum, and the second term is a modifier that makes the mean square ground displacement finite. ω_i and ζ_i are characteristic of the soil layer (see table below) and are based on classification of ground condition. ω_f and ξ_f are set equal to $0.1\,\omega_i$ and 0.6 respectively; to make the mean square ground displacement finite. The characteristic ground frequency and damping of the MKT model depend on the soil type as follow (Der Kuireghian and Neuenhofer, 1992):

Soil Type	f_i	ξ_i
Hard rock	5	0.8
Stiff	3	0.6
Medium	1.5	0.4
Soft	0.5	0.2

Characteristics of soils for the MKT model

Natural period	Ground Type	Geological definition
T_G<0.2s	I (Stiff)	Tertiary or older rock, or diluvium with H<10m
0.2<T_G<0.6s	II (medium)	Diluvium with H>10m, or alluvium with H<25m including soft layer with H<5m
0.6s<T_G	III (soft)	Other than the above (usually soft alluvium or reclaimed land)

Classification of ground condition based on the natural period of ground TG

The ground condition is commonly classified in three groups, as shown above, based on the natural period of the ground T_G (Japan Road Association 1990), as reported by Kawashima, 1998. For the purpose of the transfer function, the soil layer is assimilated to a single-degree-of-freedom oscillator of frequency f_i and damping ratio ξ_i.

The transfer function is plotted for 4 set of parameters values that idealize sites with soft, medium, stiff and hard rock soil properties.

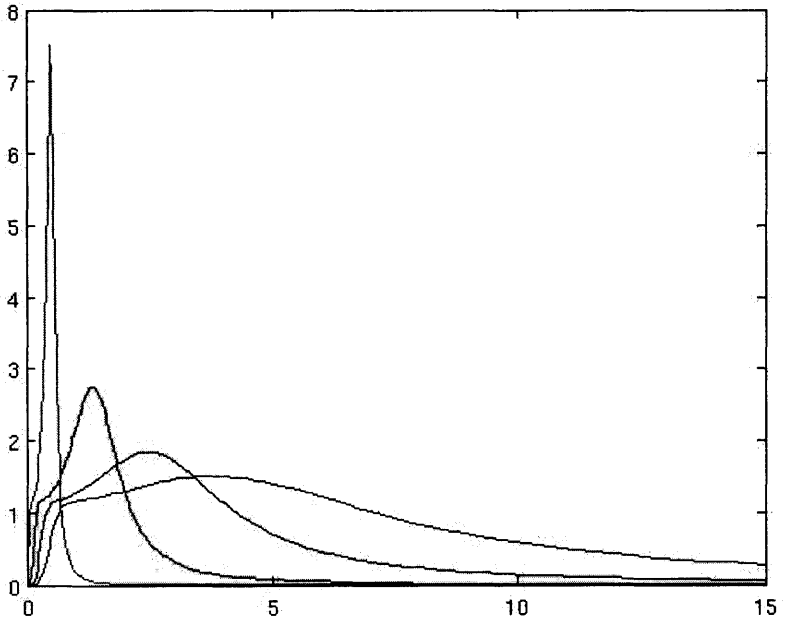

MKT Frequency-reponse functions for soils

The structural response may be obtained through random vibration analysis. The mean power spectral density of structural acceleration has the form:

$$S(\omega|M,R,soil,\omega_{st},\xi_{st}) = S_0(M,R)\left|H(\omega|\omega_i,\xi_i)\right|^2_{soil}\left|H(\omega|\omega_{st},\xi_{st})\right|^2_{structure}$$

Note that since the transfer function for soil does not distil what is known about the various factors affecting ground motion: source modelling, propagation and attenuation, the scale factor S_0 must depend on M and R. The standard deviation is obtained through integration over the full range of frequency of the transfer function, from which the peak response for a given natural period of the structure is derived (see methodology earlier in this chapter).

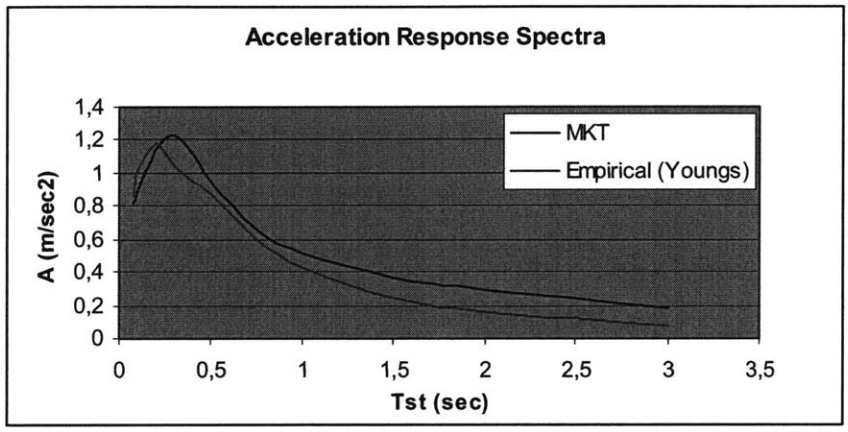

MKT Response Spectra for Firm soil

The figure above shows response spectra from the MKT model (dark line) and from an empirical relation (Youngs, 1997) in a lighter shade. We see how the theoretical model (MKT) leads to response spectra with shapes close to the empirical one. In this figure, the Youngs (1997) empirical attenuation relations if for an earthquake of magnitude 7 and epicentral distance of 100km. A coefficient specific to the couple (M,R)=(7,100) was applied to fit the theoretical spectra to the attenuation relationship of Youngs for rock.

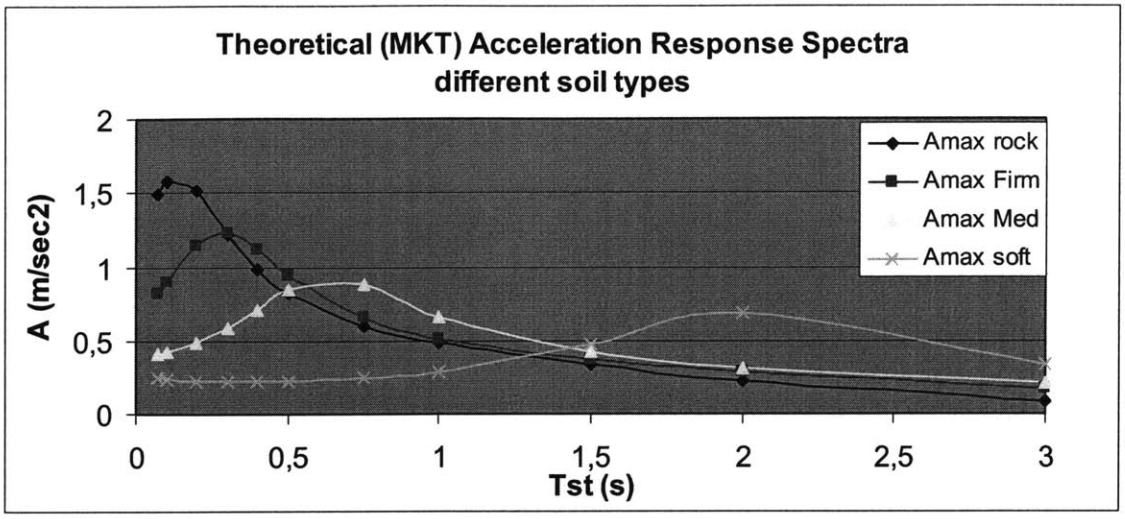

Theoretical Response Spectra for different soil conditions

The shortcoming of this method is that except for the site conditions, it does not incorporate various factors affecting ground motion, such as magnitude M, and distance to source R. Although the MKT function for soil allows a continuous modelling of soil conditions, the model requires calibrating each soil type to a PGA empirically observed on this type of soil. Hence, it implies extensive calibrations, and the empirical data provides response spectra only for a restricted number of soil conditions. Typically, only 2 soil conditions are reported – 'Rock' and 'Soil' – hence the difficulty to obtain calibrations for other soils. In addition, the calibration is likely to vary with the natural period of the structure.

Appendix III: Acceleration Response Spectra

Acceleration spectra derived from our model are presented for different earthquake scenarios. The parameters are noted as follow: 'Magnitude, Epicentral distance (km), Soil type (rock or soil)'. 'soil' refers to a soil with shear wave velocity of 350m/s, a depth of the soil column of 30m, and an impedance contrast k of 2. 'Rock' refers to a soil with shear wave velocity of 650m/s, a depth of the soil column of 30m, and an impedance contrast k of 1.

For example, '7, 100, soil' refers to our model, it stands for an earthquake of magnitude 7, an epicentral distance of 100km and on soft soil conditions.

When compared with empirical relations, those empirical relations are noted as: 'Magnitude, Epicentral distance (km), Soil type (rock or soil), Type of event (inter or intra), and name of the author (Y stands for Youngs, 1997). 'Rock' and 'Soil' refer to the Youngs (1997) study.

For example, '7, 100, soil (intra) Y' stands for an earthquake of magnitude 7, an epicentral distance of 100km from the Youngs (1997) empirical relationship for soil. The magnitude considered are: 5, 6, 7, 7.5 and 8, the distances are 100, 50 and 20 km from the source, and 2 soil conditions are considered.

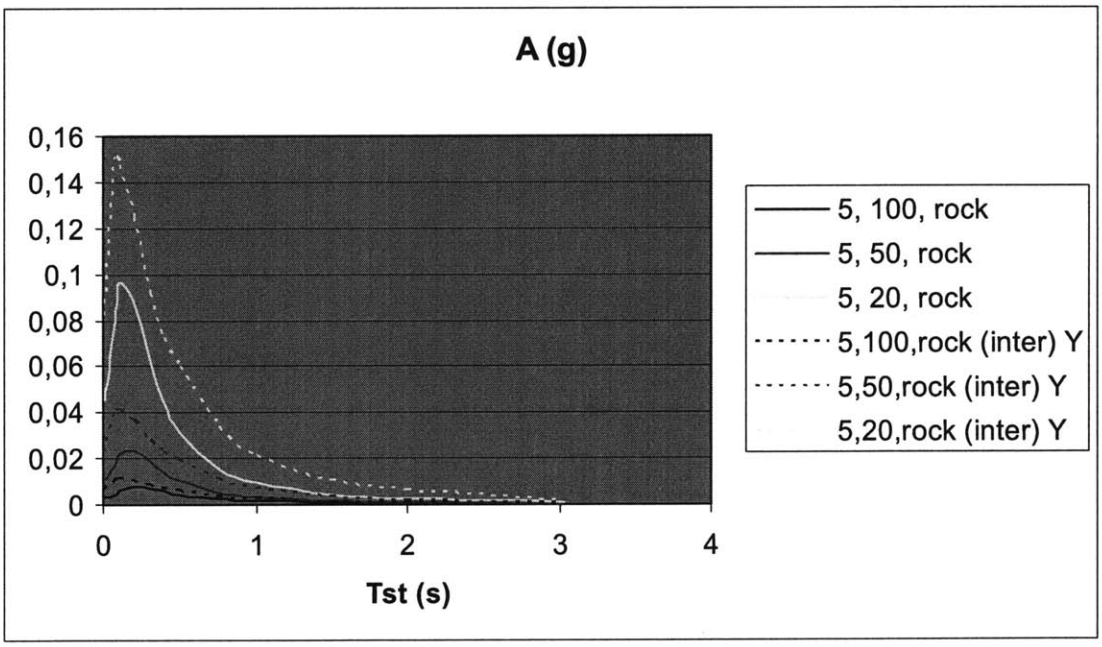

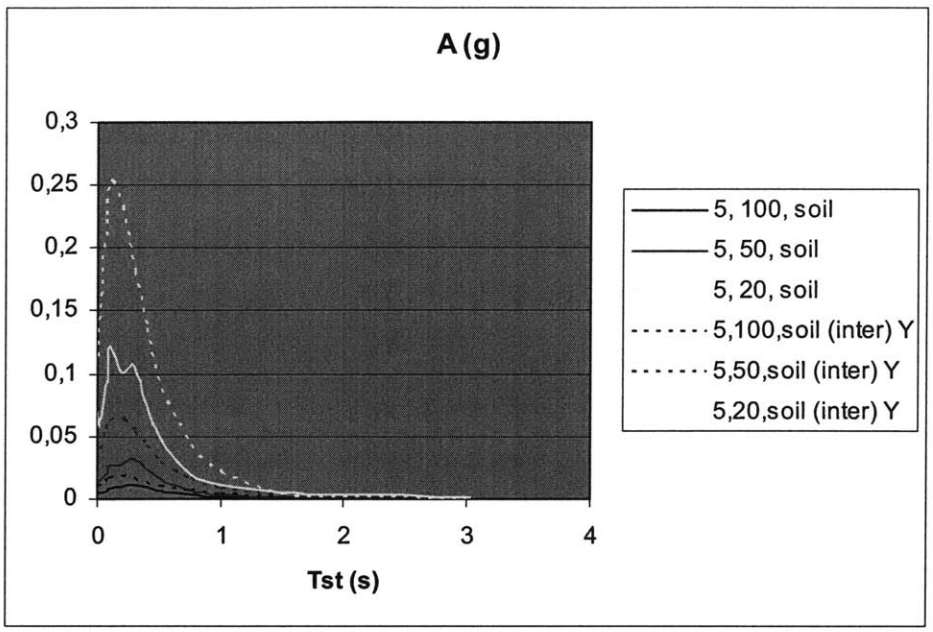
A (g)
0,3
0,25
0,2
0,15
0,1
0,05
0
0
1
2
3
4
Tst (s)
5, 100, soil
5, 50, soil
5, 20, soil
5,100,soil (inter) Y
5,50,soil (inter) Y
5,20,soil (inter) Y

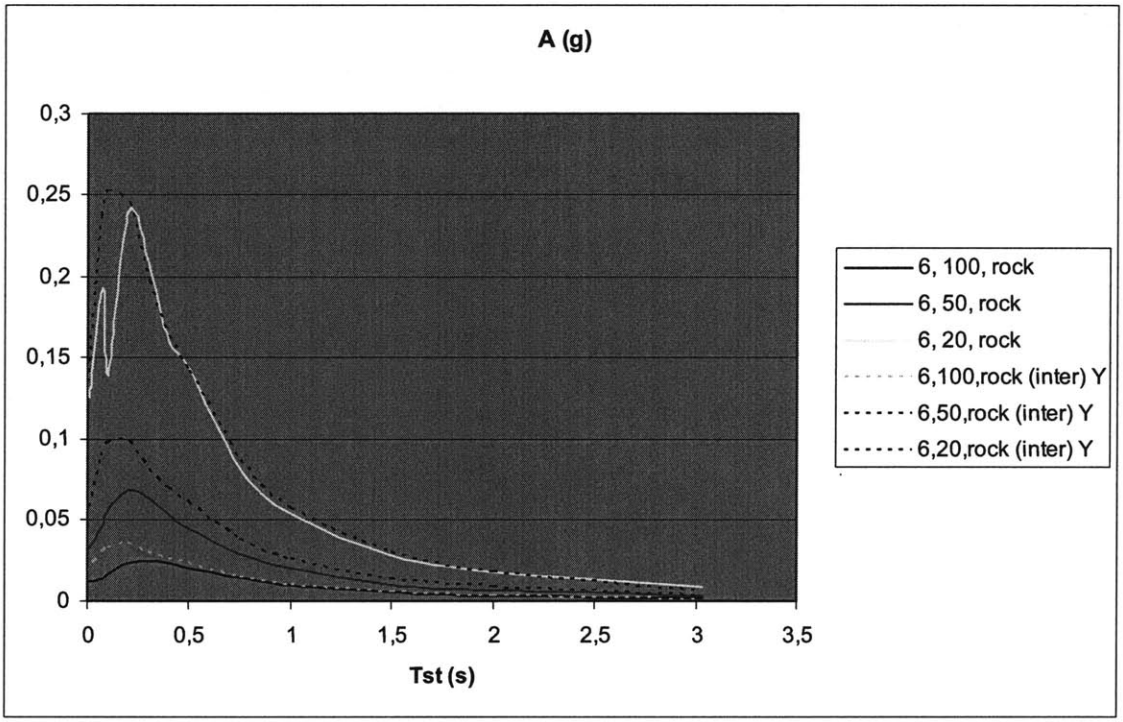
A (g)
0,3
0,25
0,2
0,15
0,1
0,05
0
0
0,5
1
1,5
2
2,5
3
3,5
Tst (s)
6, 100, rock
6, 50, rock
6, 20, rock
6,100,rock (inter) Y
6,50,rock (inter) Y
6,20,rock (inter) Y

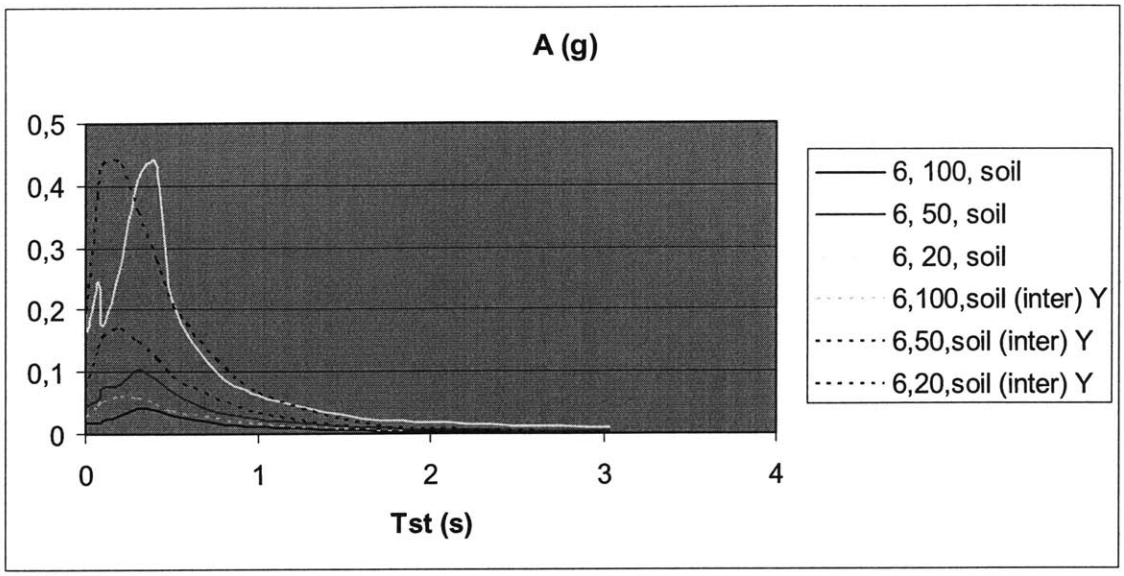
A (g)
0,5
0,4
0,3
0,2
0,1
0
0
1
2
3
4
Tst (s)
6, 100, soil
6, 50, soil
6, 20, soil
6,100,soil (inter) Y
6,50,soil (inter) Y
6,20,soil (inter) Y

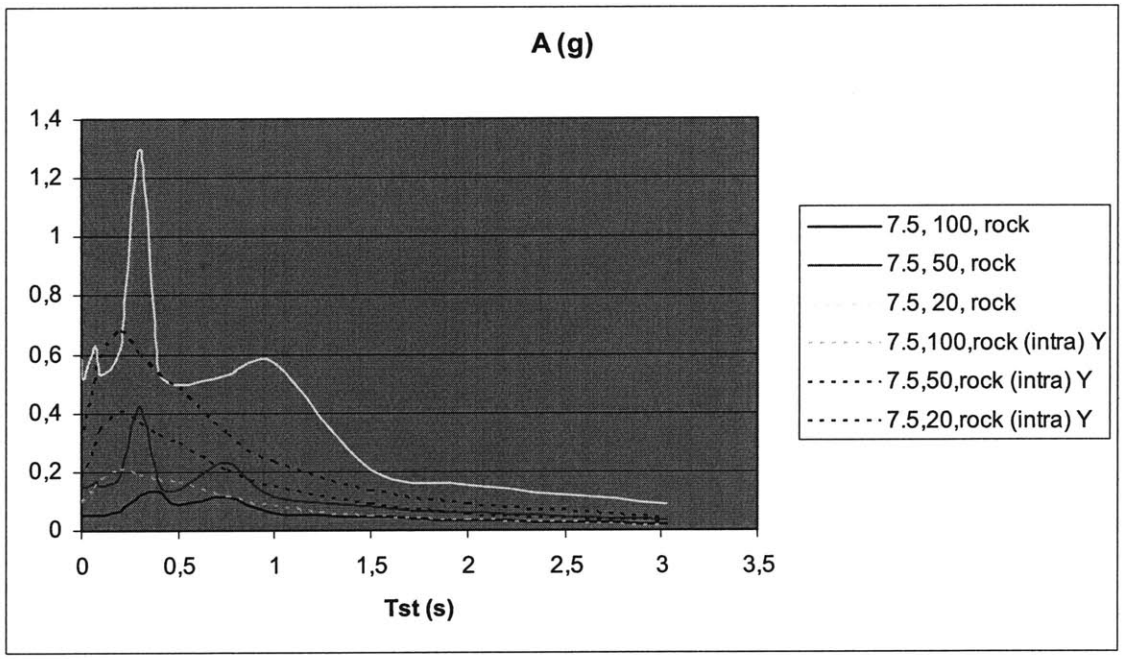
A (g)
1,4
1,2
1
0,8
0,6
0,4
0,2
0
0
0,5
1
1,5
2
2,5
3
3,5
Tst (s)
7.5, 100, rock
7.5, 50, rock
7.5, 20, rock
7.5,100,rock (intra) Y
7.5,50,rock (intra) Y
7.5,20,rock (intra) Y

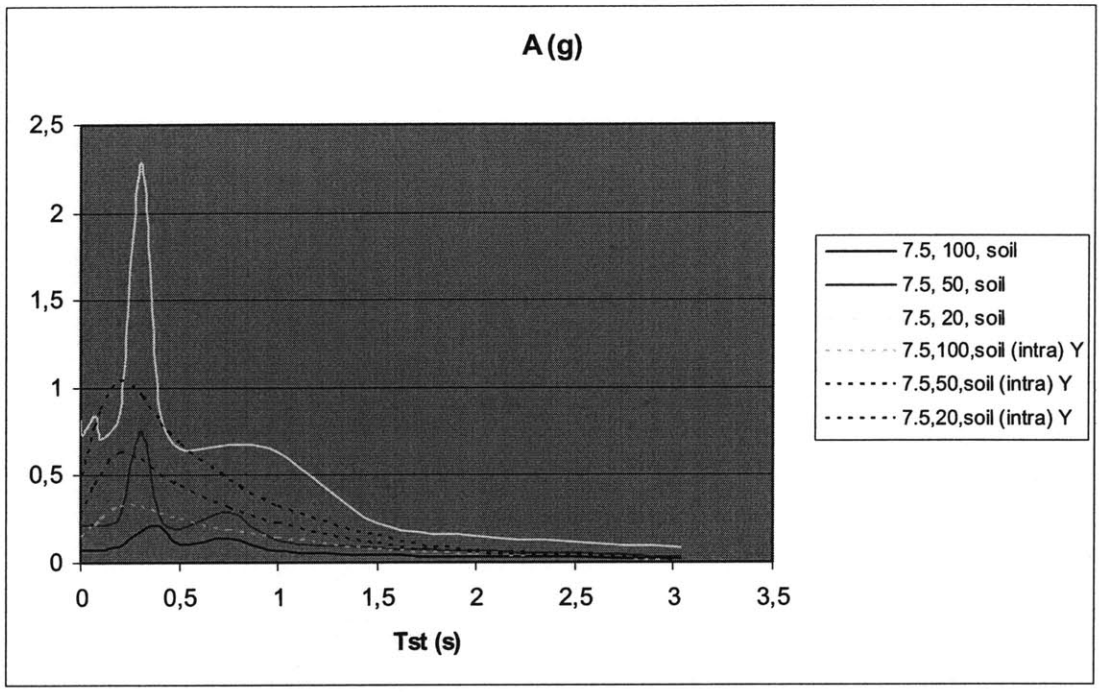
A (g)
2,5
2
1,5
1
0,5
0
0
0,5
1
1,5
2
2,5
3
3,5
Tst (s)
7.5, 100, soil
7.5, 50, soil
7.5, 20, soil
7.5,100,soil (intra) Y
7.5,50,soil (intra) Y
7.5,20,soil (intra) Y

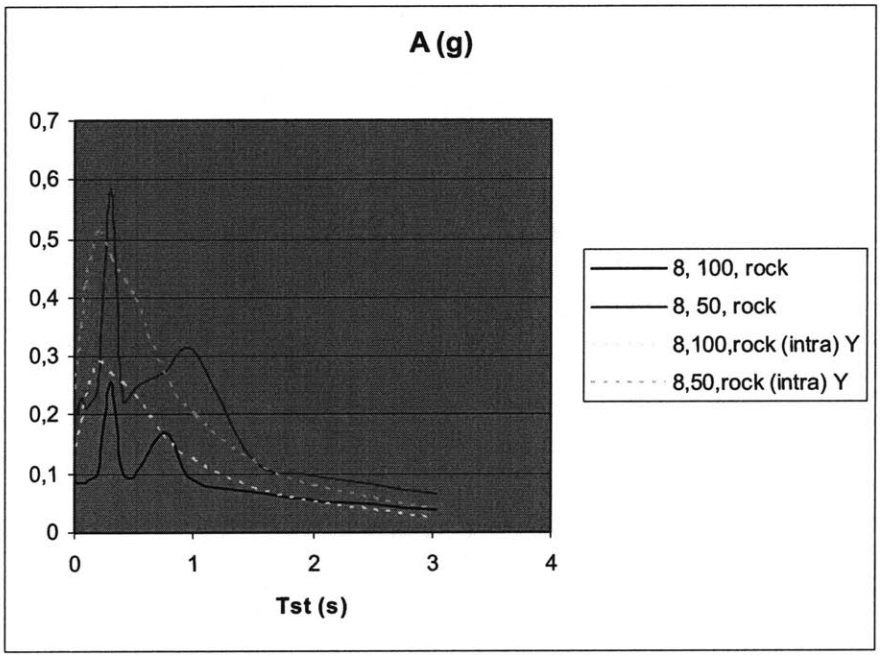
A (g)
0,7
0,6
0,5
0,4
0,3
0,2
0,1
0
0
1
2
3
4
Tst (s)
8, 100, rock
8, 50, rock
8,100,rock (intra) Y
8,50,rock (intra) Y

References

Abrahamson, N. A., Schneider, J. F., Stepp, J. C., (1991) "Empirical spatial coherency functions for application to soil-structure interaction analysis", Earthquake spectra 7, 1-28 (1991)

Alias, J. (1982), « Sans Bonnes Voies, pas de Chemin de Fer Sur », Le Rail et le Monde, No. 17.

Bender, B. (1984), "Incorporating Acceleration Variability Into Seismic Hazard Analysis" Bulletin of the Seismological Society of America, Vol. 74, No. 4, pp. 1451-1462, August 1984.

Bhatti, M.H., Garg, V.K (1984) "A review of Railway Vehicle Performance and Design Criteria" International Journal of Vehicle Design, Vol. 5, (2), 232-254.

Boore, D. M. (2003) "Simulation of Ground Motion Using the Stochastic Method" Pure and Applied Geophysics, 160 (2003) p.635-676.

Der Kiureghian, A. (1996) "A coherency model for spatially varying ground motions" Earthquake Engineering and Structural Dynamics, Vol. 25, 99-111 1996.

Der Kiureghian, A., Neuenhofer, A. (1992) "Response Spectrum Method for Multi-Support Seismic Excitations" Earthquake Engineering and Structural Dynamics, vol 21: 713-740, 1992.

Dukkipati, R. V., Amyot, J. R. (1988) "Computer-aided Simulation in Railway Dynamics" Mechanical Engineering Textbooks, Marcel Dekker, INC.

Fumal, T. E. (1978) "Correlations between seismic wave velocities and physical properties of near-surface geologic materials in the southern San Francisco Bay region" California, U.S. Geological Survey Open-File Report 78-1067 114 pp.

Garg, V. K., Dukkipati, R. V. (1984) "Dynamics of Railway Vehicle Systems" Academic Press Canada.

Harichandran, R. S., Vanmarcke, E. (1986) "Stochastic Variation of Earthquake Ground Motion in Space and Time" J. eng. mech. ASCE 112, 154-174 (1986).

Harichandran, R.S. (November 1999) "Spatial variation of earthquake ground motion: What is it, how do we model it, and what are its engineering implications?" personal notes, Dept. of Civil Eng., Michigan State University.

Igarashi, S. (1986), "Statistical Prediction of Slip Displacement due to Earthquake", Thesis, MIT, Master of Science in Civil Engineering, January 1986.

Jibson, R.W., Harp, E.L., and Michael, J.A. (1998) "A Method for Producing Digital Probabilistic Seismic Landslide Hazard Maps: An Example from the Los Angeles, California, Area" U.S. Geological Survey Open-File Report 98-113.

Kawashima, K., MacRae, G. A., Hoshikuma, J., Nagaya, K. (1998), "Residual Displacement Response Spectrum" Journal of Structural Engineering, May 1998, p.523-530.

Koffman, J.R., Barlett, D.L. (1965) "An appreciation of the practical problems: a survey of the problems and their importance" Interaction between Vehicle and Track, The Institution of Mechanical Engineers, Proceedings 1965-66, Vol. 180, Part 3F, Paper 6.

Lupoi A., Franchin P., Monti G., Pinto P. E. (2005) "Seismic design of bridges accounting for spatial variability of ground motion" Earthq. Eng. & Struct. Dyn., Vol. 34, 2005

Miranda, E. (2001) « Estimation of Inelastic Deformation Demands of SDOF Systems", Journal of Structural Engineering (ASCE) 2001; 127(9):1005-1012.

Miranda, E., Ruiz-Garcia, J. (2003), "Inelastic Displacement Ratios for Evaluation of Structures" Earthquake Engineering and Structural Dynamics, 32(9):1237-1258, 2003.

Miranda, E., Ruiz-Garcia, J. (2005) "Residual Displacement Ratios for Assessment of Existing Structures", Earthquake Engineering and Structural Dynamics, in press, Published online in Wiley InterScience (www.interscience.wiley.com) DOI: 10.1002/eqe.523 (2005)

Monti G., Pinto P. E. (1998) "Effects of multi-support excitation on isolated bridges" Tech. Report MCEER 98-0015, pp.225-247.

Newmark, N.M., 1965 "Effects of earthquakes on dams and embankments", Geotechnique, v. 15, no. 2, p. 139-160.

Papadimitriou, A., Veneziano, D. (1995). « Seismic Safety of the Tohoku Shinkensen : Assessement and Enhancement. » Cooperative JREast/MIT Research Program on Risk Assessment, Report 8, August 1995.

Profillidis, V., A. (2000). "Railway Engineering" Second edition, Ashgate Publishing Limited, 2-11-2 Static and Dynamic Analysis p. 47.

Sextos, A.G., Pitilakis, K.D., Kappos, A.J. (2003). "Inelastic Dynamic Analysis of RC Bridges Accouting for Spatial Variability of Ground Motion, Site Effects and Soil-Structure Interaction Phenomena" Earthquake Engineering and Structural Dynamics, vol. 32: 607-627, 2003.

Shimamura, M., Yamamura, K. (2005) "Development of Shinkansen Earthquake Impact Assessment System", JR EAST Technical Review.07 - Winter.2006, Special Edition Paper, Safety Research Laboratory, Research and Development Center of JR East Group.

Shinozuka M., Saxena V., Deodatis G. (2000) "Effect of spatial variation of ground motion on highway structures" Tech. Report MCEER 00-0013, December 2000.

Thomson, W. T. (1950), "Transmission of elastic waves through a stratified solid medium" J. Appl. Phys. 1950, 21.

Trifunac M. D., Brady A. G. (1975) "On the correlation of seismic intensity scales with peaks of recorded strong ground motion", Bulletin of the Seismological Society of America. 65, 139.

UIC, 703R (1989), "Layout Characteristics for Lines Used by Fast Passenger Trains", Paris.

Wickens, A.H., (2003) "Fundamentals of Rail Vehicle Dynamics: Guidance and Stability" Advances in Engineering 6.

Wills, C. J. and W. Silva (1998). "Shear wave velocity characteristics of geologic units in California" Earthquake Spectra, 14, no. 3, 533-556.

Wills, C. J. M. Petersen, W. A. Bryant, M. Reichle, G. J. Saucedo, S. Tan, G. Taylor, and J. Treiman (2000) "A site conditions map for California based on geology and shear wave velocity" Bulletin of the Seismological Society of America. 90, S187-S208.

Wilson, R.C., and Keefer, D.K., (1983) "Dynamic analysis of a slope failure from the 6 August 1979 Coyote Lake, California, earthquake" Bulletin of the Seismological Society of America, v. 73, p. 863-877.

Yamazaki, F., Ansary, M. A. (1997). "Horizontal-to-Vertical Spectrum Ratio of Earthquake Ground Motion for Site Characterization", Earthquake Engineering and Structure Dynamic, 26, 671-689 (1997).